Regulatory Roles of Cellular Diacylglycerol

BY

SVETLANA KURILOVA
B.S., Moscow State University, Russia, 2008
M.S., University of Illinois at Chicago, USA, 2014

THESIS

Submitted as partial fulfillment of the requirements
for the degree of Doctor of Philosophy in Chemistry
in the Graduate College of the
University of Illinois at Chicago, 2015

Chicago, Illinois

Defense Committee:

Wonhwa Cho, Chair and Advisor
Lawrence W. Miller
Jung-Hyun Min
Xiaojing Yang
Liang-Wei Gong, Biological Sciences

I dedicated this thesis to the ones who never stopped believing in me and supported me through all my studies. My father. My mother.

AKNOWLEDGEMENTS

I like to thank my supervisor, Prof. Wonhwa Cho, for giving me the opportunity to be a part in his research team. He patiently guided me throughout my graduate studies. I also appreciate my committee members, Dr. Larry Miller, Dr. Jung-Hyun Min, Dr. Xiaojing Yang and Dr. Liang-Wei Gong, for their valuable suggestions and support.

I am very grateful to Dr. Youngdae Yoon and Dr. Brian Page for teaching me all the technical aspects of the research and Park Lee for his help to adapt to the new working environment at the beginning of the graduate school training me on microscopy techniques.

I owe special thanks to my mentors, Dr. Vladimir Gevorgyan and Dr. William Modey, for their consistent support and encouragement in achieving my goals. I also want to extent my gratitude to the administration and support staff at the Department of Chemistry at UIC.

I would like to thank all the former and current lab members, in particular Marian Fernando, Kate Jablonski, Ewa Stec, Hyunjin Kim, Nate Lucas, Surajit Bhattacharjee, Hamid S. Afsari, Anthony Savushkin, and Olga Valueva, for all their advice and support with my projects as well as creating a good atmosphere in the laboratory.

Last but not least I like to thank my gratitude to my loving family for their support, unconditional love, time and effort. They have been a great motivational force and energy in accomplishing all I have to this day.

April 2015

Svetlana Kurilova

TABLE OF CONTENTS

LIST OF FIGURES

LIST OF TABLES

LIST OF ABBREVIATIONS

ATP	Adenosine triphosphate
BRP-DAN	MDDNK + L124C/C133S PKCγ C1b: C1b domain with N-terminal MDDNK extension and L124C/C133S mutantions
C1	Conserved domain 1 (cysteine-rich domain)
DAG	Diacylglycerol
DAN	6-acryloyl-2-dimethylaminonaphthalene, acrylodan
DGK	Diacylglycerol kinase
DMEM	Dulbecco's modified Eagle's medium
DPG	1,2-dipalmitoyl-*sn*-glycerol (16:0 DAG)
DMSO	Dimethyl sulfoxide
DTT	Dithiothreitol
EF	Calcium-binding motif composed of two helixes (E and F) joined by loop
EGFP	Enhanced green fluorescent protein
ENTH	Epsin N-terminal homology
ER	Endoplasmic reticulum
ESD	Environment sensitive dye
FBS	Fatal bovine serum
FCS	Fluorescence correlation spectroscopy
FRET	Förster resonance energy transfer *or* Fluorescence resonance electron transfer
LE	Labeling efficiency

NR	Nile Red
PC	Phosphatidylcholine
PC-PLC	Phosphatidylcholine phospholipase C
PBS	Phosphate buffered saline
PDBu	Phorbol 12,13-dibutyrate
PE	Phosphatidylethanolamine
PI	Phosphoinositide
PI(4,5)P2	Phosphatidylinositol 4,5-bisphosphate
PI-PLC	Phosphoinositide phospholipase C
PKC	Protein kinase C
PKD	Protein kinase D
PLA	Phospholipase A
PLC	Phospholipase C
PLD	Phospholipase D
PM	Plasma membrane
PMT	Photomultiplier tubes
POG	1-palmitoyl-2-oleoyl-*sn*-glycerol (16:0-18:1 DAG)
PS	Phosphatidylserine
RasGRP	RAS guanyl nucleotide-releasing protein
SAG	1-stearoyl-2-arachidonoyl-*sn*-glycerol (18:0-20:4 DAG)
SLB	Supported lipid bilayer
SMT	Single molecule tracking
TIRF	Total internal reflection fluorescence

SUMMARY

Kinetics of diacylglycerol and C1 domain interaction

Lipids in biological membranes play significant roles in cellular signaling. Lipids vary not only in head groups but also in acyl chains. It has been reported that the acyl chain of lipids plays an important role in membrane curvature and signal transduction. In this work we investigated the importance of the degree of unsaturation in the acyl chain of diacylglycerol (DAG) in its interaction with the C1 domain. Fluorescence quenching assay showed that DAG with a highly unsaturated acyl chain binds more tightly to the C1 domain than DAG with saturated acyl chains. Moreover, our single molecule tracking studies using supported lipid bilayers as a model system and NIH 3T3 cells explain the kinetic aspect of that binding. Although more unsaturated DAG binds C1 domain tighter it dissociates from the membrane faster than in case of saturated DAG. This finding can explain why unsaturated lipids participate in cell signaling when saturated lipids mainly play a role of bulk lipids. This work provides the new inside about the dynamics of protein-lipid interaction.

Extracellular function of diacylglycerol

The heterogeneous distribution of lipid molecules in biological membranes depends on a specific region and situation. Selective distribution between bilayer leaflets can be achieved through diffusion (flip-flop) across membranes. DAG is one these lipids which is able to flip-flop rapidly because of a small, uncharged head group. Since the precise cellular localization of DAG determines its function and activity, it is important to understand its distribution and dynamics

within a membrane leaflet and between inner and outer parts of cellular bilayers. We developed DAG sensor using mutagenesis and chemical labeling, which allowed accurate quantification of the lipid. Using this sensor we were able to detect very low concentration of DAG at the plasma membrane. It was found that ATP activation in NIH 3T3 cells elevates DAG in plasma membrane 5-7 times. Preliminary data suggest a significant basal level of DAG. It is known that there are two major sources of DAG: from phosphatidylinositol 4,5-bisphosphate ($PI(4,5)P_2$) and phosphatidylcholine (PC) and both can be initiated by ATP. Physiological roles of exofacial DAG remain unknown. It requires further investigation to understand the flip-flop process and its initiation. We discuss the novel four-color imaging with application of ratiometric analysis that can resolve these questions.

CHAPTER I

The effect of the *sn*-2 acyl chain of diacylglycerol on its interaction with C1 domains and its signaling role

1. Introduction

1.1. Diacylglycerol signaling

Cellular signals are transferred by complex networks of proteins and small molecules. Strict regulation of the signaling events is required to assure an accurate downstream result. In general, on the molecular level this is accomplished by definite reversible chemical modifications (for example, phosphorylation or recruitment of proteins to specific cellular compartments such as plasma membrane) [1, 2]. Less is known about cellular mechanisms of signaling processes initiated by small-molecules, lipid signaling in particular (Figure 1) [3]. It has been suggested structural diversity, localization and concentration of distinct lipid are important in lipid-mediated signaling processes [4]. Structural diversity of lipids derives from the combination of various lipid backbones and head groups and fatty acids attached to these backbones [5-7]. Importance of lipid head groups in lipid-protein interaction has been well documented but the role of fatty acid acyl chains in lipid signaling activity and specificity is not fully understood. We aim to study this unexplored issue in diacylglycerol (DAG) signaling.

We focus on DAG signaling due to its decisive role in various cellular networks such as G-protein coupled receptors as well as growth factor triggered and calcium-based signaling pathways [8-10]. Although DAG is best recognized as an activator of conventional and novel protein kinase C (PKC) isoforms through interaction with C1 domains [11, 12], DAG also induces translocation, change of conformation and as a result activation of other classes of proteins such as diacylglycerol kinase (DGK), Ras guanyl nucleotide-releasing protein (RasGRP) and protein kinase D (PKD) (Figure 2) [13]. DAG is an established second messenger critical for both short and prolonged cellular events (Figure 3). The production of DAG is

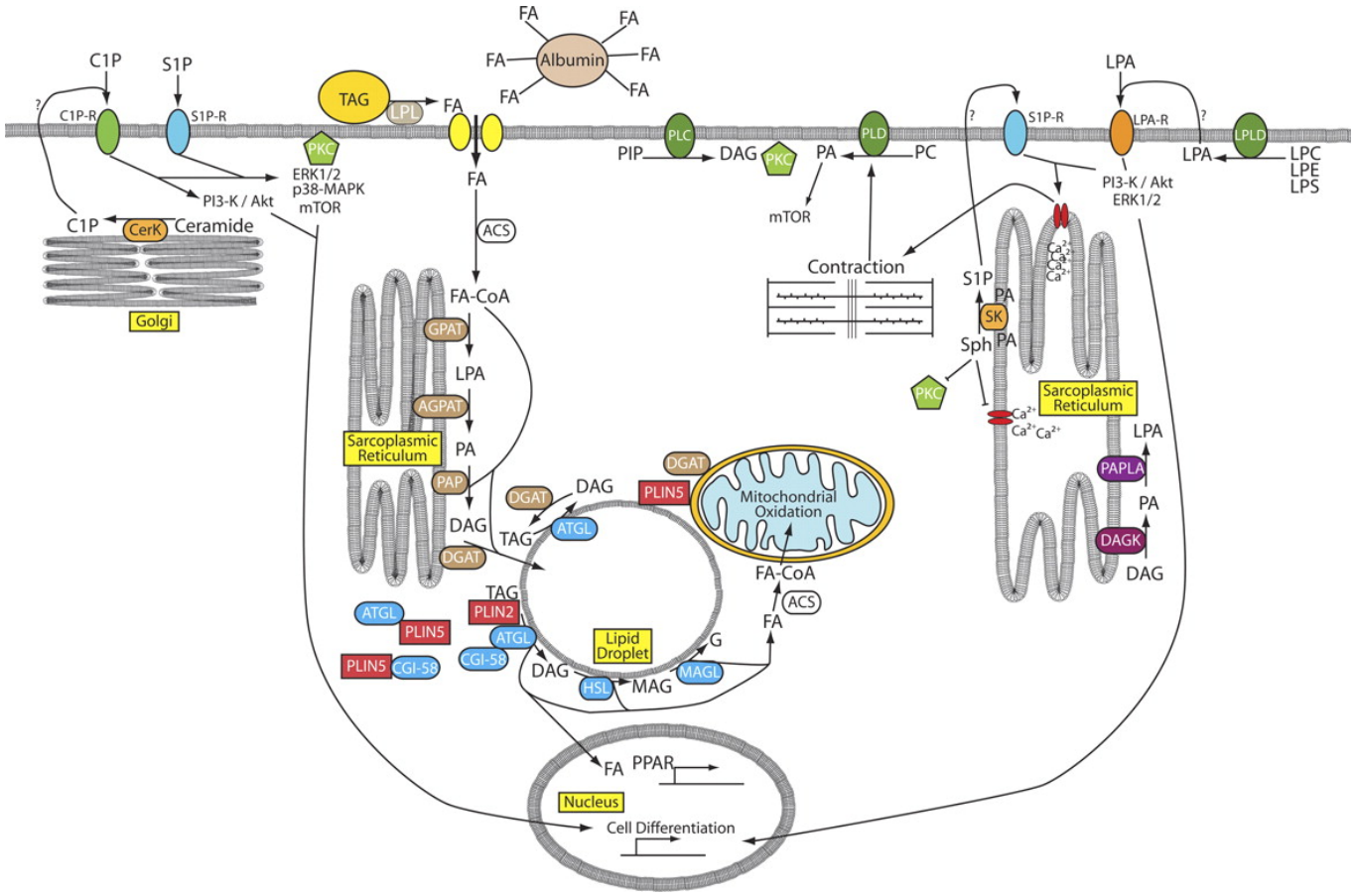

Figure 1. Lipid signaling.

Cell membranes serve as main sites for protein complex formation and networking [3]. Scheme shows the complexity of cellular signaling.

*Watt, M. J. and A. J. Hoy (2012). "Lipid metabolism in skeletal muscle: generation of adaptive and maladaptive intracellular signals for cellular function." American Journal of Physiology-Endocrinology and Metabolism **302**(11): E1315-E1328.*

initiated in response to diverse intracellular agonists such as hormones, neurotransmitters and growth factors. The location of generated DAG, its quantity and the duration of time before it gets converted to other lipids are important. It is vital for the specificity and affinity of downstream cellular processes; therefore, all the aforementioned parameters contribute to the regulation of cellular processes such as proliferation and cell growth.

DAG is a simple lipid characterized by a glycerol acyl chain in which two of hydroxyl groups are esterified with fatty acids (Figure 4,a). Mass spectral analyses of extracted mammalian plasma membranes demonstrated the coexistence up to 50 structurally distinct forms of DAG species that differ with respect to the length and the degree of unsaturation of their fatty acyl groups (Figure 4,b-d) [2, 14-16]. DAG derives from phospholipids, mainly phosphatidylinositol-4,5-bisphosphate (PI(4,5)P2) and phosphatidylcholine (PC), through the action of phospholipases. Since PI(4,5)P2, a main precursor of DAG, is mostly polyunsaturated (sn2 arachidonyl = 20:4), DAG produced by phosphoinositide-specific phospholipase C (PI-PLC) contains mainly polyunsaturated acyl chains (Figure 2). It is also known that DAG can be generated from PC through cooperative action of phospholipase D (PLD) and phosphatidic acid phosphohydrolase (PAP) at cellular surface compartments including endoplasmic reticulum (ER) and Golgi [14-17]. Since PC predominantly contains saturated (e.g., sn2 palmitoyl = 16:0) and monounsaturated (e.g., oleoyl = 18:1) acyl groups, these DAG's also have such acyl compositions [18]. In general, PI-PLC-mediated DAG production at the PM is rapid but transient, whereas DAG production by PLD and PAP at internal membranes is slower but sustained [14-17]. It has been shown that DAG's with polyunsaturated acyl chains produced by PI-PLC are more dominant in PKC activation than more saturated DAGs produced by

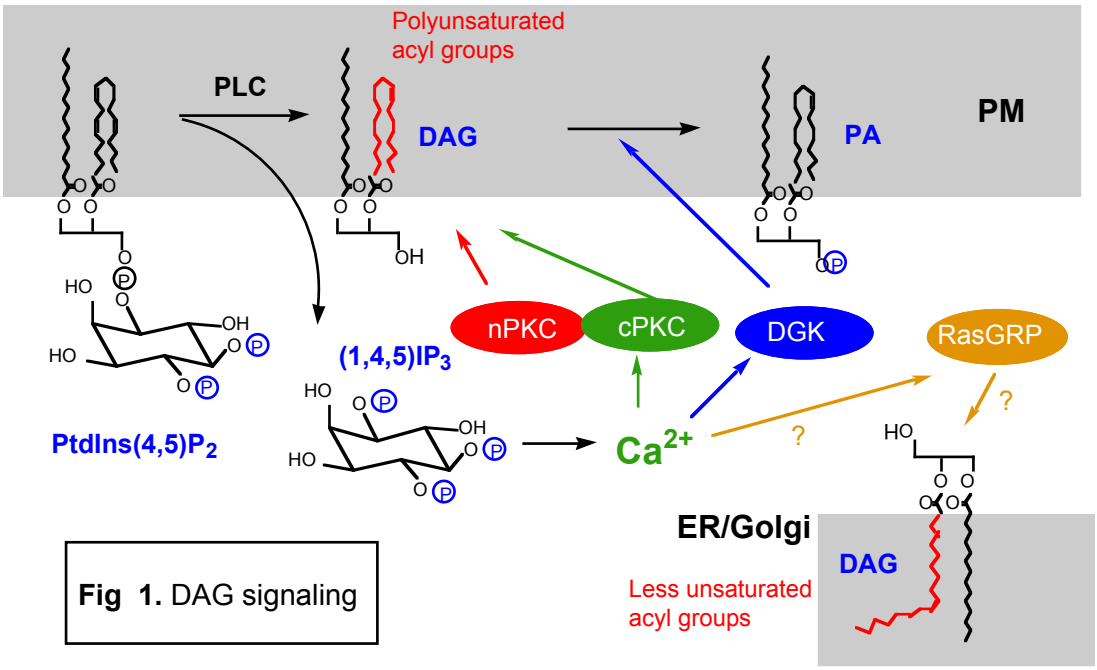

Figure 2. DAG signaling

Diacylglycerol (DAG) is an intermediate in GPCR signaling. It plays an important role as a secondary messenger as well as an activator of some proteins such as PKC and RasGRP. Recent studies shows that DAG with polyunsaturated acyl chains generated mainly by PI-PLC from PI(4,5)P2 are more effective in PKC activation than saturated forms produced by other signaling pathways.
Wonhwa Cho (2009). DAG signaling. NIH 2009 R01 GM. Studies of Diacylglycerol-Binding Proteins

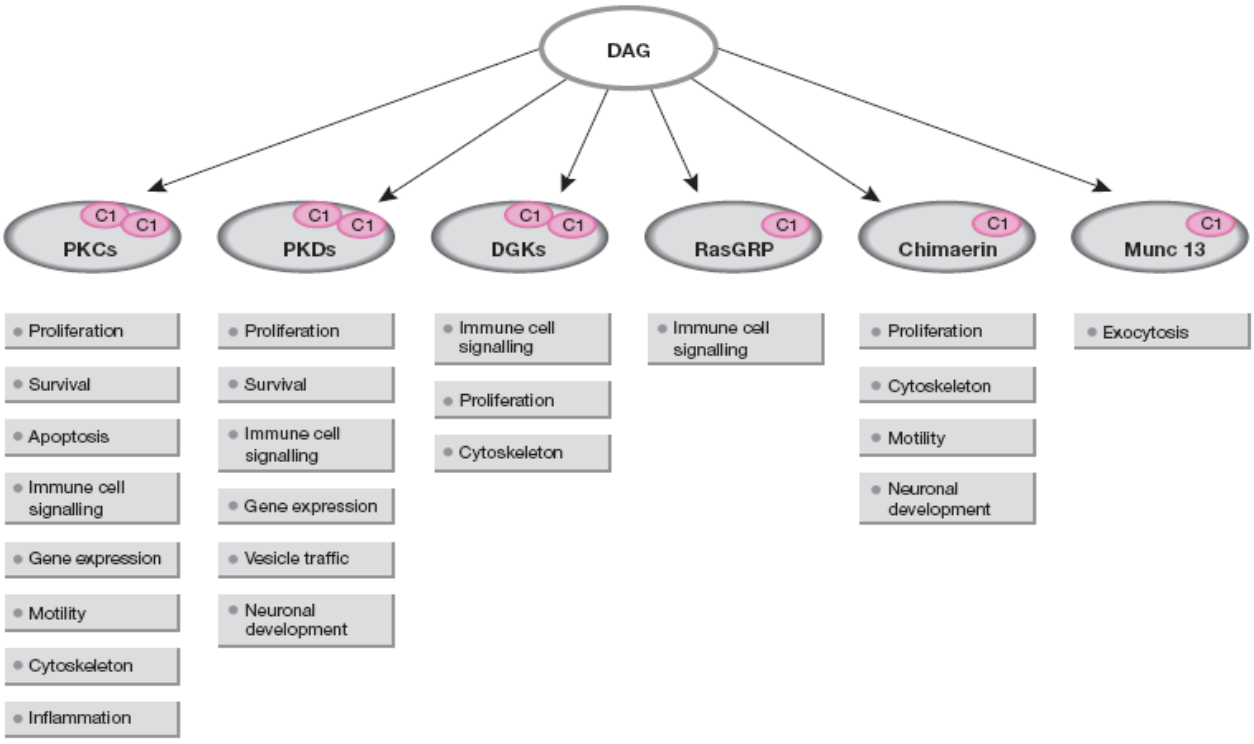

Figure 3. Transduction of diacylglycerol signaling

DAG as a second messenger is involved in various protein-lipid interactions that influence downstream of different signaling pathways and as a result effect processes such as proliferation, survival and immune cell signaling [19].
Alex Toker (2005). Several mechanisms for transducing the DAG signal. Meeting on Molecular Advances in Diacylglycerol Signalling. EMBO reports VOL 6 | NO 4 | 2005 meeting report 310

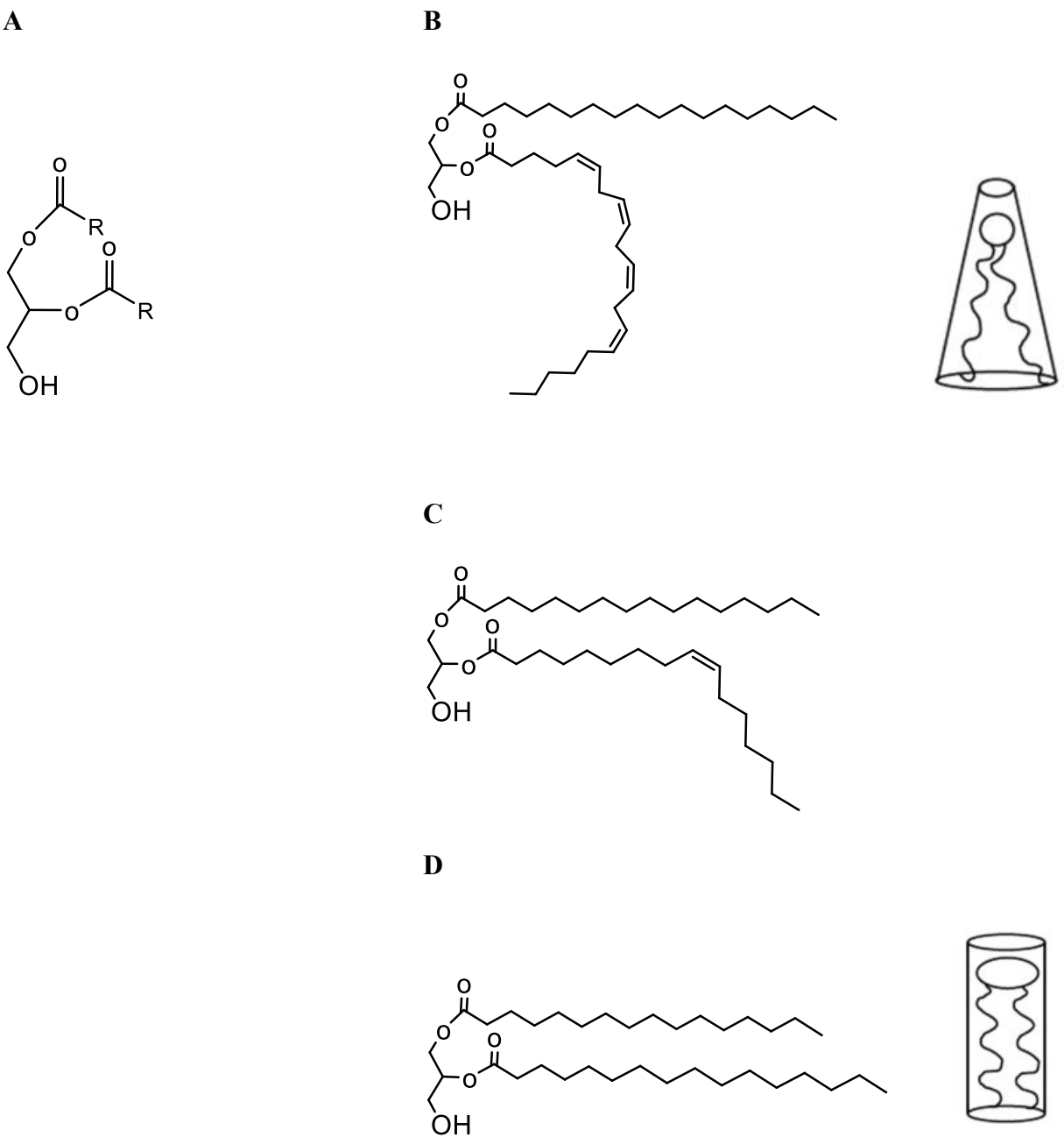

Figure 4. Structures of various diacylglycerols.

DAG is a simple lipid characterized by a glycerol backbone in which two of hydroxyl groups are esterified with fatty acids. (a) General structure consists of a glycerol molecule linked through ester bonds to two fatty acids, (b) structures of the polyunsaturated SAG, (c) saturated DPG, (d) POG. Note that the double bonds on aliphatic tail are in *cis* configuration.

other enzymatic pathways [20]. It is not known, however, whether this is due to the genuine selectivity of PKC C1 domains for DAG's with polyunsaturated acyl groups or due to the effect of these DAG's on the membrane structure. It is also unknown whether other DAG receptor proteins have similar DAG acyl group selectivity. The DAG acyl group selectivity of C1 domains was investigated in this work.

The DAG species produced from PC has distinct acyl chain compositions compared with the DAG produced from PI(4,5)P2 [21, 22]. When PC-PLC cleaves PC, the main product of the reaction is DAG with saturated acyl chain at *sn−2* position. In contrast, when PI-PLC cleaves PI(4,5)P2, produced DAG has polyunsaturated sn-2 acyl chain. In fact, the main form of DAG produced from PI(4,5)P2 is 1-stearoyl-2-arachidonoyl glycerol (SAG). The nature of the acyl chains on DAG determines its effectiveness in stimulating PKC [23, 24]. Sustained PKC activation has been shown to be oncogenic and contributes to malignant phenotypes seen in cancers [25, 26]. Only polyunsaturated DAG species were shown to be able to bind and activate PKC isoforms both *in vitro* and *in vivo* [21, 22, 27]. The relative activating ability of different DAG species is different for each PKC isoform [26], supporting the suggestion that the acyl chain of DAG influences its signaling properties. Other evidence of acyl chain specificity of DAG comes from recent studies of the activation of caged DAGs with different acyl chains [20]. Thus, the specific acyl chains are tied with signaling resulting from the PI cycle [26, 28].

1.2. C1 domain

C1 domains are approximately 50 amino acids long, enriched in cysteines structures composed of five short β strands, a short α-helix, and two zinc ions that are important for maintaining the domain folding (Figure 5) [29-33]. These domains are important in the recruitment of host proteins to the membrane. The C1 domain was originally known for its specific interaction with

DAG and phorbol ester in PKCs [34, 35]. Since then the C1 domain have been found in more than 50 different mammalian proteins from seven different classes (Figure 3) [13]. Three classes of these proteins, including PKCs, PKDs and DGKs, contain tandem C1 domains [19]. Although C1 domains exhibit a great degree of amino acid sequence homology (Figure 6) [36], small sequence differentiation in the ligand-binding pocket drastically influence the affinity for its binding partners. The X-ray structure of the PKCδ C1B domain-phorbol ester complex showed that main-chain groups (i.e., C=O and NH) in the shallow binding pocket form hydrogen bonds with the polar moieties of the phorbol ester [30]. C1 domains also have surface cationic residues that interact with the anionic membrane surface and aliphatic and aromatic residues surrounding the DAG binding pocket that are involved in partial membrane penetration. The membrane penetration is necessary for the C1 domain to interact with DAG molecules that are partially buried in the hydrophobic core of the membrane [31, 37].

1.3. C1 Domain-Containing DAG Receptor Proteins

1.3.1. PKCs

PKCs are a family of Ser/Thr kinases that mediate a wide variety of cellular processes [38, 39]. Based on structural variations in the N-terminal regulatory domain, PKCs are generally differentiated into three classes: classical PKCs (cPKC; α, β_I, β_{II}, and γ isoforms), novel PKCs (nPKC; δ, ε, η, and θ) and atypical PKCs (aPKC; ζ and λ/ι). The regulatory domains of both cPKC and nPKC contain two contiguous C1 domains (C1a and C1b). The difference is that cPKCs have a C2 domain that is responsible for Ca^{2+}-dependent membrane binding, whereas nPKCs contain a non-Ca^{2+}-binding C2 domain. Finally, the aPKC has only one C1 domain that does not bind DAG. Extensive biochemical studies have been performed to

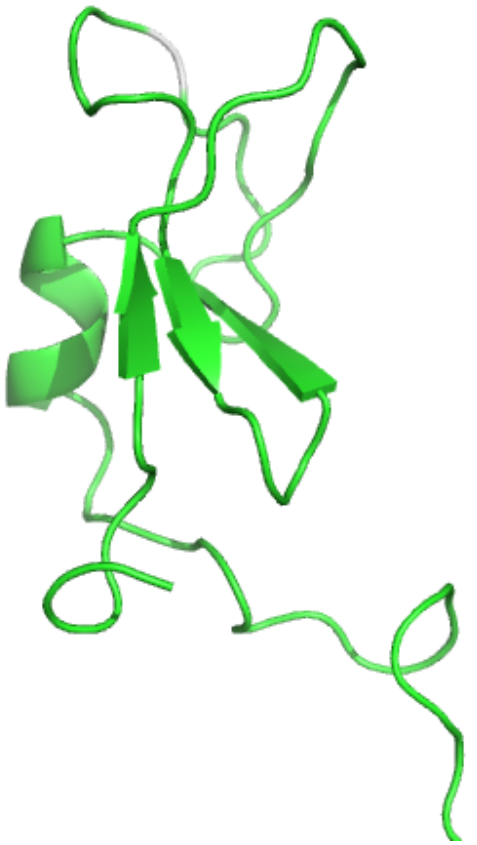

Figure 5. General Fold of the C1 Domain.

C1 domain is the cysteine-rich compact structure with five short β-strands and one short α-helix. Conserved histidines and cysteines are cordinated with two zinc ions into zinc-finger structure. *PDB 2E73*

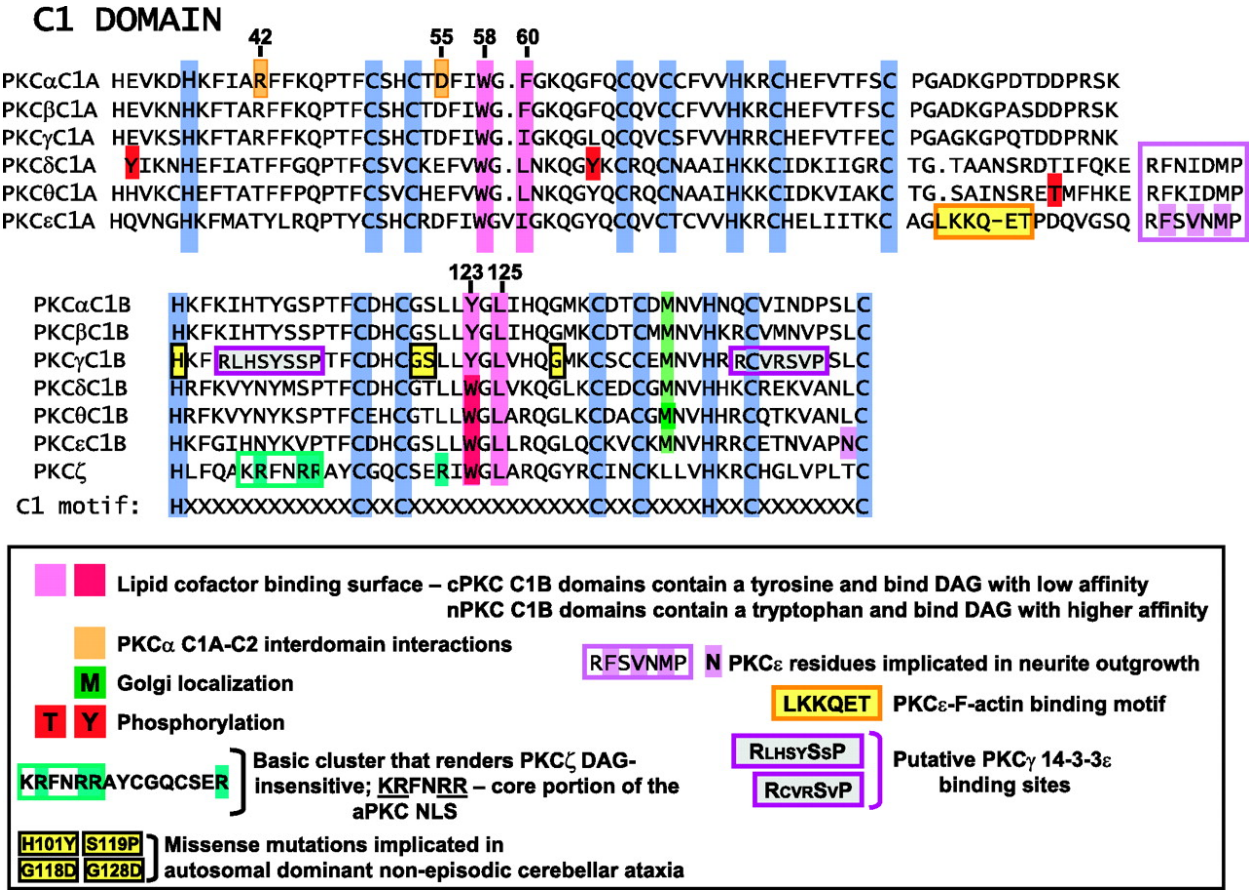

Figure 6. Amino acid sequence alignment of PKC C1 domains

Numbering is based on PKCα. Conserved histidines and cysteines are shown in blue. Other structural feature are indicated below the alignment [36].
Susan F. Steinberg (2008). Alignment of C1 domains. Structural Basis of Protein Kinase C Isoform Function. Physiological. V. 88 N. 4, 1341-1378. DOI: 10.1152/physrev.00034.2007

elucidate the roles of C1a, C1b, and C2 domains in membrane binding and activation of cPKC isoforms [40-42]. Recent studies on cPKCs showed that the C2 domain is responsible for initial Ca^{2+}-dependent electrostatic membrane binding via negatively charged PS and PI(4,5)P2 while the C1 domain is involved in membrane penetration and DAG binding which leads to conformational change of PKC and as a result its activation [37, 42, 43]. Numerous studies have indicated that C1a and C1b domains of PKCs have different ligand affinities [44-46] and distinct roles in PKC activation [45, 47].

PKCs activation contains multiple steps including PS/Ca^{2+} interaction (for cPKC), DAG binding, and phosphorylation. The translocation of PKC from the cytoplasm to the PM in response to receptor-mediated DAG production or exogenous addition of phorbol ester is a key step of PKC activation. However, recent studies using GFP-tagged PKC isoforms have illustrated that the subcellular localization and activation mechanism of PKC depends on isoform, activator, and cell type [48]. The observed complexity in PKC subcellular localization arises in part from the fact that exogenously added C1 domain ligands (phorbol ester in particular) can also move between cell membranes, depending on their hydrophobicity [49, 50]. Therefore, it is essential to determine the spatiotemporal dynamics of the C1 ligand, whether endogenously formed or exogenously added, to unambiguously elucidate the subcellular localization of PKC.

1.3.2. RasGRPs

The RasGRPs are activators of the small GTPase Ras. All RasGRPs contain a C1 domain and two EF hand motifs in the C-terminal regulatory domain [51]. Increasing number of research studies shows that RasGRPs control downstream of immune receptors in B and T cells [52-55]. Stimulation of these receptors results in PLC activation and DAG aggregation in membranes.

DAG affects RasGRPs through two mechanisms. First, the C1 domains of RasGRPs bind DAG [56, 57], as a result RasGRPs are recruited to cellular membranes [51]. Moreover, RasGRP1 and RasGRP3 can be activated through phosphorylation by PKCs [58]. Ras activation by RasGRP1 and RasGRP3 is important for cellular processes such as T cell activation and lymphocyte homeostasis [51, 52]. RasGRP4 also can interact with DAG and activates Ras [51], although regulation by PKC has not been documented [51]. Thus, it has been thought that RasGRP may act as a Ca^{2+} and DAG sensor, like cPKCs, that could link the increase in the intracellular Ca^{2+} and DAG concentration with Ras activation (Figure 2). However, the role of Ca^{2+} in RasGRP activation still remains controversial [59]. Recently, it has been reported that Ras proteins localized in Golgi and ER membranes can also play a signaling role, which is distinct from their signaling role in the PM [60]. This compartmentalized Ras signaling is particularly dominant in lymphocytes in which T cell receptor signaling seems to activate Ras only on the ER/Golgi, which is in turn mediated by RasGRP1 that translocates to the ER/Golgi in a DAG- and, arguably, Ca^{2+}-dependent manner [61]. It has been suggested that the C1 domain is mainly responsible for the ER/Golgi localization of RasGRP1 [61, 62], but the mechanism underlying this specific translocation remains controversial. For instance, a recent report suggested that the Golgi targeting of RasGRP1 is ascribed to the preference of its C1 domain for DAG with less unsaturated sn-2 acyl chains [62]. However, another study reported that RasGRP1 tightly bound to DAG with polyunsaturated sn-2 acyl chains [63]. We addressed this controversy by obtaining the information on this selectivity investigating the structural basis and cellular outcome of the acyl selectivity. Since only RasGRP1 can promote the activation of Ras in the ER/Golgi, it is imperative that the mechanism underlying the unique targeting of RasGRP1 to these membranes

can be elucidated in order to understand how compartmentalized Ras signaling works in T cells and other cells.

1.3.3. DGK

DGK converts DAG to PA and thereby down-regulates DAG signaling [64]. Up to the present, nine mammalian DGK isoforms have been identified [64]. All DGKs have tandem C1 domains (C1a and C1b) in the N-terminal regulatory part and a conserved catalytic domain in the C-terminal region. Type I DGKs (α, β, γ) contain a recoverin homology (RVH) domain and two EF-hand motifs at the N-terminus, which work in concert as a Ca^{2+} sensor. Among these DGKs, β and γ isoforms show significant binding to PDBu, while α isoform does not [65]. In agreement with this, DGKγ, but not DGKα, translocates from the cytoplasm to the PM in response to PDBu [66]. Since DAG is the substrate of DGK, the catalytic domains of all DGKs are expected to bind DAG with significant affinity; however, the DAG affinities of their C1 domains have not been reported so far.

1.4. The purpose of studying multiple DAG receptors and their C1 domains

Recent studies have shown that all of non-PKC DAG/phorbol ester receptors are involved in cellular signaling pathways that were believed to be controlled by PKCs [39, 67-74]. This functional variety between PKC and non-PKC DAG binding partners is in fact noticeable in the examination of RasGRP proteins. These proteins participate in cell proliferation, differentiation and transformation by controlling the Ras/Raf/MAP kinase signaling [75, 76]. Many studies contributed to confirmation of the crucial role of DAG regulation of non-PKC DAG receptors, demonstrating that DAG divergently and non-redundantly regulates different DAG receptors [67-71]. Therefore, it is important to characterize the *in vitro* and cellular DAG-mediated

membrane targeting of different DAG receptor proteins to fully understand the mechanisms by which DAG divergently regulates these proteins in various mammalian cells.

2. Experimental procedures

2.1 Materials

l-Palmitoyl-2-oleoyl-sn-glycero-3-phosphocholine (POPC), l-palmitoyl-2-oleoyl-sn-glycero-3-phosphoserine (POPS), 1-stearoyl-2-arachidonoyl-sn-glycerol (SAG, 18:0-20:4 DG), 1-palmitoyl-2-oleoyl-sn-glycerol (POG, 16:0-18:1 DG) and 1,2-dipalmitoyl-*sn*-glycerol (DPG, 16:0 DG) were purchased from Avanti Polar Lipids. Adenosine triphosphate and (ATP) was from Sigma Aldrich. The lipophilic membrane stains, DiI and DiO, were purchased from Life Technologies. Dabsyl-PE was synthesized by Matthew Connor from Dr. Daesung Lee's laboratory. Nikel-nitrilotriacetic acid (Ni-NTA) Aragose was purchased from Qiagen Inc. (Germany). The fluorescent labeled lipid, 4-difluoro-5,7-dimethyl-4-bora-3a,4a-diaza-s-indacene-3-propionyl)-1,2-dihexadecanoyl-sn-glycero-3-phospho-ethanolamine, triethylammonium salt (BODIPY–PE), was from Life Technologies. All other chemicals and reagents were of the highest grade and commercially available.

2.2. Vesicle preparation

Each lipid concentration was analyzed from molar percent composition. The lipids were dissolved in chloroform and aliquoted to a small glass container for a stock solution of 400 μg/mL. LUVs were prepared by drying the lipid mixture under steam of nitrogen gas, then redissolving in a TRIS/KCl buffer. The resuspended vesicles were vortex during 10 min, then sonicated for 1 min using a Branson 1200 sonifier. Then the vesicles were passed 15 times through 100 nm polycarbonates filter using a Liposofast microextruder (Avestin).

2.3. Protein expression and purification

The PCKγ C1b and PKCθ C1a+C1b were introduced in E.Coli expression vector pKTM through EcoRI/NotI digestive sites for former and NdeI/XhoI for last. The proteins were expressed as N-terminal poly-histidine tag (His-tag) and C-terminal EGFP tag fusion proteins and purified using the Ni-NTA-Tag™ resin as described [77]. The dissolved sample was quantified by Bradford assay.

For *in vivo* experiments the same single C1 domain from PCKγ and tandem C1a+C1b domain from PKCθ were inserted into the mammalian vector pEGFP-N1.

2.4. Hela and NIH 3T3 cell culture and transfection

Cells were maintained in high glucose Dulbecco's Modified Eagle Medium (DMEM, HyClone) supplemented with 10% fetal bovine serum (FBS, Invitrogen) and 2 mM glutamine (Sigma) at 37° C with 5% CO_2. Cells were transfected at 70-85% confluency with Lipofectamine 2000 (Invitrogen) in coverglass-bottom (Fisher) 8-well chamber (LabTek®). Transfections were carried out according to manufacturer's instructions. The cell medium was refreshed 4-5 h after transfection. Cells were incubated for another 24 h before experiments were performed.

2.5. Diacylglycerol delivery

Several different long chain types of DAG (SAG, POG and DPG) were used and these lipids were able to get incorporated into cellular membranes very well. Chloroform based stocks solutions of diacylglycerols were evaporated and resuspended in DMSO. The obtained solutions were diluted for addition to cells in PBS buffer so the added amount anywhere between 0.05 and 0.4 mg/mL DAG. This usually gives a final concentration of ~0.1-0.4% DMSO.

The cells also can be enriched with diacyglycerol using a small amount of DAG from chloroform stocks added directly to PBS. This method is more harmful to the cell because chloroform is more toxic than DMSO at the same concentration.

2.6. Förster resonance energy transfer (FRET)

FRET experiments were performed on F-4500 Fluorescence Spectrophotometer (Hitachi) using EGFP labeled protein as a donor of the fluorescence signal and PE-Bodipy as an acceptor. In order to excite the donor we applied excitation 390 nm and monitored the decrease of the donor signal at emission 510 nm by increasing the amount of vesicles in the system. Because EGFP signal drops with dilution the control experiment was done where buffer was added instead of lipid vesicles. That way the change of total volume was considered and data were recalculated with known dilution factor. The specific FRET signal was calculated using the following equation:

$$\Delta F/\Delta F_{\max} = [P]_b/[P]_0$$

$\Delta F/\Delta F_{max}$ is a fluorescence intensity decrease at a given lipid concentration divided by the maximal fluorescence decrease, $[P]_b$ is the concentration of a protein in its bound form and $[P]_o$ is total concentration of the protein. The fitting was performed by KaleidaGraph.

2.7. Quenching assay

All fluorescence quenching assay measurements were performed using FluoroLog3 spectrofluorometer (Horiba Scientific) at 25°C. Two milliliters of 20 mM Tris buffer, pH 7.4, containing 0.16 M KCl and 100 nM protein solution, were transferred to a quartz cuvette (Hellma Analytics), and the EGFP fluorescence was excited at 460 nm and its emission spectrum

was obtained. The change in emission intensity at 509 nm was detected after incremental addition of LUV solution and 1 min incubation [78]. Data analysis was done as described in [78].

2.8. Fluorescence correlation microscopy (FCS)

FCS assay was performed on a confocal system using a Zeiss LSM510 microscope. The signal I(t) produced by particles of fluorophore diffused through the detection volume. I(t) fluctuates around a mean value $I(t) = \langle I(t) \rangle + \delta I(t)$ [79-81] The autocorrelation function is described as $G(\tau) = \langle \delta I(t)\ \delta I(t(t+\tau) \rangle / \langle I(t) \rangle$ [82]. Due to Brownian motion of fluorescent molecules in a three dimensional Gaussian focus volume, the autocorrelation curve can be fit with the following equation whereby the concentration and the diffusion coefficient were extracted [83]:

$$G(\tau) = \frac{1}{N} \times g(\tau) = \frac{1}{N}\left(1 + \frac{T}{1-T} e^{-\tau/\tau_{Tr}}\right)\left(\frac{1}{1 + \tau/\tau_D}\right)\left(\frac{1}{1 + \tau/SS^2\tau_D}\right)^{\frac{1}{2}}$$

where N is the average number of particles of the fluorophore in the focal volume; τ_D is the correlation time of these molecules which represents their diffusion time, or the time that each molecule spends on average to pass through the laser focus volume. By definition, the correlation time is $\tau_D = \omega^2/4D$, where ω is the radius of the focus volume and D is the diffusion coefficient. The structural parameter S is the ratio of the radii of the laser beam focus in the axial and radial directions and is identified using 20 nM Fluorescein in 10 mM Tris-HCl buffer (pH 9.0) as a standard and found to be S = 4 with the focus volume 0.17 fl. triplet lifetime τ_{Tr} and the fraction of fluorescent molecules in the triplet state T are fitting parameters for the triplet characteristics in autocorrelation curves. All measurements and data analysis were performed using the SimFCS software (Laboratory for Fluorescence Dynamics, University of California Irvine).

2.9. Total internal reflection fluorescence (TIRF) microscopy

Supported lipid bilayer (SLB) was constructed as described elsewhere [84]. Single-molecule imaging of the studied proteins was performed *in vitro* (SLB) and *in vivo* applying a total internal reflection fluorescence (TIRF) system custom-built on our Olympus IX71 microscope as described formerly [85, 86]. While proteins were infused with EGFP label, SLB contained 3-5% red fluorescence dye (DiI) in order to detect the formation of the bilayer and efficiently separate the fluorescence lipid emission signal (red) from the protein signal (green). The cells expressing EGFP fusion constructs and E.Coli expressed fluorescence proteins were excited using 488 nm DPSS laser (Excelsior, Spectra-Physics), there DiI fluorescence was initiated by 561 nm DPSS laser (Excelsior, Spectra-Physics). The fluorescent signal of the sample was separated into two channels by passing it through emission filters (D630/30, Chroma and 510BP20, Omega) and detected by two EM-CCD cameras (Andor iXon 897) [86]. All single molecule tracking, data analysis and image processing were performed using an in-house written MATLAB program [86].

3. Results and Discussion

The membrane binding of lipid-dependent proteins, including PKCs is driven by combination of electrostatic and non-electrostatic interactions [87]. The membrane binding can be initiated by cationic interfacial binding residues, which mediate non-specific electrostatic interactions with anionic membranes and thereby accelerate the membrane association (Figure 7, k_a↑ effect) or by aromatic interfacial binding residues, Trp in particular, [88], that facilitate the membrane association through complex interactions with the membrane. Aromatic residues also slow the membrane dissociation (k_d↓ effect). Once membrane-associated, some proteins bind to a specific lipid (Figure 7), such as DAG and phosphoinositides, through lateral diffusion, whereas others undergo conformational changes to penetrate into the hydrophobic core of membranes (Figure 7), both of which slow the membrane dissociation (k_d↓ effect) and increase the membrane residence time. These processes are mutually exclusive because specific lipid binding often induces the membrane penetration of protein [89-91].

It was generally thought that specific localization of proteins would require protein-protein interactions. However, recent studies have suggested that high specificity and affinity can be attained through lipid-protein binding [1, 41, 92-94]. Hence, subcellular localization of proteins can be predicted by analyzing the kinetics of their binding to model membranes. The correlation k_a, k_d and K_d for *in vitro* vesicle binding of proteins with their cellular membrane translocation rates was observed. This indicates that the recruitment of proteins to the membrane can be quickly switched on and off by minor changes in kinetics as well as equilibrium parameters of interaction with membrane. Therefore, in this research we studied thermodynamics and kinetics of the binding of C1 domains to the membranes to extend our understanding about the mechanism of this process.

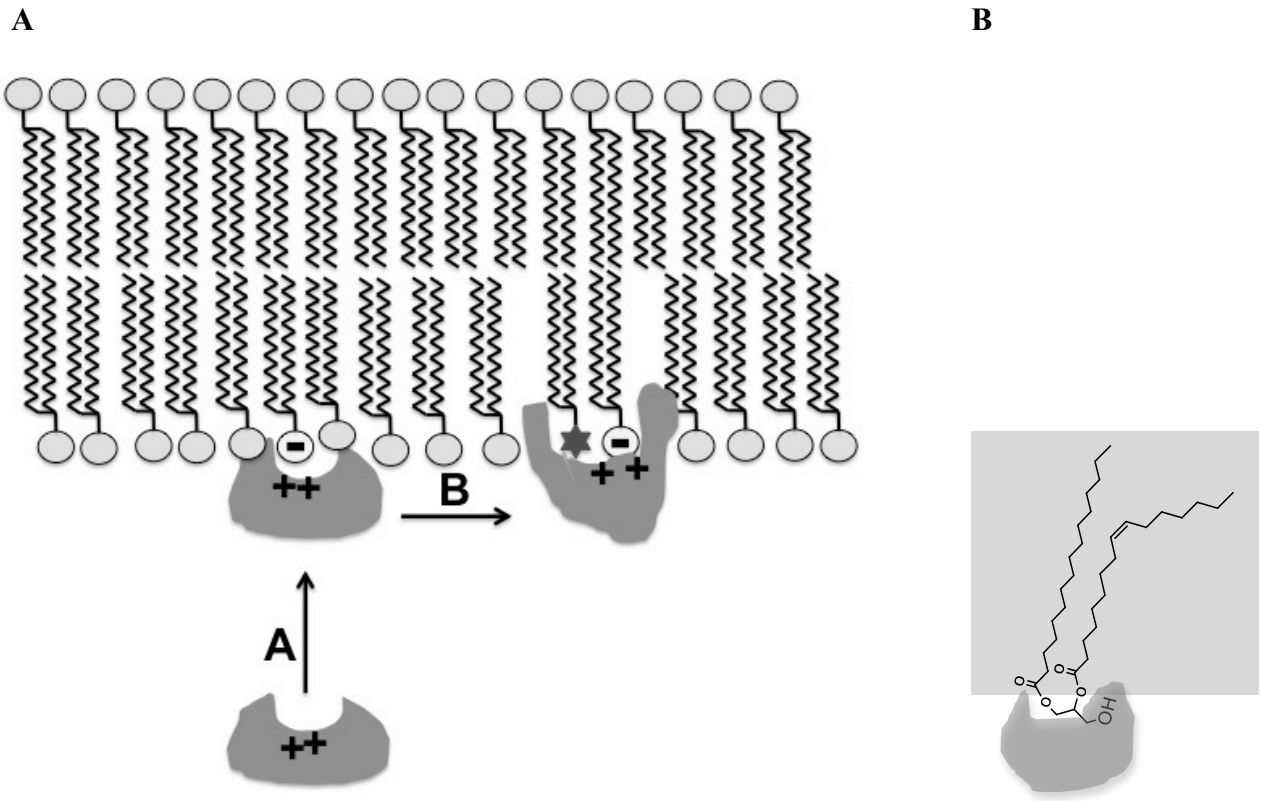

Figure 7. Binding of C1 domain to diacylglycerols

(a) The mechanism of the membrane binding: step A – electrostatic interaction, step B – hydrophobic interaction via membrane penetration and specific interaction via hydrogen bonding. (b) Cartoon of DAG-C1 domain binding.

3.1. Thermodynamics of C1 domain – DAG interactions

Based on direct correlation between size of the molecule and its diffusion coefficient, a free protein molecule moves significantly faster than the same molecule bound to a lipid vesicle. Using a fluorescently labeled protein we can detect the difference between free and bound fraction and moreover identify an exact ratio between these two. Figure 8 represents the principle of quantification of protein binding to lipid vesicles using FCS technique.

To determine the detection volume of the system we employed fluorescein with a known diffusion coefficient as a commonly used standard. Then we performed FCS measurements of free GFP-labeled C1 domain to determine its individual diffusion times. The curves for free C1 domain were fit according to [80], resulting in diffusion times of 200 μs for the protein. The curves were fit to single component equations indicating monodisperse solutions. We ran a binding assay keeping the concentration of the protein constant and increasing the amount of vesicles in a solution. To investigate the importance of degree of DAG unsaturation, we performed two sets of the experiment. In the first trial we constructed LUVs containing 5% of SAG (polyunsaturated acyl chain) and in the second trial we substituted it with saturated DPG. Figure 9 (a,b) shows the autocorrelation curves of GFP-labeled C1 domain with both free and LUV-bound. For the fitting of autocorrelation curves of solutions containing both free C1 domain and vesicle-bound C1 domain (Section 2.8), τ_{C1} was fixed to 200 μs and τ_{LUV} was enabled to float to result in the best possible fit. Fitting of this normalized autocorrelation curves (Figure 9) yields a fraction LUV-bound protein (Table S1). We found that the protein reached 100% saturation when we used LUVs containing SAG species, while we were not able to overcome 40% binding with LUVs containing DPG. We obtained binding curves (Figure 9, c)

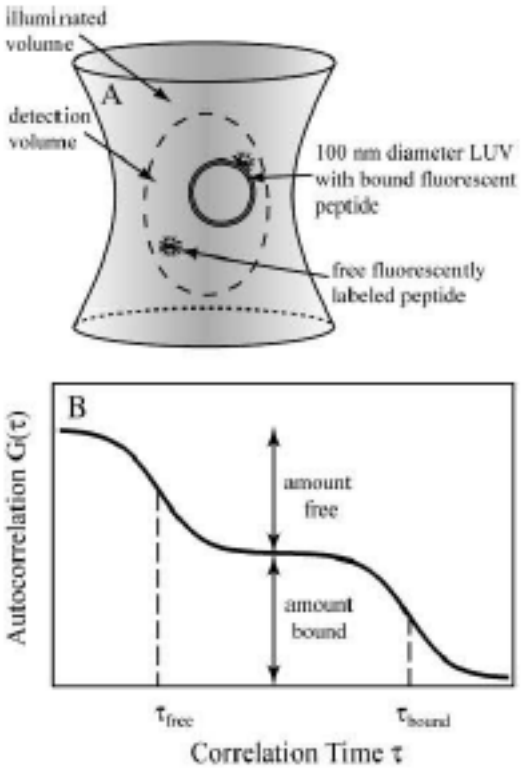

Figure 8. Determination of binding affinities of proteins for LUVs with FCS.

(a) Representation of the focal volume of the FCS microscope. A free EGFP-labeled protein and a lipid vesicle with 100 nm diameter, illustrated with a bound protein, moves through the detection volume, resulting in fluorescence intensity fluctuations. A free fluorophore molecule maintains the correlation time $\tau_{free} \approx 200$ µs, meanwhile the vesicle-bound protein holds a longer correlation time, $\tau_{bound} \approx 2$ ms because of the lower diffusion coefficient of the lipid-protein complex. With the protein concentration of 50 nM, the 0.3 fl detection volume contains roughly five free protein molecules. The focus volume of 350 nm diameter, vesicle 100 nm diameter, and protein size are shown to scale. (b) Graph of the idealized two-component autocorrelation function for $\tau_{free} << \tau_{bound}$. If the portions of free and bound fluorescent protein are equal, the molar partition coefficient, K = 1/[lipid]. The correlation times are illustrated with dashed lines. [83]

Rusu, L., A. Gambhir, S. McLaughlin and J. Radler (2004). "Fluorescence correlation spectroscopy studies of peptide and protein binding to phospholipid vesicles." Biophysical Journal 87(2): 1044-1053.

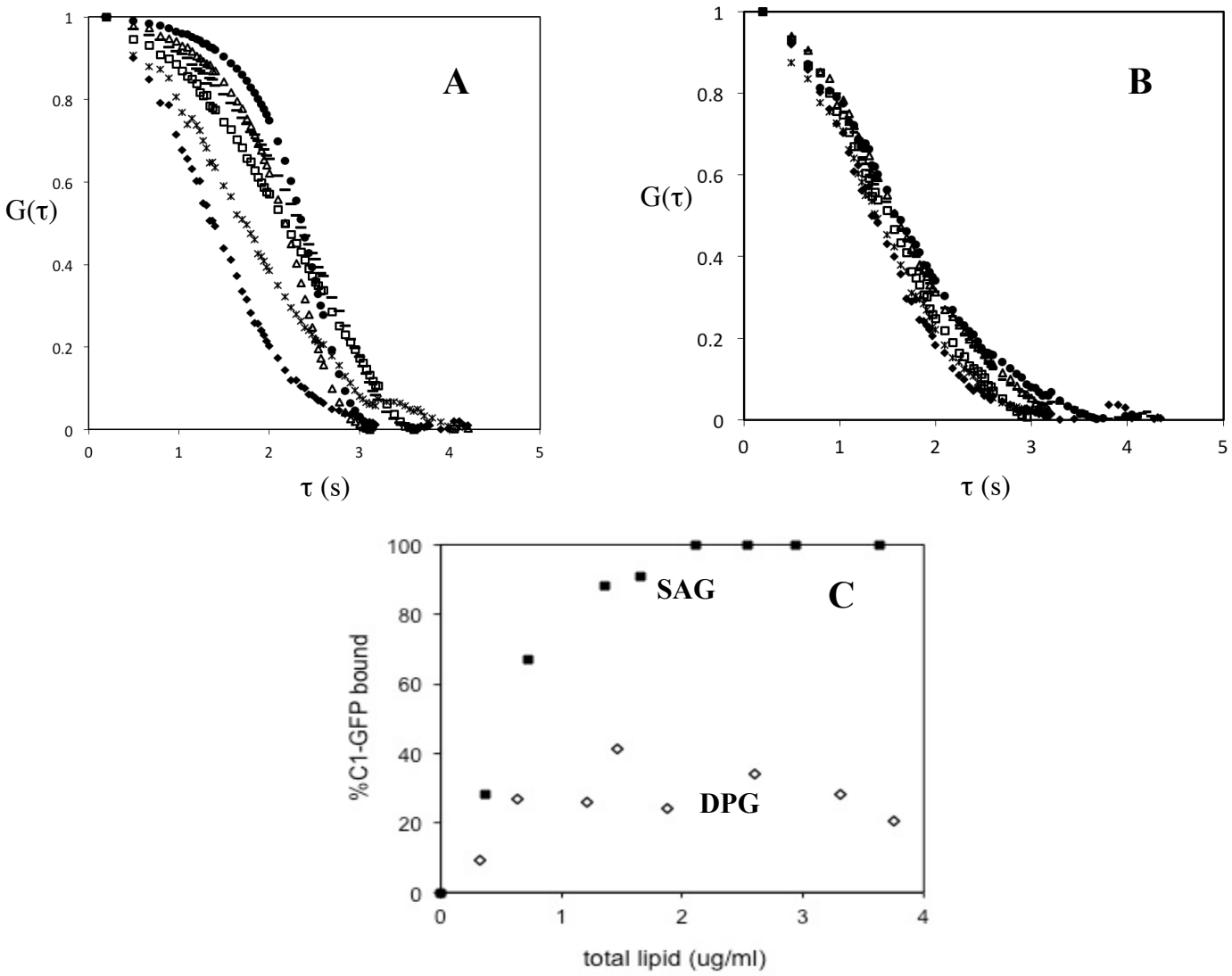

Figure 9. FCS measurements of PKC-C1-EGFP and LUV binding.

EGFP-tagged PKCgamma C1 domain (PKC-C1-EGFP) binding to PC/PC/DAG (75:20:5) LUVs. (a-b) Autocorrelation curves of PKC-C1-EGFP and LUVs, which have a diameter of 100 nm and contains polyunsaturated DAG (a) and saturated DAG (b). The diffusion coefficient for PKC-C1-EGFP was 65 mm^2/s. Auto-correlation curves obtained from a solution containing 25 nM PKC-C1_EGFP and different lipid concentrations are shown. Autocorrelation curves from left to right are shown for 0 to 5 mol.% of accessible lipid concentrations, corresponding to 0 % (◆), 25 % (×), 65 % (□), 80 % (Δ), 85 % (-) and 99 % (•) for SAG vesicles and 0 % (◆), 25 % (×), 30 % (□), 40 % (Δ), and 37 % (-) for DPG vesicles. The lines represent the best fit of two-component model. (c) FCS measurements of PKC-C1-EGFP binding to PC/PS/DAG and PC/PS LUVs. The percentage of PKC-C1-EGFP bound, deduced from data similar to those illustrated in Fig. 4(a-b) is plotted as a function of the accessible lipid concentration.

and calculated K_d values (Table 3). This result confirms the higher binding affinity of C1 domain for polyunsaturated DAG than saturated one.

To further investigate this tendency, we decided to apply FRET assay approach. Based on the principle of this method, we chose EGFP-labeled C1 domain (PKC-C1-EGFP) as a donor and Bodipy-labeled phosphoethanolamine (PE-Bodipy) as an acceptor for FRET pair. In this experiment we kept protein concentration constant and increased the amount of Bodipy-containing vesicles. FRET change can be detected by increase of an acceptor signal as well as the decrease of a donor signal. In EGFP-Bodipy pair, the donor has more drastic change than an acceptor; therefore, we were detecting the drop of the signal (Figure 10, a). To find the difference between SAG and DPG, we constructed vesicles containing PC/PS/DAG/PE-Bodipy in a mole ratio 70/20/5/5. The fluorescence decrease upon lipid addition was background corrected by the fluorescence decrease upon addition of the same volume of the buffer solution. $\Delta F/\Delta F_{max}$ was calculated as fluorescence intensity decrease at a given lipid concentration divided by the maximal fluorescence decrease (Figure 10, b). The binding isotherm was fit by nonlinear least-squares analysis using the method described in [78]. Relative K_d values are summarized in Table 1. Using this fluorescence assay we determined that C1 domain showed at least 3 times higher affinity for polyunsaturated diacylglycerol than saturated one.

With development of a new quenching-based assay in our laboratory we were able to test C1-DAG binding. Even though we confirmed our hypothesis using two completely different approaches (FCS and FRET), the novel quenching assay could further support our data. In this assay the same principle of FRET was utilized, however, instead of an acceptor of the signal (Bodipy-PE) we used a quencher of the fluorescence signal dabsyl-PE (Figure 11). Again we

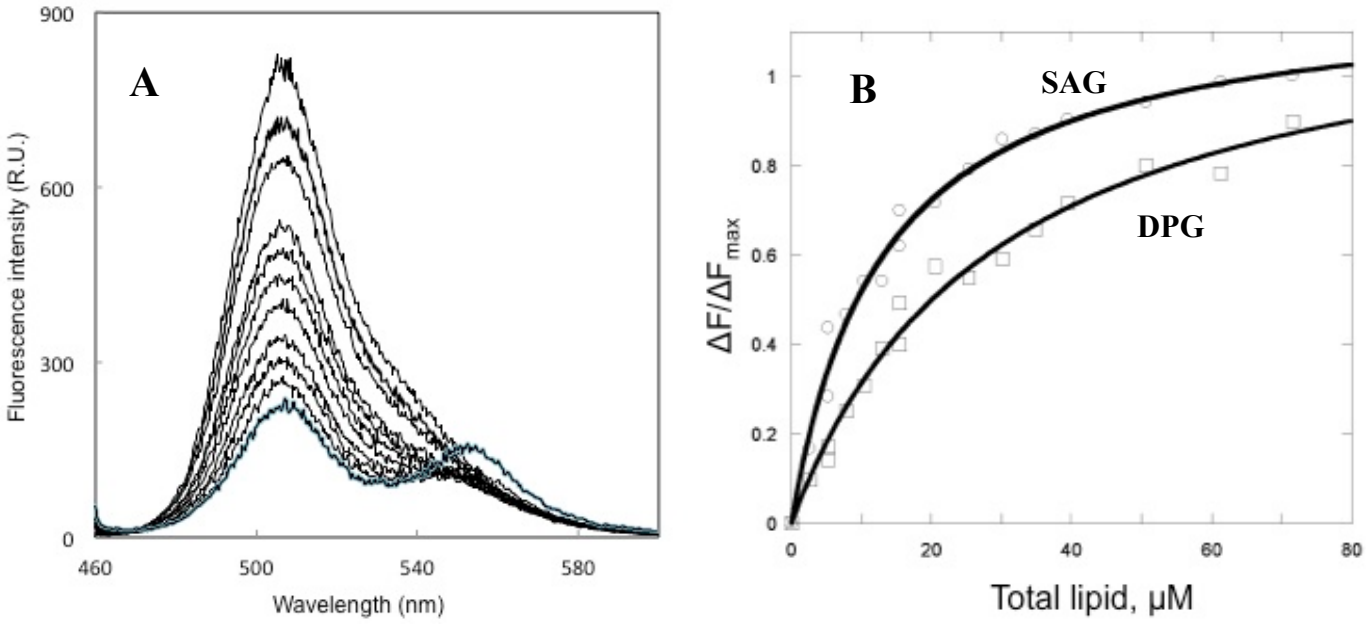

Figure 10. FRET measurements of PKC-C1-EGFP and LUV binding

Titration monitored by FRET between C-terminal EGFP-tagged PKC C1 domain (PKC-C1-EGFP) and a Bodipy-labeled LUVs. (a): Fluorescence spectra of PKC-C1-EGFP (100 nM) upon addition of Bodipy-containing vesicles (POPC/POPS/DAG/Bodipy 70:20:5:5) in buffer solution (pH = 7.40 50 mM TRIS, 160 mM KCl) with an excitation of 450 nm and emission 510 nm. Measurements were performed by the cuvette-based assay. The total lipid concentrations used were 0, 1.5, 3.0, 4.5, 6.0, 7.5, 9.0, 11.5, and 13.0 μM from top to bottom. (b): Binding isotherms of PKC-C1-EGFP with vesicles containing various DAGs, i.e., POPC/POPS/DAG/Bodiby (70:20:5:5) vesicles where DAG includes SAG and DPG. POPC/POPS/Bodipy (75:20:5) vesicles were also tested as a negative control. The fluorescence decrease upon lipid addition was background corrected by the fluorescence decrease upon addition of the same volume of the buffer solution. $\Delta F/\Delta F_{max}$ was calculated as fluorescence intensity decrease at a given lipid concentration divided by the maximal fluorescence decrease. The binding isotherm for POPC/POPS/dabsyl-PE/DAG (70:20:5:5) vesicles was fit by nonlinear least-squares analysis [78]. K_d values are summarized in Table 1.

detected the decrease of EGFP signal. Fluorescence emission signal intensity was normalized against the EGFP intensity value at 509 nm without lipid vesicles added. The fluorescence decrease upon lipid addition was background corrected by the fluorescence decrease upon addition of the same volume of the buffer solution. $\Delta F/\Delta F_{max}$ was calculated as fluorescence intensity decrease at a given lipid concentration divided by the maximal fluorescence decrease (Figure 12). The binding isotherm for POPC/POPS/dabsyl-PE/DAG (70:20:5:5) vesicles was fit by the same nonlinear least-squares analysis as we applied for FRET calculations. Values of relative K_d are summarized in Table 1.

Results from all three methods reflected the same conclusion showing higher binding affinity of C1 domain to the unsaturated DAG in comparison to saturated lipid. We proved that the binding affinity of C1 domain depends on degree of unsaturation of DAG molecule. At this stage we looked into addressing the question of what is the role of this affinity difference in the cell signaling and what is the role of each of these species. Next, we investigated the kinetics of C1-DAG interactions using the single molecule tracking technique.

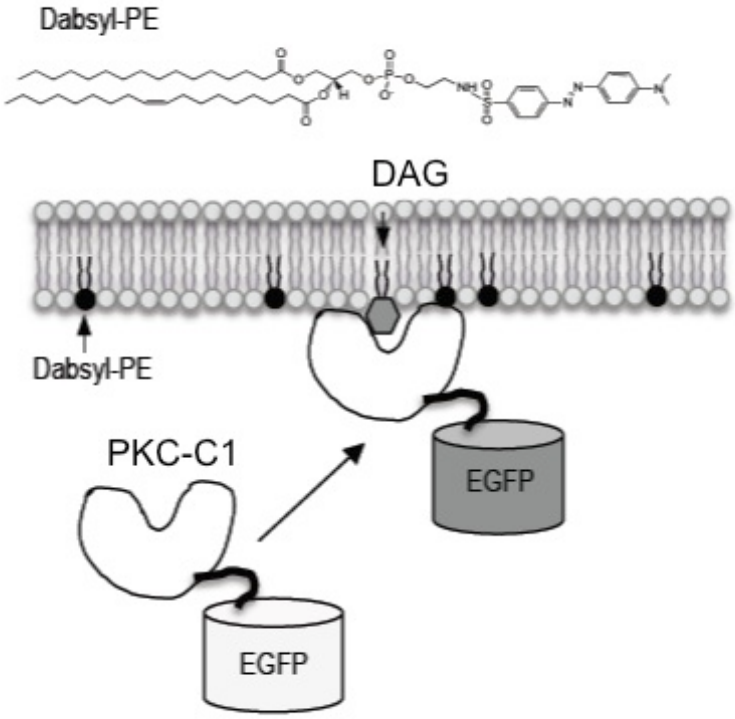

Figure 11. The strategy of a fluorescence quenching-based membrane-binding assay.

Vesicles containing the lipid of interest (DAG) and a dark quencher, dabsyl-PE, are added to the solution of EGFP-labeled protein (PKC-C1-EGFP). As the protein binds the lipid vesicle, the fluorescence emission intensity of EGFP is greatly reduced due to quenching effect of a dark quencher. This allows quantification of membrane-protein interaction.
Modified from Kim, H., H. S. Afsari and W. Cho (2013). "High-throughput fluorescence assay for membrane-protein interaction." Journal of Lipid Research 54(12): 3531-3538.

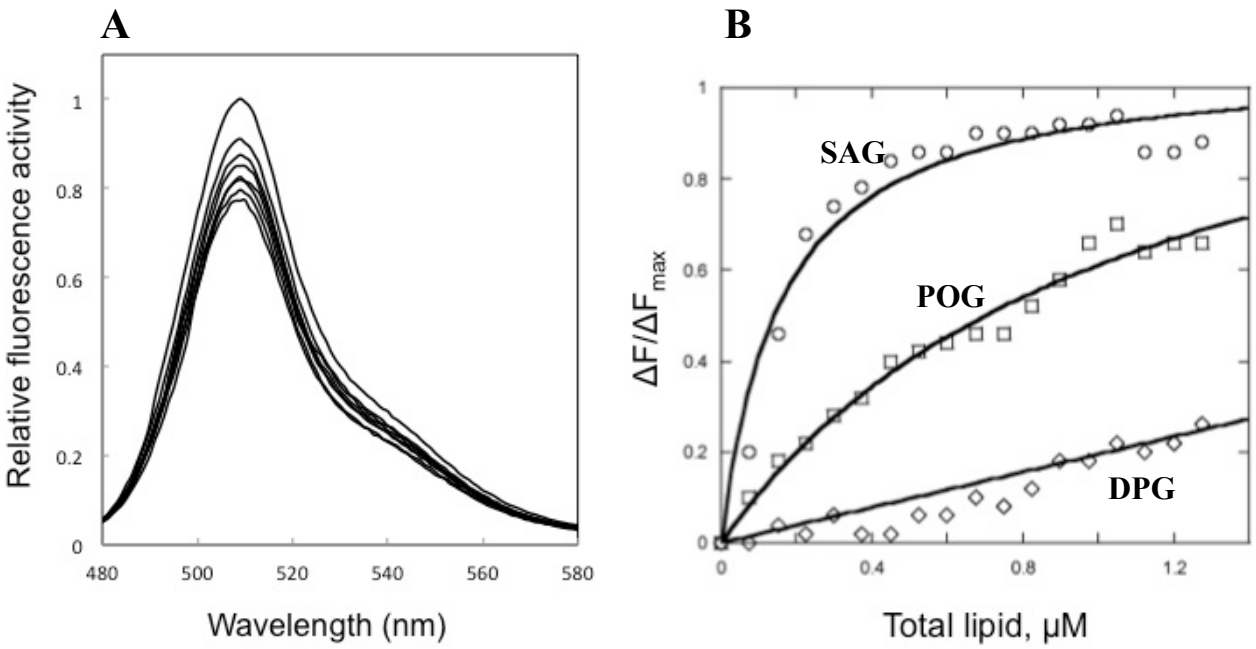

Figure 12. Fluorescence quenching of PKC-C1-EGFP by dabsyl-PE-containing vesicles

(a) Fluorescence emission spectra of GFP-tagged PKCgamma C1 domain (PKC-C1-EGFP) (100 nM) in the presence of increasing concentration of POPC/POPS/PE-dabsyl/DAG (70:20:5:5) vesicles were measured using the cuvette-based assay [78]. The total lipid concentrations used were 0, 1.5, 3.0, 4.5, 6.0, 7.5, 9.0, 11.5, and 13.0 μM from top to bottom. Fluorescence emission signal intensity was normalized against the EGFP intensity value at 509 nm without lipid vesicles added. (b) Binding isotherms of PKC-C1-EGFP with vesicles containing various DAGs, i.e., POPC/POPS/dabsyl-PE/DAG (70:20:5:5) vesicles. DAG includes SAG, POG and DPG. POPC/POPS/dabsyl-PE (75:20:5) vesicles were also tested as a negative control. The fluorescence decrease upon lipid addition was background corrected by the fluorescence decrease upon addition of the same volume of the buffer solution. $\Delta F/\Delta F_{max}$ was calculated as fluorescence intensity decrease at a given lipid concentration divided by the maximal fluorescence decrease. The binding isotherm for POPC/POPS/dabsyl-PE/DAG (70:20:5:5) vesicles was fit using data analysis described in [78]. Relative K_d*'s* are summarized in Table 1.

Table 1. Comparison of relative dissociation constants (K_d) for membrane binding of C1 domain obtained by the three different fluorescence assays

Diacylglycerol	Method		
	FCS	FRET	Quenching
SAG	1	1	1
DPG	3.0 ± 0.5	2.6 ± 0.7	2.7 ± 0.4

3.2. Kinetics of C1 domain – DAG binding

In order to investigate the binding and unbinding of individual C1 domains to membranes, we decided to use a supported lipid bilayer (SLB) as a standard membrane model of *in vitro* studies. SLB is widely implemented as biomimetic membrane systems due to eliminated cellular complexity [84, 95]. Because lipids retain their lateral motion in such a system, this synthetic bilayer supplies the sufficient PM environment that is essential for preserving the membrane binding of investigated biomolecules. Generating the bilayer on a surface of the cover slip allowed us to perform single molecule tracking using a custom built TIRF system. To ensure a proper bilayer formation, we added a small amount (3-5% of a total) of a lipophilic membrane stain, DiI, to a lipid mixture, which enabled observation of uniformity of SLBs. Because of its spectral properties (red excitation/emission spectra 553/570 nm maxima), the DiI fluorescence signal is well separated from the EGFP signal permitting simultaneous imaging of both dyes. Therefore, we expressed EGFP-tagged single and tandem C1 domains from the bacterial expression vector to perform this experiment. Interaction of C1 domain with the DAG-containing bilayer was monitored at high temporal resolution (13 ms/frame). Single molecule tracking analysis was performed from the images using our in-house algorithm. First we identified the positions of fluorescent proteins in each frame using the Gaussian intensity distribution as estimate of point spread function of the fluorescent signal. Then determined positions in each frame of the processed image of acquired movies were used to reconstruct the trajectories of individual protein molecules. We applied obtained trajectories for determining the diffusion coefficients as a main indicator of the C1 domain diffusion behavior. Furthermore, we examined how lipid composition of SLB affects the C1 domain binding process.

In order to understand how the membrane composition (the degree of unsaturation of DAG, in particular) modulates the residence time of C1 domain on the model membrane, we calculated the dissociation rate constant, k_{off}, from defined trajectories. By definition the dissociation rate constant corresponds to $\ln(2)/t_{1/2}$ (half-life of reaction). The dissociation rate constant, together with the association rate constant (k_{on}), determines the protein's membrane binding affinity. Previous studies on other peripheral proteins, such as the ENTH domain indicated that k_{off} is a more factor in determining the cell signaling activity of proteins than k_{on} because the former determined their residence time in the membrane for signal transduction activity. We thus hypothesized that in case of the C1 domain k_{off} is also a critical parameter for its cell signaling activities [84, 96-98].

Single molecule measurement is the most rigorous technique to determine the dissociation rate constant of membrane-bound proteins because it eliminates the need to synchronize the dissociation of multiple molecules for accurate dissociation measurements. We built a histogram as a dependency of a number of molecules from the residence time using the experimentally obtained distribution of residence times. In order to find the dissociation rate constant, k_{off}, as well as the time needed for a half of molecule population to dissociate, $t_{1/2}$, we applied the exponential fit of the first order reaction (Figure 13). The dissociation rate constant can be calculated from this fit as $A = A_o\, e^{(-t/koff)}$. To have a better reflection of real kinetic properties of the C1 domain, we eliminated the first frame, which greatly reduced the noise as well nonspecific binding signals. Using this technique, we determined the dependence of the C1 domain dissociation rate constant on the SLB containing various DAG. As shown in Figure 13, the C1 domain k_{off} is increased with the increasing degree of DAG unsaturation. The dissociation rate constant for SAG and DPG containing supported bilayers was measured to be 3.5 ± 0.8 and

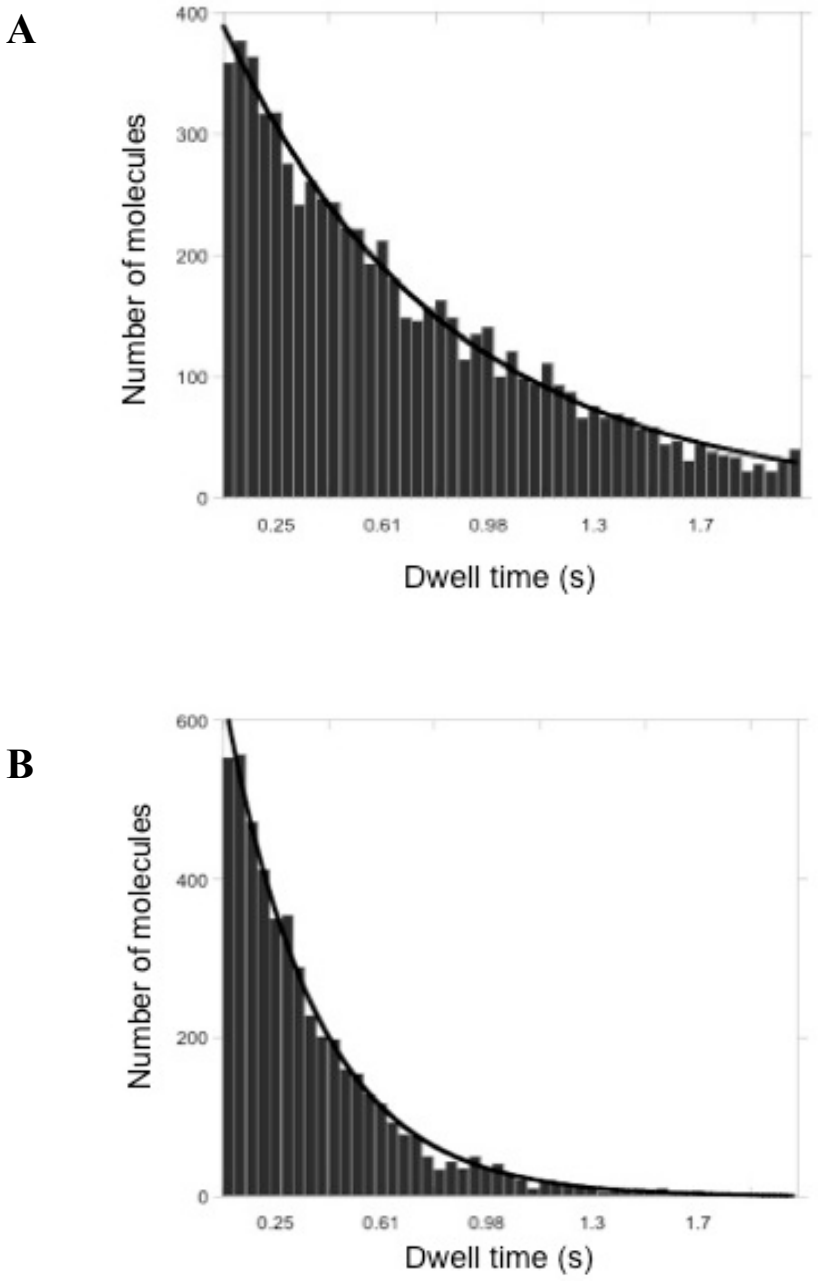

Figure 13. Single molecule tracking of EGFP-tagged PKCϴ C1a+C1b domain in vitro

A single-exponential fit to the distribution of PKC-C1-EGFP residence times. The resulting k_{off} values are 3.5 ± 0.8 and 1.2 ± 0.5 s^{-1} for SAG (a) and DPG-containing (b) SLB, respectively. In this example, the SLB composition is 72 mol % POPC, 20 mol % POPS, 3 mol % DiI and 5 mol % DAG, the buffer is 20 mM TRIS, 150 mM KCl, pH 7.4, and the EGFP-labeled PKCϴ C1a+C1b domain in bulk solution has the concentration of 50 nM.

$1.2 \pm 0.5\ s^{-1}$, respectively. This result supports our hypothesis that in comparison tosaturated DAGs the C1 domain possesses a stronger affinity to polyunsaturated DAGs and at the same time dissociates quicker from them. These membrane binding properties would allow C1 domain-containing signaling proteins to bind (i.e., the association rate constant is almost ten times higher for SAG than for DPG) and unbind the membrane faster, thereby securing fast and tightly controlled signaling processes.

The C1 domain possesses a stronger affinity to polyunsaturated DAGs and at the same time dissociates quicker from them. These membrane binding properties would allow C1 domain-containing signaling proteins to bind (i.e., the association rate constant is almost ten times higher for SAG than for DPG) and unbind the membrane faster, thereby securing fast and tightly controlled signaling processes.

To test the physiological significance our *in vitro* results, we chose Hela cells as a model system for *in vivo* application. Cells were transfected with full length PKCΘ and treated with 100 μM ATP. We followed the same single molecule tracking procedure as in supported lipid bilayer experiments. It has been reported [42, 99, 100] that the binding of full length PKC is a complex process that involves several crucial steps of binding. In order to simplify the system and isolate the interaction of our interest we decided to move to a single and tandem C1 domain. This could help to eliminate involvement of electrostatic binding between C2 domain and PS lipid as well as conformational changes and pseudosubstrate binding. PI-PLC can be activated by ATP treatment of the cell; this activation initiates production of DAG on a plasma membrane (PM). Using this approach we performed a single particle measurements before and after addition of ATP. It has been published previously [26, 36, 101] that the main downstream

product of PI(4,5)P2 is polyunsaturated SAG. As shown on Figure 14 the dissociation rate constant is $3.7 \pm 0.6\ s^{-1}$, which aligns with results for a supported lipid bilayer.

To confirm the obtained result, we performed an additional experiment. Taking under the consideration the fact that DAG has a small head group and therefore flip-flops freely between inner and outer PM, we used the enrichment technique where DAG was dissolved in a mixture TRIS buffer and small quantities of DMSO and then added to the cells. Originally, we carried out this procedure using chloroform instead of DMSO, which resulted in a high toxicity and quick cell death. To keep the experimental conditions closer to physiological, chloroform was substituted by DMSO for all DAG enrichment tests. We were able to detect attraction of the C1 domain to PM by this procedure. Significant interactions of the C1 domain with PM over several tens of milliseconds were detectable, resulting in a measured dissociation rate constant of $3.3 \pm 0.4\ s^{-1}$ (Figure 15). Therefore, these experiments clearly demonstrate that the C1 domain interaction with DAG enriched membranes has a clear correlation with *in vitro* studies. As it was mentioned recently in literature [99, 100], with improved CCD camera resolution details of specific and nonspecific interactions of this binding process could be further investigated in order to identify mechanisms of acceleration of membrane proteins targeting to their binding partners.

Our combined results demonstrate (Table 3) that DAGs with polyunsaturated acyl chain and saturated ones have clearly distinguishable binding properties. Not only the former have a higher affinity to the binding partner C1 domain, they also undergo faster dissociation process. Hence, the rate of association is almost ten times higher for SAG than for DPG.

It has been proved that various lipids including phosphoinositides play an important role in cell signaling. The question whether the fatty acid composition has crucial role remains open. Further investigations are required address this important issue.

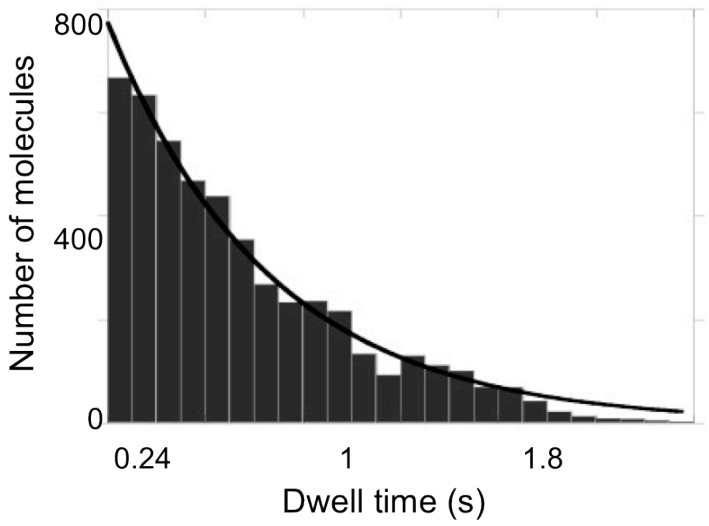

Figure 14. Single molecule tracking of EGFP-tagged PKCΘ C1a+C1b domain *in vivo* after DAG enrichment

A single-exponential fit to the distribution of PKC-C1-EGFP residence times. The resulting k_{off} value is $3.7 \pm 0.6\ s^{-1}$ for SAG-enriched Hela cell. In this example, the cells were pretreated with DAG dissolved in 20 mM TRIS, 160 mM KCl, pH 7.4 solution in presence of small amounts of DMSO. The cell were transfected EGFP-labeled PKCθ C1a+C1b mammalian expression vector at least 24 hours prior the experiment.

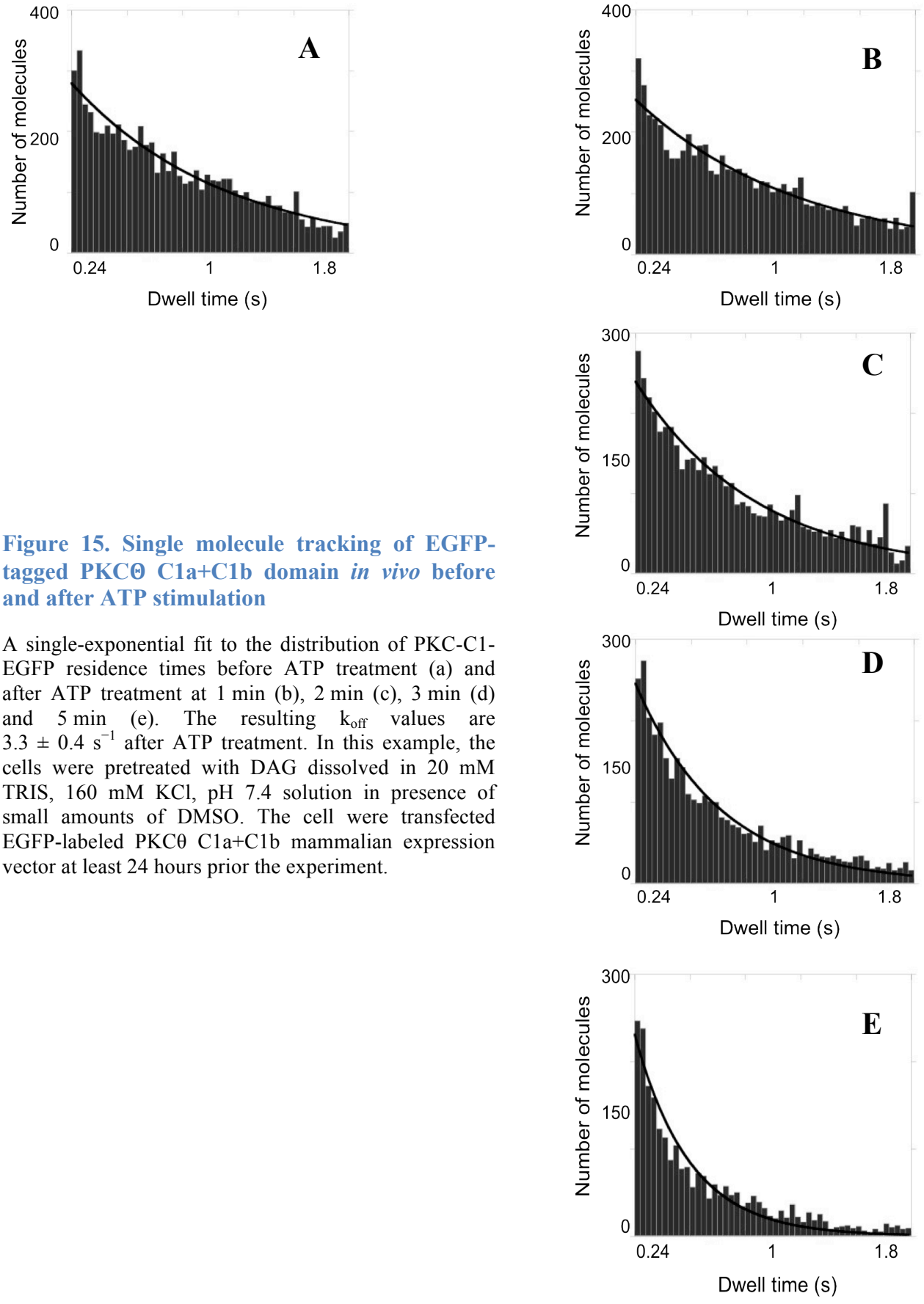

Figure 15. Single molecule tracking of EGFP-tagged PKCΘ C1a+C1b domain *in vivo* before and after ATP stimulation

A single-exponential fit to the distribution of PKC-C1-EGFP residence times before ATP treatment (a) and after ATP treatment at 1 min (b), 2 min (c), 3 min (d) and 5 min (e). The resulting k_{off} values are 3.3 ± 0.4 s^{-1} after ATP treatment. In this example, the cells were pretreated with DAG dissolved in 20 mM TRIS, 160 mM KCl, pH 7.4 solution in presence of small amounts of DMSO. The cell were transfected EGFP-labeled PKCθ C1a+C1b mammalian expression vector at least 24 hours prior the experiment.

Table 2. Comparison of binding properties (relative values for K_d, k_{on} and k_{off}) of C1 domain for polyunsaturated and saturated DAGs

Diacylglycerol	K_d	k_{off}	k_{on}	k_{on}(SAG)/k_{on}(DPG)
SAG	1	3	3	9
DPG	3	1	0.3	1

4. Cited literature

1. Bhattacharyya, R.P., et al., *Domains, motifs, and scaffolds: The role of modular interactions in the evolution and wiring of cell signaling circuits*, in *Annual Review of Biochemistry*. 2006. p. 655-680.
2. Quehenberger, O., et al., *Lipidomics reveals a remarkable diversity of lipids in human plasma.* Journal of Lipid Research, 2010. **51**(11): p. 3299-3305.
3. Watt, M.J. and A.J. Hoy, *Lipid metabolism in skeletal muscle: generation of adaptive and maladaptive intracellular signals for cellular function.* American Journal of Physiology-Endocrinology and Metabolism, 2012. **302**(11): p. E1315-E1328.
4. Sampaio, J.L., et al., *Membrane lipidome of an epithelial cell line.* Proceedings of the National Academy of Sciences of the United States of America, 2011. **108**(5): p. 1903-1907.
5. Quann, E.J., et al., *Localized diacylglycerol drives the polarization of the microtubule-organizing center in T cells.* Nature Immunology, 2009. **10**(6): p. 627-U96.
6. Subramanian, D., et al., *Activation of membrane-permeant caged PtdIns(3)P induces endosomal fusion in cells.* Nature Chemical Biology, 2010. **6**(5): p. 324-326.
7. Yoon, Y., et al., *In situ quantitative imaging of cellular lipids using molecular sensors.* Nature Chemistry, 2011. **3**(11): p. 868-874.
8. Ananthanarayanan, B., et al., *Activation mechanisms of conventional protein kinase C isoforms are determined by the ligand affinity and conformational flexibility of their C1 domains.* Journal of Biological Chemistry, 2003. **278**(47): p. 46886-46894.
9. Carrasco, S. and I. Merida, *Diacylglycerol, when simplicity becomes complex.* Trends in Biochemical Sciences, 2007. **32**(1): p. 27-36.
10. Oda, K., et al., *A comprehensive pathway map of epidermal growth factor receptor signaling.* Molecular Systems Biology, 2005. **1**.
11. Giorgione, J., et al., *Contribution of the C1A and C1B domains to the membrane interaction of protein kinase C.* Biochemistry, 2003. **42**(38): p. 11194-11202.
12. Newton, A.C., *Protein kinase C: poised to signal.* American Journal of Physiology-Endocrinology and Metabolism, 2010. **298**(3): p. E395-E402.
13. Brose, N. and C. Rosenmund, *Move over protein kinase C, you've got company: Alternative cellular effectors of diacylglycerol and phorbol esters.* Journal of Cell Science, 2002. **115**(23): p. 4399-4411.
14. Wakelam, M.J., *Diacylglycerol--when is it an intracellular messenger?* Biochim Biophys Acta, 1998. **1436**(1-2): p. 117-26.
15. Hodgkin, M.N., et al., *Diacylglycerols and phosphatidates: which molecular species are intracellular messengers?* Trends Biochem Sci, 1998. **23**(6): p. 200-4.
16. Goni, F.M. and A. Alonso, *Structure and functional properties of diacylglycerols in membranes.* Prog Lipid Res, 1999. **38**(1): p. 1-48.
17. Pagano, R.E., *What is the fate of diacylglycerol produced at the Golgi apparatus?* Trends Biochem Sci, 1988. **13**(6): p. 202-5.
18. Pettitt, T.R., et al., *Diacylglycerol and phosphatidate generated by phospholipases C and D, respectively, have distinct fatty acid compositions and functions. Phospholipase D-derived diacylglycerol does not activate protein kinase C in porcine aortic endothelial cells.* J Biol Chem, 1997. **272**(28): p. 17354-9.

19. Toker, A., *The biology and biochemistry of diacylglycerol signalling - Meeting on molecular advances in diacylglycerol signalling.* Embo Reports, 2005. **6**(4): p. 310-314.
20. Nadler, A., et al., *The Fatty Acid Composition of Diacylglycerols Determines Local Signaling Patterns.* Angewandte Chemie-International Edition, 2013. **52**(24): p. 6330-6334.
21. Pettitt, T.R. and M.J.O. Wakelam, *Diacylglycerol kinase epsilon, but not zeta selectively removes polyunsaturated diacylglycerol, inducing altered protein kinase C distribution in vivo.* Journal of Biological Chemistry, 1999. **274**(51): p. 36181-36186.
22. Madani, S., et al., *Implication of acyl chain of diacylglycerols in activation of different isoforms of protein kinase C.* Faseb Journal, 2001. **15**(14): p. 2595-2601.
23. Marignani, P.A., R.M. Epand, and R.J. Sebaldt, *Acyl chain dependence of diacylglycerol activation of protein kinase C activity in vitro.* Biochemical and Biophysical Research Communications, 1996. **225**(2): p. 469-473.
24. Torrecillas, A., et al., *Activation of protein kinase C alpha by lipid mixtures containing different proportions of diacylglycerols.* Biochemistry, 2001. **40**(49): p. 15038-15046.
25. Koivunen, J., V. Aaltonen, and J. Peltonen, *Protein kinase C (PKC) family in cancer progression.* Cancer Letters, 2006. **235**(1): p. 1-10.
26. D'Souza, K. and R.M. Epand, *Enrichment of phosphatidylinositols with specific acyl chains.* Biochimica Et Biophysica Acta-Biomembranes, 2014. **1838**(6): p. 1501-1508.
27. Pettitt, T.R., et al., *Diacylglycerol and phosphatidate generated by phospholipases C and D, respectively, have distinct fatty acid compositions and functions - Phospholipase D-derived diacylglycerol does not activate protein kinase C in porcine aortic endothelial cells.* Journal of Biological Chemistry, 1997. **272**(28): p. 17354-17359.
28. D'Souza, K. and R.M. Epand, *Catalytic Activity and Acyl-Chain Selectivity of Diacylglycerol Kinase epsilon Are Modulated by Residues in and near the Lipoxygenase-Like Motif.* Journal of Molecular Biology, 2012. **416**(5): p. 619-628.
29. Hommel, U., M. Zurini, and M. Luyten, *SOLUTION STRUCTURE OF A CYSTEINE-RICH DOMAIN OF RAT PROTEIN-KINASE-C.* Nature Structural Biology, 1994. **1**(6): p. 383-387.
30. Zhang, G.G., et al., *CRYSTAL-STRUCTURE OF THE CYS2 ACTIVATOR-BINDING DOMAIN OF PROTEIN-KINASE C-DELTA IN COMPLEX WITH PHORBOL ESTER.* Cell, 1995. **81**(6): p. 917-924.
31. Xu, R.X., et al., *NMR structure of a protein kinase C-gamma phorbol-binding domain and study of protein-lipid micelle interactions.* Biochemistry, 1997. **36**(35): p. 10709-10717.
32. Zhou, M., et al., *Solution structure and functional analysis of the cysteine-rich C1 domain of kinase suppressor of Ras (KSR).* Journal of Molecular Biology, 2002. **315**(3): p. 435-446.
33. Shen, N., O. Guryev, and J. Rizo, *Intramolecular occlusion of the diacylglycerol-binding site in the C-1 domain of munc13-1.* Biochemistry, 2005. **44**(4): p. 1089-1096.
34. Kazanietz, M.G., et al., *ZINC-FINGER DOMAINS AND PHORBOL ESTER PHARMACOPHORE - ANALYSIS OF BINDING TO MUTATED FORM OF PROTEIN KINASE-C-TAU AND THE VAV AND C-RAF PROTOONCOGENE PRODUCTS.* Journal of Biological Chemistry, 1994. **269**(15): p. 11590-11594.

35. Zhao, F., et al., *Are Zinc-Finger Domains of Protein Kinase C Dynamic Structures That Unfold by Lipid or Redox Activation?* Antioxidants & Redox Signaling, 2011. **14**(5): p. 757-766.
36. Steinberg, S.F., *Structural basis of protein kinase C isoform function.* Physiological Reviews, 2008. **88**(4): p. 1341-1378.
37. Medkova, M. and W.H. Cho, *Interplay of C1 and C2 domains of protein kinase C-alpha in its membrane binding and activation.* Journal of Biological Chemistry, 1999. **274**(28): p. 19852-19861.
38. Mellor, H. and P.J. Parker, *The extended protein kinase C superfamily.* Biochemical Journal, 1998. **332**: p. 281-292.
39. Linch, M., et al., *Functional implications of assigned, assumed and assembled PKC structures.* Biochemical Society Transactions, 2014. **42**: p. 35-41.
40. Mamidi, N., et al., *Synthesis and protein kinase C (PKC)-C1 domain binding properties of diacyltetrol based anionic lipids.* Molecular Biosystems, 2014. **10**(11): p. 3002-3013.
41. Kashiwagi, K., et al., *Importance of C1B domain for lipid messenger-induced targeting of protein kinase C.* Journal of Biological Chemistry, 2002. **277**(20): p. 18037-18045.
42. Ziemba, B.P., et al., *Single-Molecule Studies Reveal a Hidden Key Step in the Activation Mechanism of Membrane-Bound Protein Kinase C-alpha.* Biochemistry, 2014. **53**(10): p. 1697-1713.
43. Nalefski, E.A. and A.C. Newton, *Membrane binding kinetics of protein kinase C beta II mediated by the C2 domain.* Biochemistry, 2001. **40**(44): p. 13216-13229.
44. Irie, K., et al., *Comparison of chemical characteristics of the first and the second cysteine-rich domains of protein kinase C gamma.* Bioorganic & Medicinal Chemistry, 1997. **5**(8): p. 1725-1737.
45. Irie, K., et al., *Molecular basis for protein kinase C isozyme-selective binding: The synthesis, folding, and phorbol ester binding of the cysteine-rich domains of all protein kinase C isozymes.* Journal of the American Chemical Society, 1998. **120**(36): p. 9159-9167.
46. Irie, K. and H. Ohigashi, *Synthesis and functional analysis of the cysteine-rich domains of protein kinase C (PKC) for development of new medicinal leads with PKC isozyme and C1 domain selectivity.* Journal of Synthetic Organic Chemistry Japan, 2002. **60**(6): p. 563-572.
47. Szallasi, Z., et al., *Non-equivalent roles for the first and second zinc fingers of protein kinase C delta - Effect of their mutation on phorbol ester-induced translocation in NIH 3T3 cells.* Journal of Biological Chemistry, 1996. **271**(31): p. 18299-18301.
48. Shirai, Y. and N. Saito, *Activation mechanisms of protein kinase C: maturation, catalytic activation, and targeting.* J Biochem (Tokyo), 2002. **132**(5): p. 663-8.
49. Wang, Q.J., et al., *Differential localization of protein kinase C delta by phorbol esters and related compounds using a fusion protein with green fluorescent protein.* J Biol Chem, 1999. **274**(52): p. 37233-9.
50. Wang, Q.J., et al., *The lipophilicity of phorbol esters as a critical factor in determining the pattern of translocation of protein kinase C delta fused to green fluorescent protein.* J Biol Chem, 2000. **275**(16): p. 12136-46.
51. Song, X., et al., *RasGRPs Are Targets of the Anti-Cancer Agent Ingenol-3-Angelate.* Plos One, 2013. **8**(8).

52. Stone, J.C., *Regulation and Function of the RasGRP Family of Ras Activators in Blood Cells.* Genes & cancer, 2011. **2**(3): p. 320-34.
53. Botelho, R.J., et al., *Localized Diacylglycerol-dependent Stimulation of Ras and Rap1 during Phagocytosis.* Journal of Biological Chemistry, 2009. **284**(42): p. 28522-28532.
54. Qu, H.Q., et al., *Association of RASGRP1 with type 1 diabetes is revealed by combined follow-up of two genome-wide studies.* Journal of Medical Genetics, 2009. **46**(8): p. 553-554.
55. Zha, Y., et al., *T cell anergy is reversed by active Ras and is regulated by diacylglycerol kinase-alpha.* Nature Immunology, 2006. **7**(11): p. 1166-1173.
56. Carrasco, S. and I. Merida, *Diacylglycerol-dependent binding recruits PKC theta and RasGRP1 C1 domains to specific subcellular localizations in living T lymphocytes.* Molecular Biology of the Cell, 2004. **15**(6): p. 2932-2942.
57. Tognon, C.E., et al., *Regulation of RasGRP via a phorbol ester-responsive C1 domain.* Molecular and Cellular Biology, 1998. **18**(12): p. 6995-7008.
58. Roose, J.P., et al., *A diacylglycerol-protein kinase C-RasGRP1 pathway directs Ras activation upon antigen receptor stimulation of T cells.* Molecular and Cellular Biology, 2005. **25**(11): p. 4426-4441.
59. Tognon, C.E., et al., *Regulation of RasGRP via a phorbol ester-responsive C1 domain.* Mol Cell Biol, 1998. **18**(12): p. 6995-7008.
60. Chiu, V.K., et al., *Ras signalling on the endoplasmic reticulum and the Golgi.* Nat Cell Biol, 2002. **4**(5): p. 343-50.
61. Bivona, T.G., et al., *Phospholipase Cgamma activates Ras on the Golgi apparatus by means of RasGRP1.* Nature, 2003. **424**(6949): p. 694-8.
62. Carrasco, S. and I. Merida, *Diacylglycerol-dependent binding recruits PKCtheta and RasGRP1 C1 domains to specific subcellular localizations in living T lymphocytes.* Mol Biol Cell, 2004. **15**(6): p. 2932-42.
63. Madani, S., et al., *Diacylglycerols containing Omega 3 and Omega 6 fatty acids bind to RasGRP and modulate MAP kinase activation.* J Biol Chem, 2004. **279**(2): p. 1176-83.
64. Kanoh, H., K. Yamada, and F. Sakane, *Diacylglycerol kinases: emerging downstream regulators in cell signaling systems.* J Biochem (Tokyo), 2002. **131**(5): p. 629-33.
65. Shindo, M., et al., *Synthesis and phorbol ester binding of the cysteine-rich domains of diacylglycerol kinase (DGK) isozymes. DGKgamma and DGKbeta are new targets of tumor-promoting phorbol esters.* J Biol Chem, 2003. **278**(20): p. 18448-54.
66. Shirai, Y., et al., *Subtype-specific translocation of diacylglycerol kinase alpha and gamma and its correlation with protein kinase C.* J Biol Chem, 2000. **275**(32): p. 24760-6.
67. Ron, D. and M.G. Kazanietz, *New insights into the regulation of protein kinase C and novel phorbol ester receptors.* Faseb J, 1999. **13**(13): p. 1658-76.
68. Kazanietz, M.G., *Novel "nonkinase" phorbol ester receptors: the C1 domain connection.* Mol Pharmacol, 2002. **61**(4): p. 759-67.
69. Brose, N. and C. Rosenmund, *Move over protein kinase C, you've got company: alternative cellular effectors of diacylglycerol and phorbol esters.* J Cell Sci, 2002. **115**(Pt 23): p. 4399-411.
70. Yang, C. and M.G. Kazanietz, *Divergence and complexities in DAG signaling: looking beyond PKC.* Trends Pharmacol Sci, 2003. **24**(11): p. 602-8.

71. Brose, N., A. Betz, and H. Wegmeyer, *Divergent and convergent signaling by the diacylglycerol second messenger pathway in mammals.* Curr Opin Neurobiol, 2004. **14**(3): p. 328-40.
72. Clarke, M., et al., *Curvature recognition and force generation in phagocytosis.* Bmc Biology, 2010. **8**.
73. Egea-Jimenez, A.L., S. Corbalan-Garcia, and J.C. Gomez-Fernandez, *The C1B domains of novel PKCepsilon and PKCeta have a higher membrane binding affinity than those of the also novel PKCdelta and PKCtheta.* Biochimica et biophysica acta, 2014. **1838**(7): p. 1898-909.
74. Stahelin, R.V., *Ready, set, go! How protein kinase C manages dynamic signaling.* Chem Biol, 2014. **21**(4): p. 433-4.
75. Dower, N.A., et al., *RasGRP is essential for mouse thymocyte differentiation and TCR signaling.* Nat Immunol, 2000. **1**(4): p. 317-21.
76. Jones, D.R., et al., *T lymphocyte nuclear diacylglycerol is derived from both de novo synthesis and phosphoinositide hydrolysis.* Int J Biochem Cell Biol, 2002. **34**(2): p. 158-68.
77. Stahelin, R.V., et al., *Contrasting membrane interaction mechanisms of AP180 N-terminal homology (ANTH) and epsin N-terminal homology (ENTH) domains.* Journal of Biological Chemistry, 2003. **278**(31): p. 28993-28999.
78. Kim, H., H.S. Afsari, and W. Cho, *High-throughput fluorescence assay for membrane-protein interaction.* Journal of Lipid Research, 2013. **54**(12): p. 3531-3538.
79. Blin, G., et al., *Quantitative analysis of the binding of ezrin to large unilamellar vesicles containing phosphatidylinositol 4,5 bisphosphate.* Biophysical Journal, 2008. **94**(3): p. 1021-1033.
80. Rhoades, E., et al., *Quantification of alpha-synuclein binding to lipid vesicles using fluorescence correlation spectroscopy.* Biophysical Journal, 2006. **90**(12): p. 4692-4700.
81. Melo, A.M., A. Coutinho, and M. Prieto, *Quantifying Protein Binding to Lipid Vesicles Using Fluorescence Correlation Spectroscopy (FCS).* Biophysical Journal, 2011. **100**(3): p. 509-509.
82. Daniels, C.R., et al., *Fluorescence correlation spectroscopy study of protein transport and dynamic interactions with clustered-charge peptide adsorbents.* Journal of Molecular Recognition, 2012. **25**(8): p. 435-442.
83. Rusu, L., et al., *Fluorescence correlation spectroscopy studies of peptide and protein binding to phospholipid vesicles.* Biophysical Journal, 2004. **87**(2): p. 1044-1053.
84. Rozovsky, S., et al., *Single Molecule Kinetics of ENTH Binding to Lipid Membranes.* Journal of Physical Chemistry B, 2012. **116**(17): p. 5122-5131.
85. Sheng, R., et al., *Cholesterol modulates cell signaling and protein networking by specifically interacting with PDZ domain-containing scaffold proteins.* Nature Communications, 2012. **3**.
86. Sheng, R., et al., *Cholesterol selectively activates canonical Wnt signalling over non-canonical Wnt signalling.* Nature Communications, 2014. **5**.
87. Manna, D., et al., *Differential roles of phosphatidylserine, PtdIns(4,5)P(2), and PtdIns(3,4,5)P(3) in plasma membrane targeting of C2 domains - Molecular dynamics simulation, membrane binding, and cell translocation studies of the PKC alpha C2 domain.* Journal of Biological Chemistry, 2008. **283**(38): p. 26047-26058.

88. Sumandea, M., et al., *Roles of aromatic residues in high interfacial activity of Naja naja atra phospholipase A(2).* Biochemistry, 1999. **38**(49): p. 16290-16297.
89. Hurley, J.H., *Membrane binding domains.* Biochimica Et Biophysica Acta-Molecular and Cell Biology of Lipids, 2006. **1761**(8): p. 805-811.
90. Cho, W. and R.V. Stahelin, *Membrane binding and subcellular targeting of C2 domains.* Biochimica Et Biophysica Acta-Molecular and Cell Biology of Lipids, 2006. **1761**(8): p. 838-849.
91. Melowic, H.R., et al., *Mechanism of diacylglycerol-induced membrane targeting and activation of protein kinase C theta.* Journal of Biological Chemistry, 2007. **282**(29): p. 21467-21476.
92. Lemmon, M.A., *Membrane recognition by phospholipid-binding domains.* Nature Reviews Molecular Cell Biology, 2008. **9**(2): p. 99-111.
93. Hurley, J.H. and T. Meyer, *Subcellular targeting by membrane lipids.* Current Opinion in Cell Biology, 2001. **13**(2): p. 146-152.
94. Bennett, W.F. and D.P. Tieleman, *The importance of membrane defects-lessons from simulations.* Acc Chem Res, 2014. **47**(8): p. 2244-51.
95. Tamm, L.K. and H.M. McConnell, *SUPPORTED PHOSPHOLIPID-BILAYERS.* Biophysical Journal, 1985. **47**(1): p. 105-113.
96. Cho, W.H. and R.V. Stahelin, *Membrane-protein interactions in cell signaling and membrane trafficking*, in *Annual Review of Biophysics and Biomolecular Structure*. 2005. p. 119-151.
97. De Camilli, P., et al., *The ENTH domain.* Febs Letters, 2002. **513**(1): p. 11-18.
98. Lai, C.L., et al., *Membrane Binding and Self-Association of the Epsin N-Terminal Homology Domain.* Journal of Molecular Biology, 2012. **423**(5): p. 800-817.
99. Knight, J.D., et al., *Single Molecule Diffusion of Membrane-Bound Proteins: Window into Lipid Contacts and Bilayer Dynamics.* Biophysical Journal, 2010. **99**(9): p. 2879-2887.
100. Knight, J.D. and J.J. Falke, *Single-Molecule Fluorescence Studies of a PH Domain: New Insights into the Membrane Docking Reaction.* Biophysical Journal, 2009. **96**(2): p. 566-582.
101. Ueda, Y., et al., *Regulation of the transbilayer movement of diacylglycerol in the plasma membrane.* Biochimie, 2014. **107 Pt A**: p. 43-50.

CHAPTER II

Quantification and Membrane Dynamics of Diacylglycerol

1. Introduction

1.1. Lipids as regulators of cellular processes

Lipids are amphipathic molecules, which have a tendency to aggregate together by hydrophilic parts, and in the same time, they may interact with water phase. These properties allow lipids to form bilayers and become biomembranes [1-3].

Phospholipids, the main component of eukaryotic cellular membranes, are divided into two classes, glycero- and sphingophospholipids. Phospholipids are not thought to be sufficiently water-soluble to permit diffusion through the aqueous cytosol [3, 4].

In contrast to phospholipids, many intermediates in the biosynthetic pathways leading to the formation of these lipids or phospholipid hydrolysis products in signaling pathways are not limited in their distribution to bilayer structures. Monoacylglycerolipids exhibit detergent-like properties, while lysophosphotidic acids are readily water-soluble. Therefore, these lipids may equilibrate between different lipid bilayer structures. However, as in the case for phospholipids, redistribution in the absence of active transport is topographically restricted by the presence of charged head groups [3, 5-8]. Neutral lipid, like DAG or ceramide, containing long-chain fatty acids, remain confined to membrane structures in the absence of transport proteins, but may "flip-flop" between inner and outer leaflets. Smaller uncharged molecules, such as fatty acids, easily equilibrate throughout the cell [9-12].

Based on their properties in the absence of transport proteins, intermediates and products of lipid synthesis and degradation are divided into five categories: (1) precursor molecules limited in distribution to the aqueous phase (choline, serine); (2) amphipathic molecules that are water mixable but not topologically restricted (free fatty acids); (3) amphipathic molecules that are water mixable but topologically restricted (LPA); (4) amphipathic molecules present in lipid

bilayers which may “flip-flop” between leaflets (DAG, ceramide); and (5) amphipathic molecules that are limited in their distribution to bilayers structures and are topologically restricted (phospholipids).

The combination of these properties of cellular lipids, together with compartmentalization of proteins involved in biosynthesis and lipid transport, will determine the lipid composition of membranes in different subcellular structures. The composition may vary significantly depending on intracellular compartment [13-15].

Lipids regulate many cellular activities mainly by serving as site-specific membrane indicators that mediate the membrane recruitment and activation of various proteins [2, 16]. Lipids are an important component of the cell; they give the structural foundation of cellular membranes. Various lipids participate in regulation of various biological processes such as cell proliferation, differentiation, cell survival and membrane trafficking [1, 17, 18]. Spatial and temporal distributions of different lipids are tightly regulated by lipid-signaling enzymes such as lipid kinases, phosphatases and phospholipases [17, 19, 20]. These enzymes play an important role in the production of lipid messengers as well [1]. Mutations in lipid-metabolizing enzymes are associated with the development of diseases, including psychiatric and neurological disorders, cancer, diabetes and allergy [21]. In many cases, lipid-mediated cell regulation pathways are major targets for drug development [22].

Although much is known about the biology of lipid signaling, there is still limited information about the spatiotemporal dynamics and fluctuation of cellular lipids, which restricts mechanistic understanding of lipid-mediated cell regulation and development of specific therapeutic agents targeted for these signaling pathways [20]. The development of sensor-based

fluorescence imaging technique that allows accurate quantification of specific lipids helps to overcome this problem [23, 24].

1.2. Strategies for lipid quantification

Reversible conversion of lipids (for example, PI(4,5)P2 from/to DAG) and the heterogeneous distribution of these lipids determine the cellular membrane nature. Recent improvements in techniques for detection of various lipids and development new imaging methods to study their distribution and changes have significantly improved the study of this important class of biological molecules [23, 25-27]. The developed approaches have helped to have a better understanding of the physiological role of lipids and the significance of their metabolic dysfunction in disease. Incorporation of detection methods allows the characterization of a specific lipid and its biological role. This result may lead to the comprehension of lipid signaling. Here, we review current techniques used for the study and manipulation of cellular PIs and also discuss advantages and disadvantages associated with the various methods [21].

Biochemical detection techniques now allow quantification of all seven PIs, and the use of fluorescently tagged PI-binding domains enables real-time visualization of most of them in intact cells [21, 28, 29]. Together, these and other methods now allow us to examine the dynamics of the seven PIs at different levels, from global changes in cells and tissues down to changes in a specific PI in a cellular subcompartment. Parallel to the development of detection techniques, new techniques for the chronic or acute, cell-wide or spatially localized manipulation of PIs have been developed [21]. Available methodology for the analysis and manipulation of PIs, compare the strengths and weaknesses of different methods and also suggest future directions for this field of PI biology is summarize below.

Biochemical methods are the most commonly used for the detection of various lipids [30, 31]. The presence of the particular lipid in the lipid extract is detected by different chromatography methods such as ion-exchange or thin layer. Mass spectrometry has been gaining its popularity as widely used method of lipid detection [32]. It has a great sensitivity and enables to distinguish lipids not only by a head group but also an acyl chain. The major advantage of these detection methods is a simultaneous detection/separation of lipid mixture. Although these methods provide a good sensitivity and specificity, there are a lot of limitations in their application. Biochemical techniques give information about a fixed composition of the lipid membranes and do not provide specific lipid localization and distribution. In order to perform biochemical measurements lipids are extracted from fractioned cells. This step may also lead to lipid modification. Another disadvantage is deficit of information about the dynamic range of each lipid through the time [18, 21, 33].

The microscopy-based methods became the dominating approach in visualization, localization and quantification of lipid molecules [34, 35]. Wild-field epifluorescence and confocal microscopies allow obtaining high-quality images of cells or tissue sections. In cases of plasma membrane studies, total internal reflection fluorescence (TIRF) microscopy permits detection of lipid changes with high temporal and special precision [17]. Monitoring of a specific lipid is usually done using fluorescent proteins that have a high affinity to a given lipid. A lot of fluorescent-fused domains were designed for visualization of lipids such ENTH-EGFP binding to PI(4,5)P2 and C1 domain-EGFP binding to DAG.

The most established one is the Forster resonance energy transfer (FRET)-based approach, where interacting partners are labeled with donor and acceptor molecules [21]. The interaction event results in an energy transfer between the proximal donor and acceptor,

providing the analytical signal. Though the approach is robust, it requires double labeling, which is complicated and cannot be realized in many screening assays. It is very common method of identification of location of lipids but this approach does not provide any quantitative information. To overcome this limitation FRET can be used in several different set-ups [36, 37]. For example, biosensors based on intra-molecular FRET require coexistance of two fluorescence tags that allows for FRET to occur between these fluorophores [26, 37]. When not bound to a membrane, fluorescent tags of the protein are far apart and FRET between the donor and acceptor fluorophore is low. Upon recruitment to the membrane by an increase in the appropriate lipid, FRET increases and can be detected with fluorescence-based microscopy techniques. FRET is considered as a semi-quantitative technique and gives a relative concentration usually expressed in percent of increase/decrease of the fluorescent energy transfer. This method allows to monitor physiological responses in live cell and also can be miniaturized for high-throughput assays of combinatorial products [20]. However, FRET must consider rotational diffusion and average orientation, dimerization in GFP, may be limited in the range of possible fluorophore pairs. Using this technique CCD has high background noise, corrections with computer image processing are necessary Autofluorescence, natural fluorescence of cells, has to be addressed in the image processing.

Another method that provides semi-quantitative information about a particular lipid is antibody-based detection. Commercial antibodies are available against the majority of lipid and are widely used in immunofluorescence experiments. However, these methods have complicated sample preparation and provide a snapshot of the cell because of specimen fixation.

We developed a new ratiometric imaging method of the accurate lipid quantification [19] that consists of three main steps: 1) lipid binding domain engineering, 2) chemical labeling using

environment sensitive dyes, and 3) cell delivery and intracellular quantification (Figure 16). The principle of ratiometric analysis is the sensitivity of chosen fluorescent probes to given environmental change [38, 39]. These environmental changes contain pH, the concentration of specific ions such as Na^+ as well as the polarity and viscosity of surroundings. A lipid biosensor binds to the membrane surface this biosensor experiences a dramatic environmental change from a polar environment of a cell cytoplasm to a nonpolar lipid surroundings; therefore a polarity-sensitive fluorophores such as acrylodan (6-acryloyl-2-dimethylaminonaphthalene, DAN for short) introduced to the lipid-binding surface exhibit the expected spectral characteristics upon lipid binding [40]. These fluorophores show either a major increase in fluorescence emission intensity and/or a large spectral shift upon binding a lipid in the membrane that can be used for ratiometric fluorescence analysis for lipid quantification [41, 42]. By measuring the ratio of intensities on digital images captured at the wavelengths of the membrane-bound and free biosensor the precise lipid concentration at different locations can be calculated [19]. This method is very sensitive to low concentrations of lipids, independent of the biosensor concentration and allows obtaining lipid amount at the specific location on the membrane with a high precision [19]. The biggest challenge in application of the ratiometric technique is the successful protein labeling and limited number of fluorophores [43].

1.3. *In situ* quantification of PI(4,5)P2 on plasma membrane

Typically, lipid-binding domains and proteins have usually a positively charged membrane-binding surface responsible for a non-specific interaction with a surface of the cellular membrane as well as a lipid-binding groove, which takes care of specific interaction with a given lipid. Therefore, optimization of lipid-binding characteristics involves engineering of specific ans non-

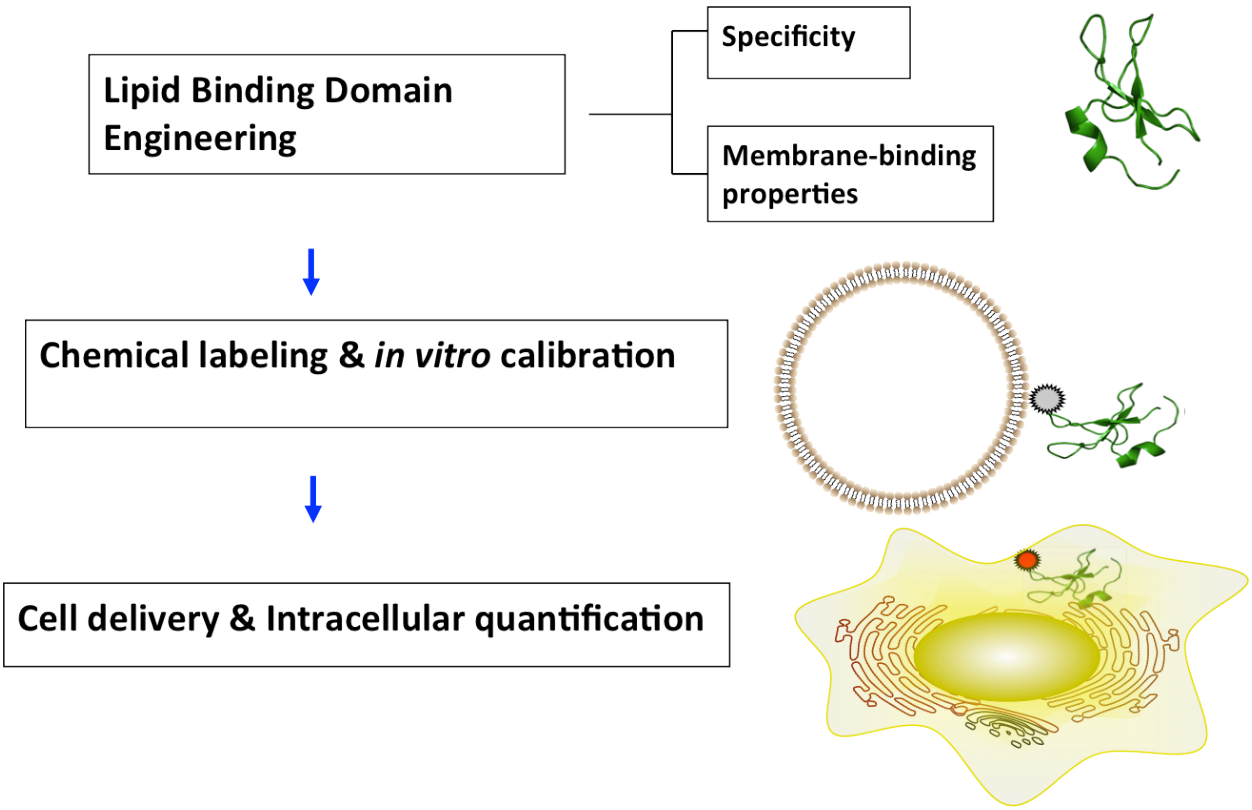

Figure 16. Strategy for *in situ* quantification

The strategy consist of three major steps: engineering the domain with high sensitivity and specificity to a lipid, chemical labeling with environment sensitive dye and quantification of lipid concentration *in vivo* and *in vitro* using ratiometric analysis. The basis of the ratiometric analysis is the sensitivity of fluorophores to certain environmental changes.
Wonhwa Cho (2010). Chemical Biology of Biosensors. UIC

specific binding sites of the sensor [34, 44-46]. Epsin N-terminal homology (ENTH) domain is one of lipid-binding domains that bind PI(4,5)P2 with relatively high specificity and was used as a template for sensor protein engineering. As confirmed by surface plasmon resonance (SPR) analysis, ENTH domain shows a high selectivity for PI(4,5)P2 over other PIs [19]. Mutagenesis can further improve lipid introduced to the membrane-binding pocket and surface located near that area. It was found that Trp usually increases the lipid-binding affinity [47]. When the best mutant is identified, the chemical labeling takes place. As was mentioned earlier (section 1.2), The transformation of a high binding affinity lipid biosensor into a fluorescence 'switch-on' biosensor can be obtained using chemical labeling of the domain with an organic fluorescent probe that exhibit either a drastic amplification (often from an insignificant background) of fluorescent emission signal at a specific wavelength and/or a significant shift in the emission spectra upon lipid binding. As a result the obtained biosensor can be applied for lipid quantification using ratiometric analysis. Because of the sufficient change of environment going from aqueous solution to a membrane-bound non-polar membrane surface, it was proved in recent studies that environment-sensitive fluorescent dyes attached to the lipid-binding surface illustrate the desired spectral characteristics upon binding to lipid membrane surfaces [39, 40]. It is important to eliminate all Cys exposed to the surface of the domain since they all can easily react with fluorophore via thiol-alkene reaction:

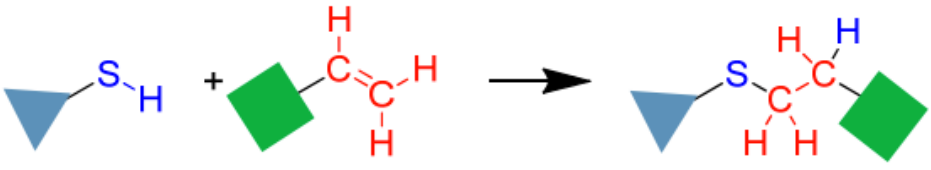

After efficient labeling the biosensor was used in GUV calibration. Using the binding curve we performed the cellular imaging delivering a PIP2 sensor by microinjection and using earlier described ratiometric analysis for lipid quantification.

1.4. Environment sensitive dyes

Monitoring biomolecular interactions is a fundamental issue in biosensing, with numerous applications ranging from basic biological research to clinical diagnostics. Fluorescence techniques are particularly well suited for this purpose [40, 48]. With all advantages of FRET method, it takes dual labeling for detection and quantification of one cellular interaction. Therefore, single fluorescence labeling techniques, where only one biomolecule in binding pair is labeled, specificity and the overall membrane affinity of the ENTH domain where various mutations are would significantly simplify the technical part of the experimentation. One such approach is implementation of environment-sensitive dyes (ESD) [40, 49, 50]. ESD change their fluorescence properties in response to physical or chemical changes in their molecular environment [51]. Unlike classical dyes commonly used as markers of biological molecules, ESD can be utilized as sensors for monitoring the various biomolecular interactions. The ESD change to the environment is initiated in one of three ways: excited-state reactions (conformational change, electron transfer, etc.), non-covalent interactions (van der Waals, dipole–dipole, etc.), and specific H-bonding [40, 52].

Two types of ESD are received a special attention with their ability to be used in various biomolecular applications: molecular rotors and solvatochromic fluorescent dyes [41, 53, 54]. First one is a class of molecular rotors, which change their emission intensity with the change of the solvent viscosity [53]. In viscous environments, such as biomembranes, their rotation mobility is limited; as a result their fluorescence quantum efficiency significantly increases. In

other words, molecular rotors can turn on their fluorescence with a change in rigidify of their environment. Unfortunately, the application of these dyes is still at the stage of the development. Another type of ESD composes solvatochromic fluorophores [40, 55]. Usually they exhibit emission shifts and frequently drastic change in fluorescence intensity. These changes happen in response to a polarity change in molecular surroundings [40, 55, 56]. In these dyes, the dipole moment increases significantly upon electronic excitation (S_0->S_1 transition) because of an intramolecular charge transfer from the electron-donor group to the electron-acceptor group (Figure 17). Polar solvents relax efficiently the excited molecules to the S_1(solv) state as a result of polarization of the solvent dipoles around the fluorophore dipole. The energy of the S_1(solv) state usually is elevated with decreasing the solvent polarity, as a result the emission spectra shifts to the right in a direction of longer wavelengths (red shift) (Figure 17). Therefore, dipole–dipole interactions in polar solvents can initiate the red emission shift of these dyes while nonpolar solvents can introduce the blue shift. Most environment-sensitive fluorophores exhibit low fluorescence intensity in water. Thus, incorporation of these dyes into proteins and their application in studies of lipid-protein interactions where the dye would experience the dramatic environmental polarity change often significantly increases their fluorescence.

1.5. Diacylglycerol sensor

MDDNK + L124C/C133S PKCγ C1B as a DAG-sensor

1,2-diacyl-sn-glycerol (DAG) is a key lipid second messenger that mediates a wide variety of cellular processes, including cell proliferation, differentiation and cell cycle progression [16, 57, 58]. Thus, DAG signaling pathways offer multiple targets for anticancer therapy. As it has been found, various DAG receptors are present in mammalian cells. It is important to understand how DAG regulates these proteins in the cells [59-63].

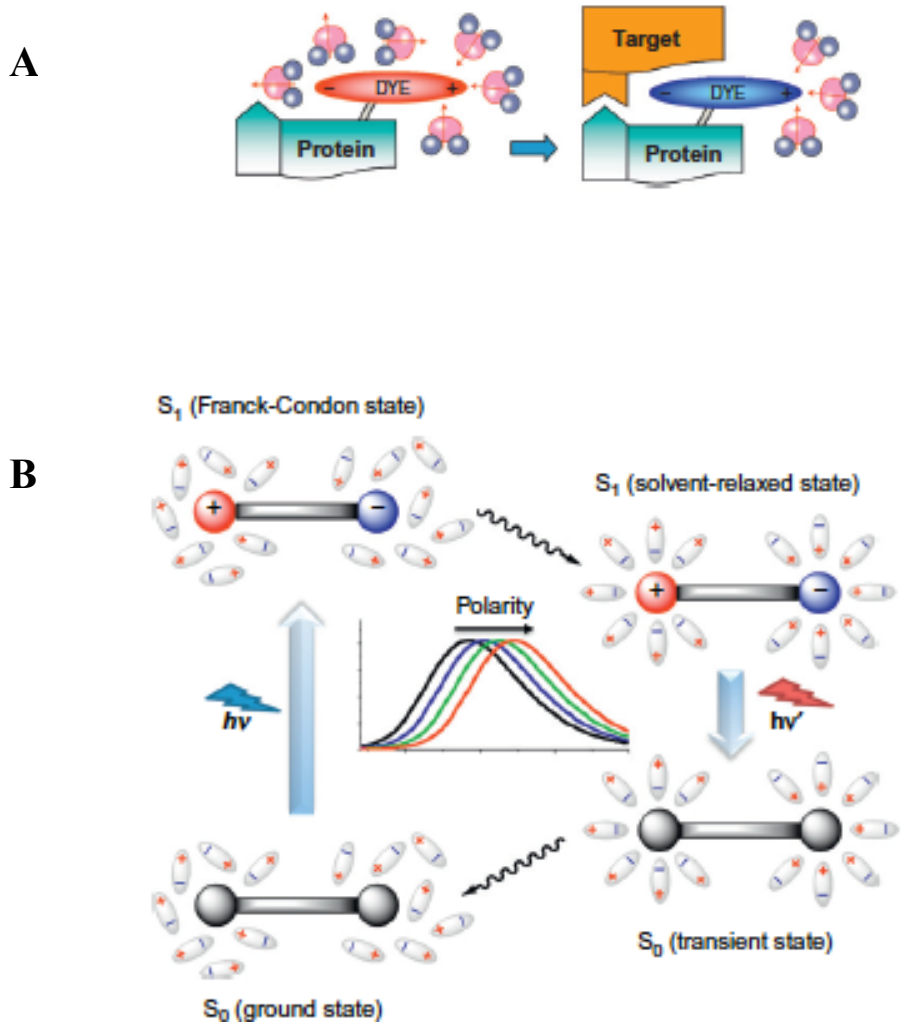

Figure 17. Monitoring molecular interactions by environment sensitive dyes

a) Solvatochromic fluorophores response to a polarity change in molecular surroundings. b) Simplified diagram explaining the phenomenon of solvatochroism. Environment sensitive dyes exhibit emission shifts and frequently drastic change in fluorescence intensity.
Klymchenko, A.S. and Y. Mely, Chapter Two - Fluorescent Environment-Sensitive Dyes as Reporters of Biomolecular Interactions, in Progress in Molecular Biology and Translational Science, C.M. May, Editor. 2013, Academic Press. p. 35-58.

Therefore, elucidation of the spatiotemporal dynamics of DAG fluctuation and the mechanisms by which DAG's divergently regulate the activities of their receptors are of great significance and of broad interest. This information also helps to develop a new strategy to modulate the cellular activities of overexpressed or hyper-activated DAG receptors in a spatiotemporally specific manner without interfering with normal DAG signaling pathways.

To fully understand the mechanisms by which DAG mediates divergent membrane targeting and activation of receptor proteins, it is necessary to quantitatively monitor the cellular DAG fluctuation and correlate the spatiotemporal dynamics of DAG with specific protein translocation [64].

The C1b domain of PKCγ labeled with DAN was suitable to satisfy three requirements for a successfully working lipid biosensor. First of all, the chosen protein domain has a significant affinity for DAG, particularly when it is labeled with DAN. Next, the this fluorescent label helps to penetrate the cellular membrane and demonstrate significant modification of fluorescent intensity through lipid binding, and finally, the domain is stable and stay active for the time of experiments at different conditions (Figure 18).

On the early stage of DAG sensor development Dr. Brian Page found that the cationic patches of the sensor were crucial nonspecific binding to the glass surface of the microinjector, which lead to unsuccessful microinjection. To overcome this problem as well as enhance domain stability, few key mutations were introduced and the sequence was extended from the N-terminal site [64].

1.6. Simultaneous quantitative imaging of multiple sensors

Simultaneous quantification of two lipids requires two dyes with a clear spectral separation for dual ratiometric analysis. Using two sensors labeled with DAN and NR3, respectively, we can

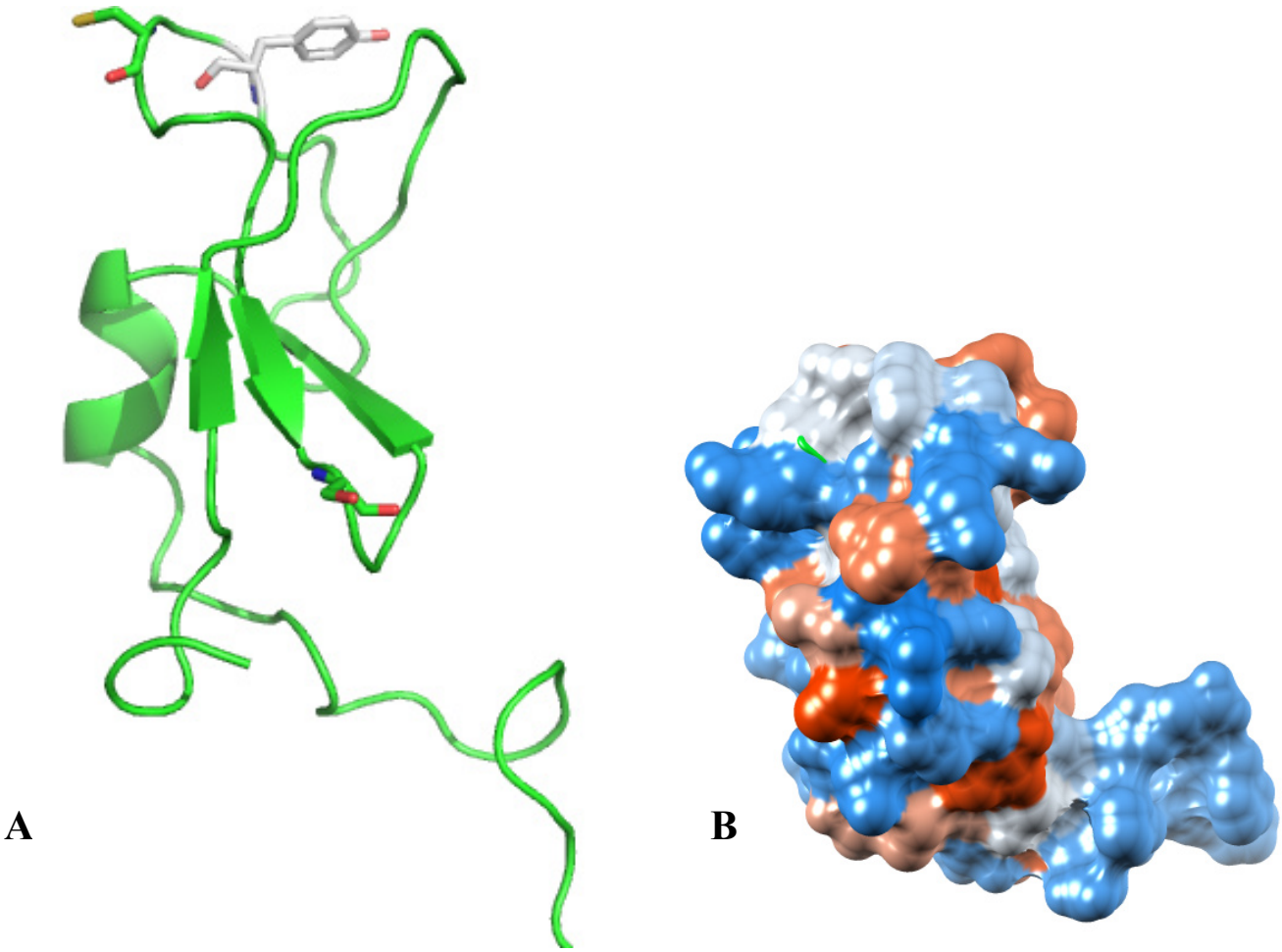

Figure 18. Structure of original DAG sensor (BRP) PKCγ C1 domain L124C/C133S with MNNKK N-terminal extension

a) Ribbon structure shows all key mutations of the first generation DAG sensor. b) The same structure is represented as electrostatic surface. The C1 domain domain is a very small structure with a lot of cationic and anionic patches.

perform binary lipid quantification in mammalian cells according to the established protocol [19]. Several sensors with a high specificity such as PI(4,5)P2, PI(3,4,5)P3, DAG and PS were developed using established approach of engineering of lipid binding domains [65]. Because lipids are tightly correlated in conversion, it would be beneficial to design a system where we are able to not just see correlation between different classes of lipids but also quantify their amounts and changes in time with a high precision. There are a lot of possible pairs, which could give an inside of lipid metabolism. We chose to test several combinations: PIP2-DAG, PIP2-PIP3 and PS_{inner}-PS_{outer}. In each of these pairs we tested both DAN and NR3 labeling to find the best composite (Figure 19).

To perform fluorescent imaging, we have constructed a custom-built, two-laser multichannel two-photon microscope [66]. A block diagram of the optical layout of the microscope, detailed in Figure 20, shows the two laser sources. Each laser is tuned to a specific wavelength, which allows a separated excitation of an isolated labeled sensor. A standard Ti:Sapphire laser with femtosecond pulses (Tsunami-Millennia) has been employed for fluorescence dyes' excitation in 720–900 nm range of the spectra (blue and green dyes). The second laser consists of an automatically tunable femtosecond pulsed Ti:Sapphire laser (Mai-Tai) and an OPO (Opal), and this laser is more suitable for long-wavelength excitations in the range of 900-1000 nm (orange, red and far-red dyes).

Simultaneous quantification of two different lipids requires orthogonal lipid biosensors that enable simultaneous ratiometric quantification of two lipids. The availability of amphipathic ESDs is significantly limited, that thwarts the successful production of diverse lipid biosensors. Hence we looked for such ESDs that we could use simultaneously with well-established and widely utilized thiol-reactive amphipathic ESD, 2-dimethylaminonaphthaloyl DAN [67]. The

protein is labeled with DAN via a cysteine residue located in close-proximity to lipid-binding pocket. The DAN-labeled protein experiences a significant green-to-blue shift in an emission spectra and also shows a great increase in fluorescence signal when the protein interacts with its binding partner on the plasma membrane. These important properties enable the application of ratiometric analysis for finding the content of specific membrane lipids using *in vitro* calibration [19]. To perform simultaneous quantification of two lipids on the plasma membrane we searched for ESD that could demonstrate all crucial properties of amphipathic fluorophore as well as be differentiated from DAN by emission spectra, possibly having a spectral shift in a longer (red) range of wavelengths. Examination of known red fluorescent dyes suggests that Nile Red has required properties and its maleimide derivatives can be adjusted for cysteine labeling [39-41, 68]. Unfortunately, Nile Red derivatives have a strongly hydrophobic nature; therefore they show extremely low water solubility. This aspect negatively affects the protein labeling efficiency in physiological conditions; it influences the protein folding and can disturb lipid-binding properties of the labeled proteins. To succeed in dealing with these difficulties, we aimed to improve properties of ESDs through design of derivatives and modification of the labeling procedure.

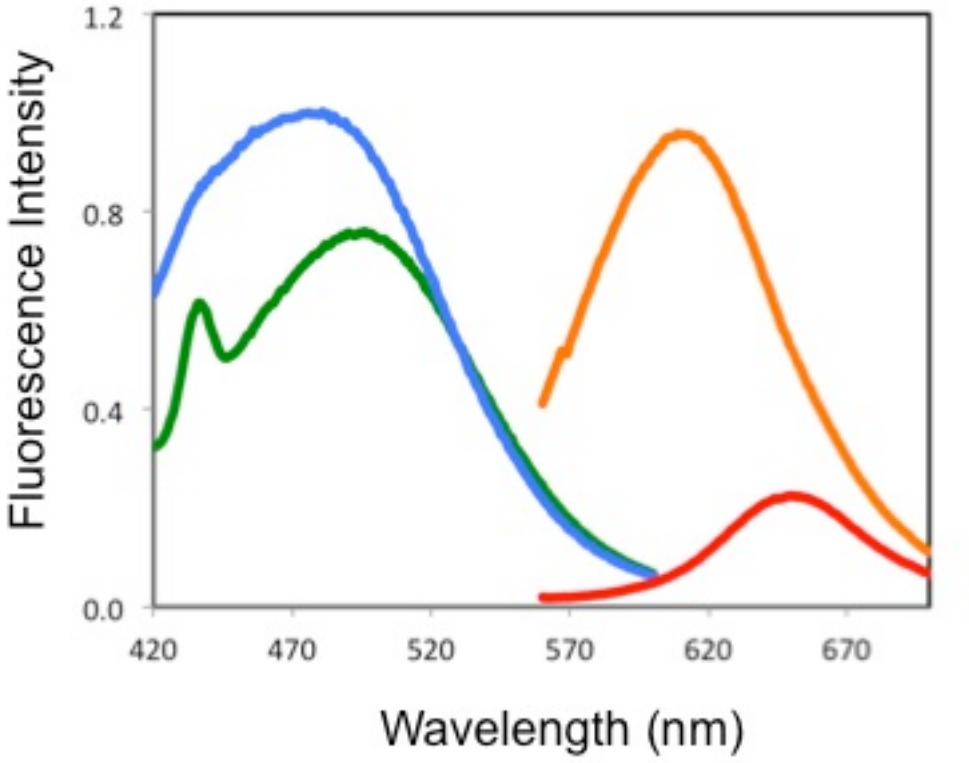

Figure 19. Spectral separation of two environment sensitive dyes (ESD)

Acrylodan (DAN) labeled lipid sensor shows emission at 520 nm for free and 450 nm for lipid-bound protein. Nile Red 3 (NR3) labeled lipid sensor shows emission at 650 nm for free and 600 nm for lipid-bound protein. The spectra demonstrate the possibility of simultaneous detection of the fluorescence signal for a pair of lipid sensors.

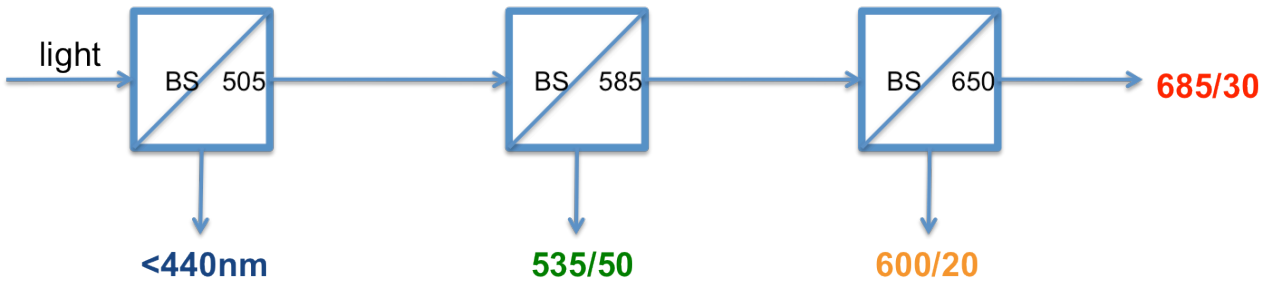

Figure 20. Simultaneous four-color imaging

Scheme of simultaneous four channel detection: the emitted light passes through the series of longpass (LP) beamsplitters (BS): 405 nm, 585 nm and 650 nm. Optical layout of custom-built two-photon microscope with two lasers and four channels provides excitation at 720–850 nm and 900–1,040 nm where emission is collected into four isolated channels. We used a Millennia-pumped Tsunami laser for excitation of wavelengths < 900 nm and a Mai Tai laser for those between 900 and 1,020 nm.

2. Experimental procedures

2.1. Materials

Thrombin and the thiol reactive acrylodan (6-acryloyl-2-dimethylaminonaphthalene) were purchased from Invitrogen. l-Palmitoyl-2-oleoyl-sn-glycero-3-phosphocholine (POPC), l-palmitoyl-2-oleoyl-sn-glycero-3-phosphoserine (POPS) and 1-stearoyl-2-arachidonoyl-*sn*-glycerol (SAG) were purchased from Avanti Polar Lipids. Adenosine triphosphate (ATP) and lysophosphatidic acid (LPA) were from Sigma Aldrich. The fluorescence labeled lipids, TopFluor PtdIns(4,5)P2 (l-oleoyl-2-(6-[4-(dipyrrometheneboron difluoride)butanoyl]amin)-hexanoyl-s-glycero-3-phosphoinositol-4,5-bisphosphate) and rhodamine-PE were purchased from Avanti Polar Lipids. All supplementary materials were of the highest grade commercially available.

2.2. Mutagenesis

The cloning procedures have been described in specific details elsewhere. Briefly, Y123W mutation was introduced in PKCγ C1b and the modified sequence was inserted into bacterial vector pET21a via NdeI/XhoI restriction sites. Cysteine that didn't coordinate zinc-finger formation was mutated to serine. One additional cysteine residue was introduced to the sequence in lipid-binding area of protein. The same mutations were carried on few other C1 domains. All constructs included N-terminal extension (MDDNK) and C-terminal His-tag.

2.3. Protein expression and purification

The PKCγ C1b and PKCθ C1a+C1b mutants were expressed as C-terminal poly-histidine tag (His-tag) fusion proteins and purified using the Ni-NTA-Tag™ resin (Novagen) as described [69]. Protein concentration was determined by the Bradford protein assay.

2.4. Labeling

The labeling reaction contained 20 μM protein and 80 μM acrylodan (ratio 1:4) in 5 ml of 50 mM TRIS buffer in a presence of 300 mM KCl, pH 7.5. Labeling reaction was held overnight at 4°C, then all unreacted fluorescent dye and remaining impurities were removed by extensive washing with TRIS buffer containing low concentration imidazole (10, 15, 20 μM). The labeled protein was eluted with 300 μM imidazole TRIS buffer. All collected fractions were checked for a spectral properties and labeling efficiency. Specific labeling for each protein was adjusted.

Variety of different red dyes (see Appendix) were kindly provided by Dr. Daesung Lee and tested for label efficiency and spectrofluorometric properties. The labeling procedure was identical to acrylodan/thiol reaction except the washing step. It was challenging to remove a free dye completely, therefore low concentration on DMSO and ethanol (up to 10 %) were added in order to eliminate as much remaining free dye as possible following the principle: Like dissolves like.

For efficient labeling via cysteines we used the method described in [70]. Precipitation as well as storage was maintained with addition of 5-10 mM DTT. DTT is crucial in breaking all intermolecular disulfide, in addition it helps to keep slightly basic pH. The efficiency of a chemical labeling conjugation to the protein precipitate was estimated using the protocol [70]

2.5. Labeling efficiency

Desalted proteins were quantified using GENESYS^{TM} 20 Visible spectrophotometer (Thermo Fisher Scientific). Dye labeling efficiency (LE) was calculated based on the extinction coefficient of each reagent: ε_{280}(protein) = 8000 M^{-1} cm^{-1}; ε_{372}(DAN) = 16400 M^{-1}. Absorbance at 280 nm was corrected by a correction factor (CF) defined as $CF_{280} = A_{280}$ (freedye)/A_{max} (freedye). The labeling efficiency (LE) for the dye was calculated according to: LE (Dye) = [ε_{280}

(protein) × $A_{\lambda max}$(Dye)]/[A_{280}(corr) × $\varepsilon_{\lambda max}$(Dye)], where $A_{\lambda max}$(Dye) is absorbance at the emission maximum of the dye and A_{280} is absorbance of the protein sample at λ=280 nm [67, 70, 71].

2.6. Giant Unilamellar Vesicle (GUV) Formation

GUVs were prepared by the electroformation technique as described previously [51, 64, 72]. These lipids (POPC/POPS/DAG 80-x:20:x where x was 0-7 mol%) were dissolved in chloroform with a stock concentration of lipids 0.4-0.5 mg/ml. Next the obtained solution was spread onto the indium tin oxide electrode surface, and the surface was dried under vacuum to form a uniform lipid film. To grow lipid vesicles we use 350 mM sucrose solution with an electric field (3 V, 20 Hz frequency) for 4-5 hours at room temperature. The size of obtained vesicles varied between 5 and 20 µm. Small amount of sucrose-loaded GUV solution (typically 1-2 µl) was added into an 8-well plate chamber with glass coverslip bottom. The well contained 400 µm 20 mM Tris-HCl buffer with 160 mM KCl at pH 7.4. The protein was added to the buffer to the final concentration 100 nM and gently mixed prior the addition of GUVs. The plate was placed on the stage of the Zeiss 200M microscope. After GUVs were sedimented on the bottom of the well, several GUVs were scanned with point scanning Hamamatsu photomultiplier tubes (PMT) controlled by SimFCS software (Laboratory for Fluorescence Dynamics, University of California Irvine) at room temperature. Every image was an average of 10 frames.

2.7. Calibration DAG on GUV using fluorescence microscopy

In vitro calibration of DAG-DAN sensor was performed using GUVs composed of POPC/POPS/DAG (80-x:20:x) (x = 0-7 mol%). The surface concentration of DAG on the vesicle (pmoles/m^2) was calculated from the average cross-sectional area of a lipid head group

(70 A^2/molecule) [19] and the known mol% of DAG in each vesicle. GUVs were mixed with DAG-DAN sensor in the concentration range of 0-300 nM and fluorescence measurements were carried out at room temperature using the custom-built two-photon, four-channel microscope that was described previously [73]. Measurements were controlled by the SimFCS (Laboratory for Fluorescence Dynamics, University of California Irvine), and after systems upgrade all imaging was done using PrairieView software (Prairie Technologies, Inc.). The DAG-DAN was two-photon excited at 780 nm by Ti:sapphire pulsed laser MaiTai (Spectra Physics, Fremont, CA) and the fluorescence emission of the membrane-bound and free sensor species were separated by 436 ± 10 nm (for blue channel) and the 525 ± 25 nm (for green channel) band pass filters, respectively. Each image of 512 x 512 pixels was collected with the pixel dwell time of 20 milliseconds using Peltier-cooled 1477P style Hamamatsu PMT. For each DAG concentration, 5 GUVs were selected and for each of them, 10 frames were collected and an averaged image was utilized in further data processing in MATLAB. The averaged photon counts in green and blue channels were read into a 512 x 512 matrix to obtain an averaged snapshot. After that a binary mask of the image was made from the averaged image by the choosing GUVs surface area and eliminating the background of GUV's inside and outside area. Then original averaged snapshot was multiplied by its binary mask to extract the photon counts of GUV membrane. The GUV's total number of photon counts in each channel, F_B or F_G, was divided by the number of pixels that contributed to the signal coming from the membrane of each GUV. To calculate the photon counts per area, we used a conversion of pixel size into metric system value, F_B and F_G (counts/m^2). Average values of F_B and F_G for each DAG concentration were then used to prepare the calibration curves for both single-channel (i.e., green-channel only) and ratiometric (F_B/F_G) analyses. Because the intensity in green channel was on average the

same, it was possible to proceed calculation using a single (blue) channel. For the blue-channel analysis, F_B versus data was fit using the equation: $F_B = (F_B)_{max}/(1 + K_d/[DAG])$ where K_d and $(F_B)_{max}$ values were determined from non-linear least-squares analysis (Figure 25). Then, [DAG] from an unknown sample was calculated using the equation; $[DAG] = K_d F_B/((F_B)_{max} - F_B)$. For the ratiometric analysis, K_d and $(F_B/F_G)_{max}$ values were calculated from non-linear least-squares analysis of the (F_B/F_G) versus [DAG] plot using the equation; $(F_B/F_G) = (F_B/F_G)_{max}/(1 + K_d/[DAG])$ and the theoretical calibration curve was constructed using these values (Figure 25). Then, [DAG] from an unknown sample was calculated using the equation; $[DAG] = K_d(F_B/F_G)/((F_B/F_G)_{max} - (F_B/F_G))$.

2.8. Spectrofluorometric Measurements

FluoroLog3 spectrofluorometer (Horiba Scientific) was used for all cuvette-based fluorescence measurements, and it was used for binding specificities of sensor toward diacylglycerol. DAG-DAN (500 nM) was added to POPC/POPS/DAG (80-x:20:x) (x = 0-5 mol%) LUV and the emission spectra of DAN were measured with excitation wavelength set at 380 nm. The same measurements were repeated with control LUVs made of POPC/POPS (80:20).

2.9. Determination of DAG content *in vivo*

NIH 3T3 cells were seeded into glass bottom Petri dishes and grown at 37 °C in a humidified atmosphere with 5% CO_2 in Dulbecco's modified Eagle's medium (DMEM) (Invitrogen) supplemented with 10% (v/v) fatal bovine serum (FBS) (Invitrogen). DAG-DAN was delivered into the cells by microinjection using the Eppendorf InjectMan NI 2 system. All microscopy measurements and data analysis were performed as described above. The cellular [DAG] was determined from the observed (F_B/F_G) (ratiometric) values using the *in vitro* calibration curves (Figure 24) determined for POPC/POPS/DAG. The angular profile of photon counts in the

cellular plasma membrane was calculated by MATLAB with the following algorithm implementation. First, a binary image mask around the plasma membrane was created as described above. Then, another triangular shaped binary mask that connects the center of the cell, any position on the plasma membrane and the second position on the plasma membrane that is advanced from the first position by 2 degree. The two masks and the cell's image matrix were multiplied to calculate the average local photon counts. This operation was repeated for every 2 degrees around the plasma membrane in a counterclockwise manner.

3. Results and Discussion

3.1. Engineering C1 domain as the second generation of DAG sensor

C1 domains illustrate an independent folding and play an important role in a complex mechanism of recruitment of PKC proteins and other C1 containing proteins to cellular membranes via nonspecific interactions with negatively charged lipids and specific interaction with crucial second messenger DAG. Through the membrane binding a host protein (PKC, RasGRP, DGK, etc.) change the conformation and converted to the active state to continue downstream signaling. The DAG threshold content is defined by the DAG binding affinity and it varies for every protein containing C1 domain. The diversity of this value is required for the propagation and selectivity of signaling response among DAG receptors in the cellular processes. Although the structural basic of C1 domains is well known, it does not explain the molecular foundation of differentiation in their binding affinities to DAG [74]. Solution NMR methods and molecular dynamics simulations showed that the mutant, Y123W, of the C1b domain of protein kinase Cα (C1bα) did not perturb the C1bα structure, yet resulted a considerable change in conformational dynamics as well as more than 100-fold increase in DAG binding affinity [74]. The review of various binding studies proposes [47, 75] that the conformational dynamics and specific location of the tryptophan residue at the binding surface of C1 domain are important modulators of the DAG binding properties.

To improve DAG binding affinity of the first generation of DAG sensor (MDDNK + L124C/C133S PKCγ C1b) we introduced Y123W mutation. In addition to that we also engineered few constructs of other C1 domains reflecting the same mutation [64]. All generated mutants were tested for binding affinity and specificity as well as for desired spectral properties

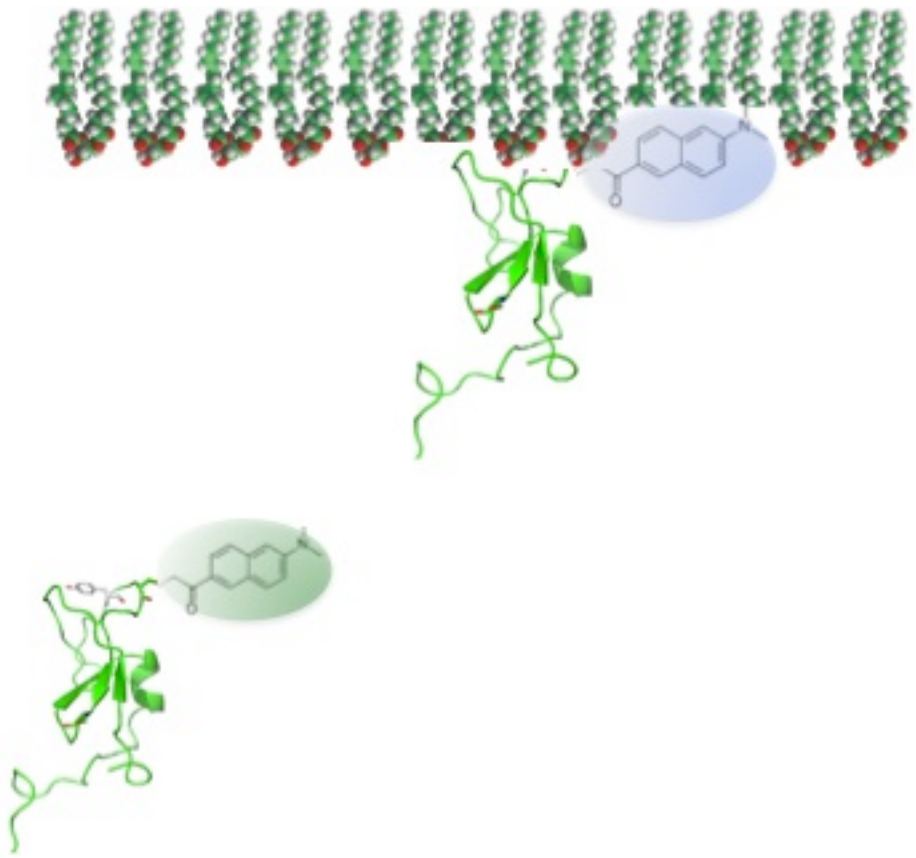

Figure 21. Lipid sensor labeled with environment sensitive dye (ESD)

Lipid sensors labeled with ESD change their emission spectra when bound to the lipid membrane.

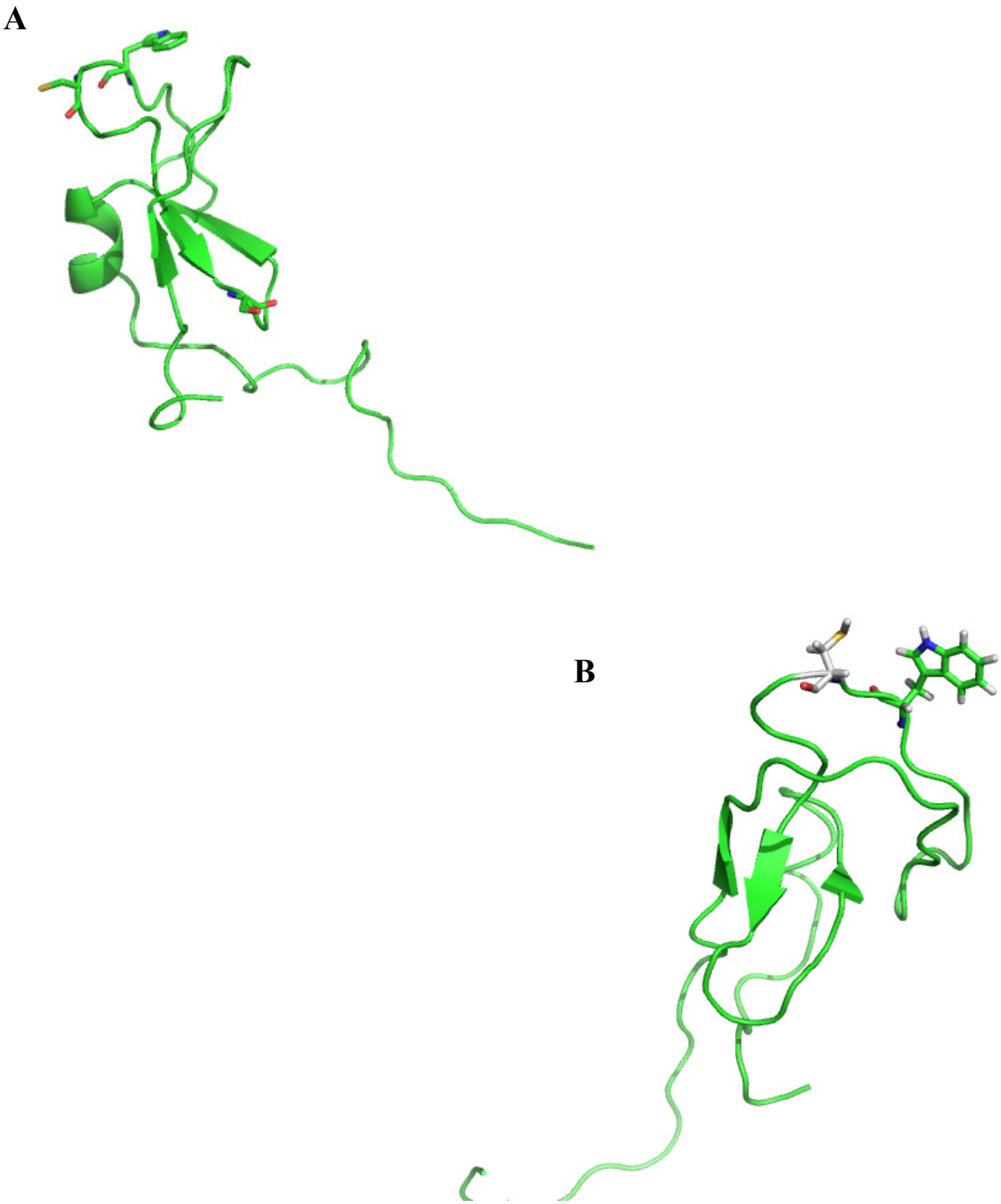

Figure 22. Structures of DAG sensor candidates

a) BRP+Y123W, b) PKCθ C1ab (mutations), only C1b is shown

of the labeled sensor. Two candidates, BRP+Y123W and PKCθ C1ab (Figure 22), demonstrated significantly increased binding affinity.

3. 2. Spectral emission shift of a sensor upon lipid binding

To check the capability of being used for DAG quantification, we first measured the change in fluorescence emission of DAG-DAN sensor upon membrane binding by spectrofluorometry. As shown in Figure 23, DAG-DAN demonstrated a significant blue-shift with a maximal increase in emission intensity (F) at 450 nm (F450) upon binding to large unilamellar vesicles (LUV) with varying composition of DAG; i.e., POPC/POPS/DAG (80-x:20:x). We measured a blue shift against LUVs containing only POPC/POPS (80:20) as a control and it indicated a negligible increase and no shift of the fluorescent signal. This again demonstrated high specificity of our sensor. DAG-DAN also exhibited increase of emission at 450nm (F450) corresponding to increase of total amount of vesicles with fixed DAG mol% (not shown). The DAG concentration can be determined by ratiometric analysis at two wavelengths (Figure 23). Since we need to know the exact concentration of the sensor in a single wavelength measurement, which can be challenging to identify in *in vivo* experiments, we decided to apply ratiometric approach for all following data analysis.

We performed calibration for original DAG sensor (BRP-DAN) and both mutants (Y123W-PKCγ C1b and Y123W-PKCθ-C1a+C1b). The standard calibration curves showed that the second generation of mutants gives the lower K_d values (Figure 24). This results confirms that Trp residue is crucial in lipid –protein binding and the presence of this aromatic residue enhances the binding affinity of the domain [47, 76, 77]

A

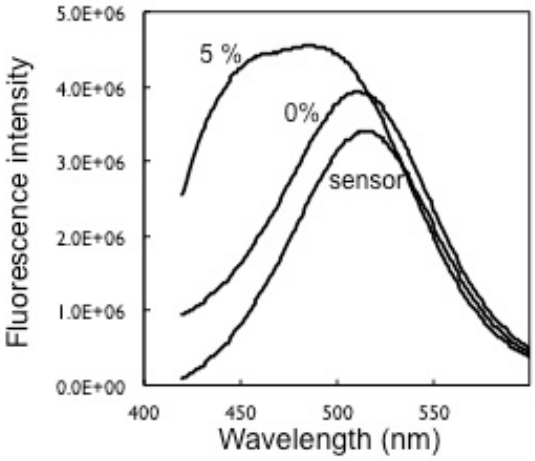

B

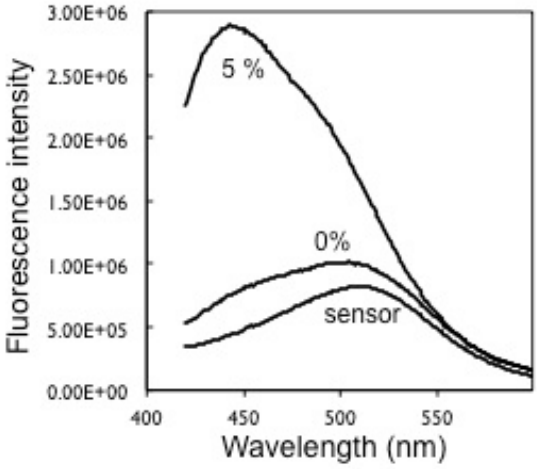

C

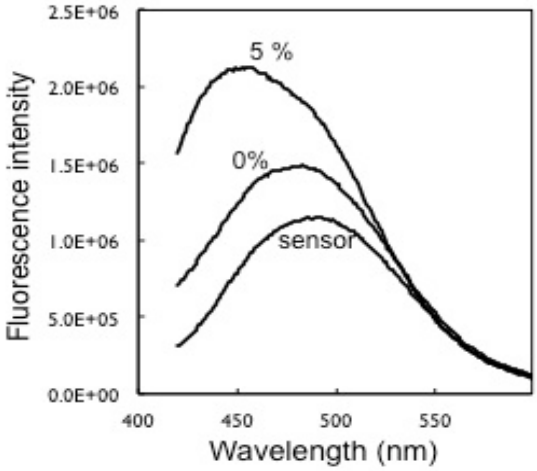

Figure 23. Spectral properties of DAG sensors

a–c) Spectral properties of DAG sensors. Fluorescence emission spectra of BRP-DAN (a), PKCγC1b-Y123-DAN (b) and PKCΘC1ab-Y123W-DAN (c) measured spectro-fluorometrically with large lipid vesicles containing (PC:PS:DAG 80-x:20:x) where x indicates mole% of DAG. The excitation wavelength was 380 nm. All exhibited a dramatic blue shift upon DAG binding. 20mM Tris buffer, pH 7.4, containing 0.16M KCl was used for all measurements.

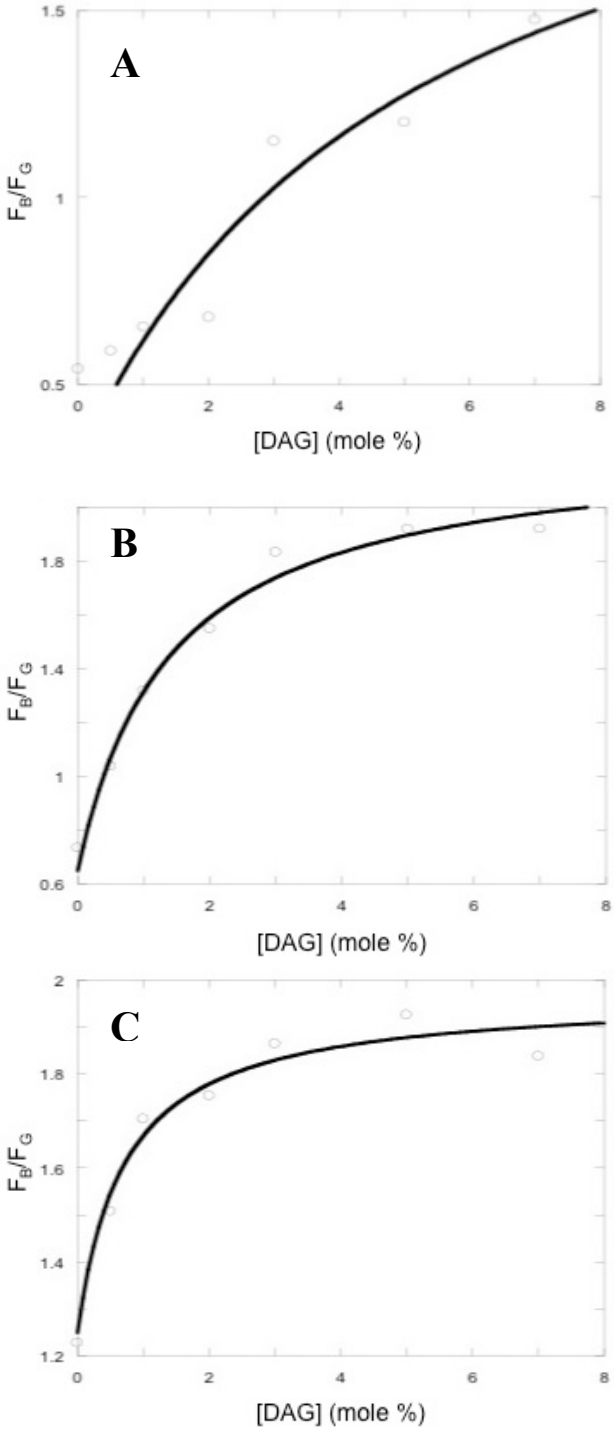

Figure 24. Standard curves for quantification of DAG using DAG sensors by fluorometry

a-c) Ratiometric calibration curves of DAG sensors: (a) BRP-DAN, (b) PKCγC1b-Y123-DAN and (c) PKCΘC1ab-Y123W-DAN. The DAG sensors were screened using a two-photon microscope in the presence of PC/PS/DAG (80-x:20:x) GUVs. Obtained data was fit using the equation $F_B/F_G=(F_B/F_G)_{max}/(1+K_d/[DAG])+C$ by nonlinear least-squares. The calibration curves are constructed using K_d,$(F_B/F_G)_{max}$, and C values. F_B and F_G indicate fluorescence intensities of the blue and green channels, respectively. K_d is the equilibrium dissociation constant (in mole%), $(F_B/F_G)_{max}$ is the highest calculated F_B/F_G value, and C the arbitrary parameter. A blue channel represents a membrane-bound sensor meanwhile a green channel gives information about a membrane-bound as well as a free sensor. 20 mM Tris buffer, pH 7.4, 0.16 M KCl was used for all calibration experiments.

3.3. Determination of DAG on GUV by Fluorescence Microscopy

To calibrate the DAG-DAN sensors for cellular DAG quantification, we then performed giant unilamellar vesicles (GUV) binding assay using two-photon microscopy. We collected fluorescence intensities measured in photon counts in the blue channel (F_B; 436 ± 10 nm band pass filter) and the green channel (FG; 525 ± 25 nm band pass filter) when DAG-DAN was added to the solution of GUV with the composition of POPC/POPS/DAG (80-x:20:x with x = 0-5 mol%)) (Figure 25). The GUVs containing different mol% of DAG were added into the wells that contained DAG-DAN which was mixed well, and then 10 frames of the image was collected in both channels by the point-scanning two-photon microscope. The averaged images from both green (fluorescence signal at 520 nm) and blue (fluorescence intensity at 450 nm) channels were analyzed and the photon counts of each pixel were extracted by MATLAB software. We applied the second copy of the same averaged image to create a mask of the GUV membrane using Photoshop. This step allows us to isolate the signal coming from the vesicle membrane and eliminate the noise. Then the mask and the original image are multiplied by corresponding pixels in MatLab. The total photon count from the membrane was normalized by total number of pixels in order to get the value of photon count per pixel (average photon count value). The ratio of average photon count from the blue channel to average photon count of the green channel was plotted versus known mol% DAG. We applied the obtained calibration curves to quantify concentration of DAG on plasma membrane surface. Here, we converted mol% of DAG to the surface concentration of this lipid. The surface concentration of DAG was calculated from the experimentally found DAG mol% and the approximated size of diacylglycerols. Because of ratiometric analysis, the ratio between fluorescence signal in blue and green channels is independent of lipid sensor concentration and stays constant even at the highest [DAG]

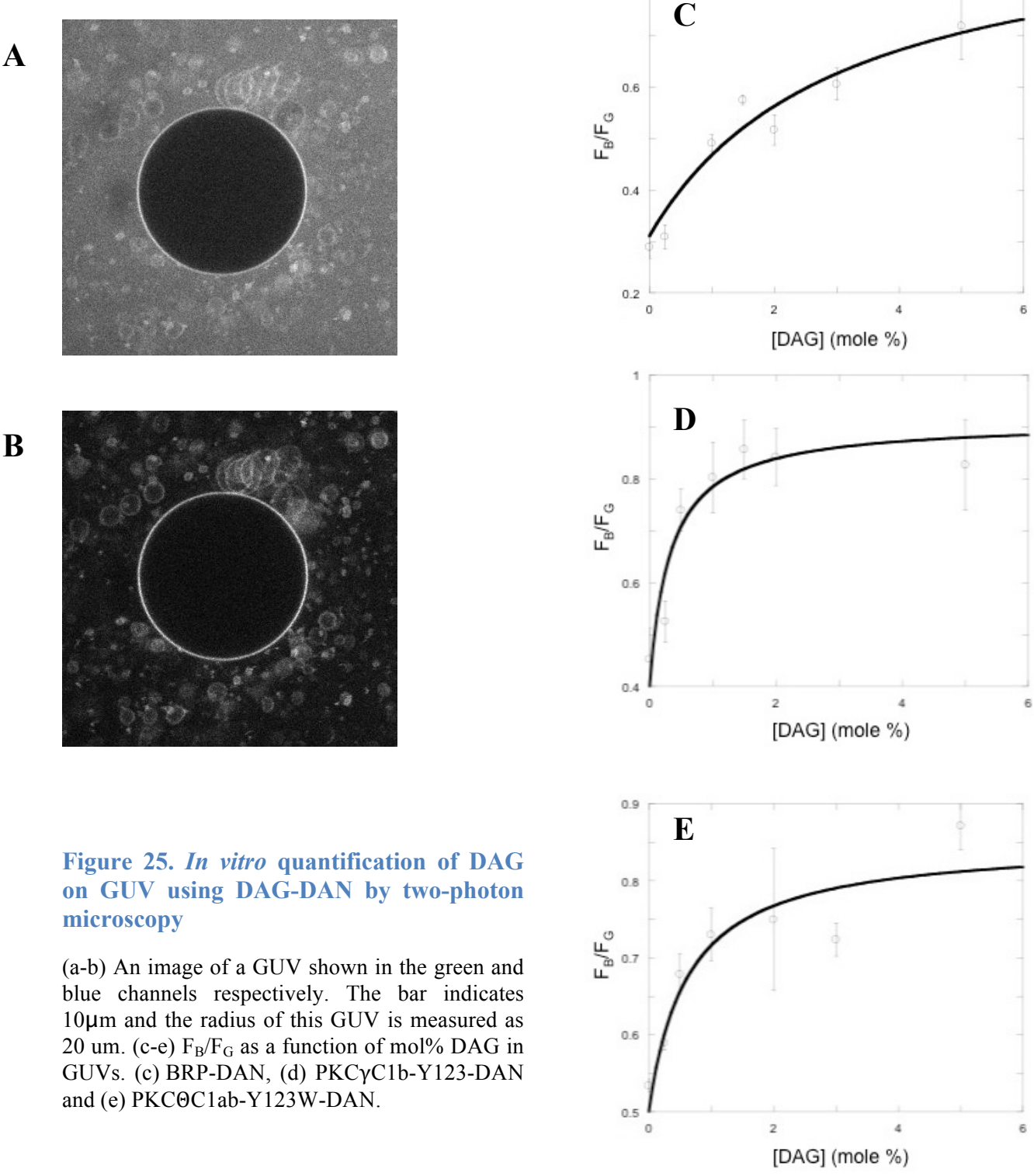

Figure 25. *In vitro* quantification of DAG on GUV using DAG-DAN by two-photon microscopy

(a-b) An image of a GUV shown in the green and blue channels respectively. The bar indicates 10μm and the radius of this GUV is measured as 20 um. (c-e) F_B/F_G as a function of mol% DAG in GUVs. (c) BRP-DAN, (d) PKCγC1b-Y123-DAN and (e) PKCΘC1ab-Y123W-DAN.

employed, indicating that the ratiometric analysis can be used effectively for DAG quantification in vivo without concern about challenging determination of the protein concentration. The resulting (F_B/F_G) versus [DAG] (Figure 25) calibration curves were used for ensuing DAG quantification in GUVs and in mammalian cells.

3.4. Detection of DAG dynamics by Fluorescence Microscopy

The concentration of DAG on GUV was determined by the ratiometric method using molecular sensor, DAG-DAN. This approach allowed us to quantify the amount of DAG *in vitro* with a good precision*;* therefore, we tested the feasibility of the developed sensor in the living cells.

We loaded DAG-DAN into mammalian cells, including Hela, HEK and NIH 3T3 cells, by microinjection for *in vivo* imaging and determined cellular [DAG] by ratiometric analysis. The fluorescence signal in the green channel representing DAG-bound as well as free DAG-DAN demonstrates that this lipid biosensor is delivered into cells and well-distributed in the cytosol and PM. In contrast, the blue channel signal representing DAG-bound sensor shows that cellular DAG is highly enriched in the cytosol, in particularly in consistent with previous reports (Figure 26). When the second generation mutant (PKCγC1b-Y123-DAN and PKCϴC1ab-Y123W-DAN) improved DAG affinity was injected, it was directly localized on the plasma membrane showing that the both mutants exhibit higher affinity to DAG and can be used for detection of basal level of this lipid.

Using the GUV calibration curve (Figure 25) we calculated spatiotemporal concentration of DAG in NIH 3T3 cells and it showed dramatic local heterogeneity in the plasma membrane at a given time (Figure 26). However, the heterogeneous spatial distribution of DAG quickly fluctuated over time (Figure 26) and, consistently, the time-averaged [DAG] displayed relatively homogenous spatial distribution) with an average of 0.5%.

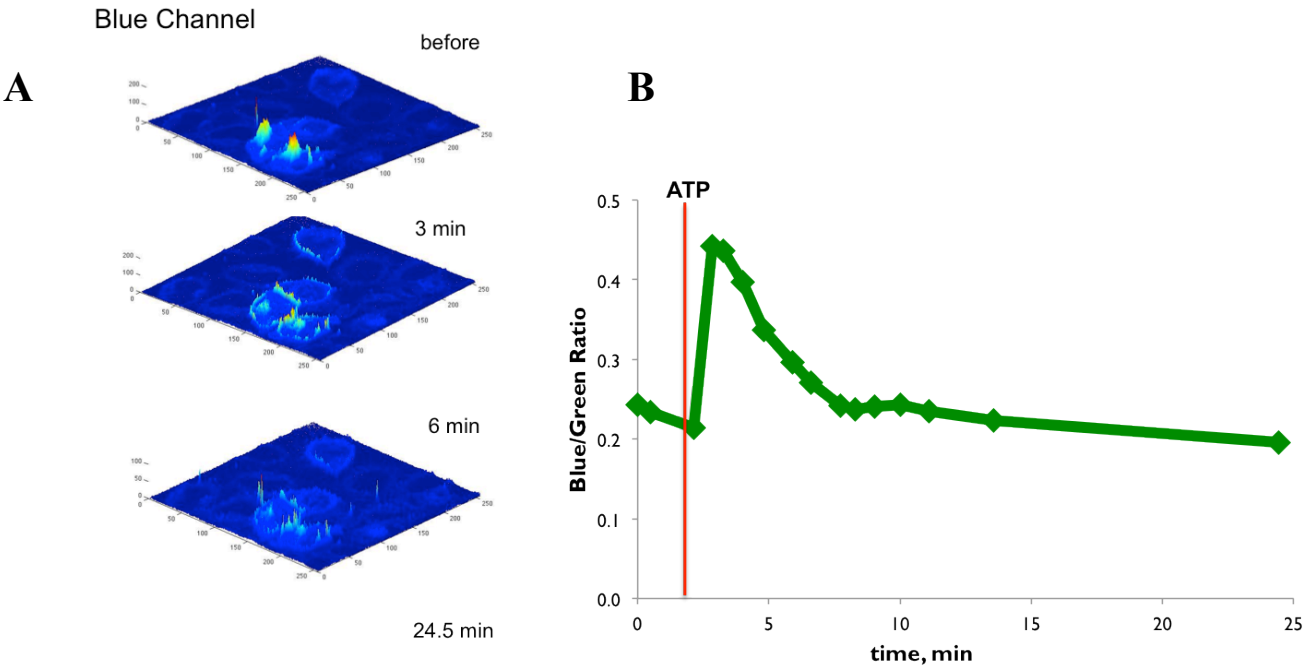

Figure 26. *In situ* quantification of DAG in NIH 3T3 cells by the sensor

(a) A blue channel image of a representative cell showing relatively random cytosolic distribution of the DAG-DAN sensor right after microinjection, 3min, 6min and 24.5min after ATP treatment. (b) The time courses of spatially averaged [DAG] in the plasma membrane upon 100 uM ATP treatment.

3.5. Red labeling

The lipid signaling is a complex process where lipid molecules not only transduce signal through interactions with proteins but also tightly regulate the location and amount of specific lipid by metabolic reactions. Contemporaneous determination and quantification of several related lipids using ratiometric approach allows better understanding of the correlation between key lipids in a living cell. Orthogonal quantification of two lipids requires biosensors that enable robust binary ratiometric analysis. The small number of amphipathic ESDs makes the generation of lipid biosensors very challenging. Thus we looked for the ESD that might be employed with widely used thiol-reactive amphipathic ESD, DAN. The best ESD choice would be an amphipathic fluorophore that can be used in combination with DAN and demonstrate a red-to-orange spectral shift binding to a specific lipid, which enables successful separation of emission signal. A comprehensive screening of known red fluorescent dyes shows that Nile Red has a required qualities and can be successfully modified for the use of thiol-alkene labeling. Although derivatives of Nile Red have very limited water solubility and as a result have low labeling efficiencies, affect the protein structure, its stability, and lipid-binding, these difficulties can be solved by a deep analysis of the structure and synthesis of cysteine-specific Nile Red derivatives with improved characteristics. Because of the unique the ENTH domain structure, this domain was chosen for development of the first red-labeled ratiometric sensor. The ENTH has unstructured region in N-terminal, which undergoes the conformational changes and forms α-helix when it binds to PI(4,5)P2 (Figure 27). This property allows observing significant environmental change; therefore, it enables to improve the spectral properties of the labeled sensor.

The first-generation fluorophore NR1 exhibited suitable spectral characteristics, yet its water solubility remained low leading to a low protein-labeling efficiency. Hence, in the second generation, NR2 (bisacrylate) and NR3 (monoacrylate), extra hydroxyl group were introduced to the linker with a purpose of increasing the solubility in water. Out of synthesized derivatives, NR3 offered the greatest labeling efficiency to the ENTH that has been successfully employed in the past as the PIP2 sensor. The NR3-labeled ENTH (ENTH-NR3) demonstrated desired characteristics, containing low aggregation as well as nonspecific interactions with other lipids and glass surface. In addition, ENTH-NR3 exhibited a significant PIP2 concentration-dependent spectral shift and a large fluorescent signal increase when it bound to PIP2-containing vesicles (Figure 28). This sensor was tested in vivo by injecting ENTH-NR3 to NIH 3T3 cells and gave a satisfactory result (Figure 28). A minimal spectral overlap between ENTH-NR3 and ENTH-DAN (Figure 19) suggests that DAN and NR3 may be used together for dual lipid measurements.

Besides Nile Red and its derivatives we tested other ESDs that potentially can be used in long-wavelength region in ratiometric analysis (Figure 32). We found several promising hits, which enhance blue shift and dramatic fluorescence intensity increase with a decrease of polarity of the surroundings. These dyes showed a desired specificity to PI(4,5)P2 in *in vitro* experiments but were unsuccessful in live cell imaging (data not shown).

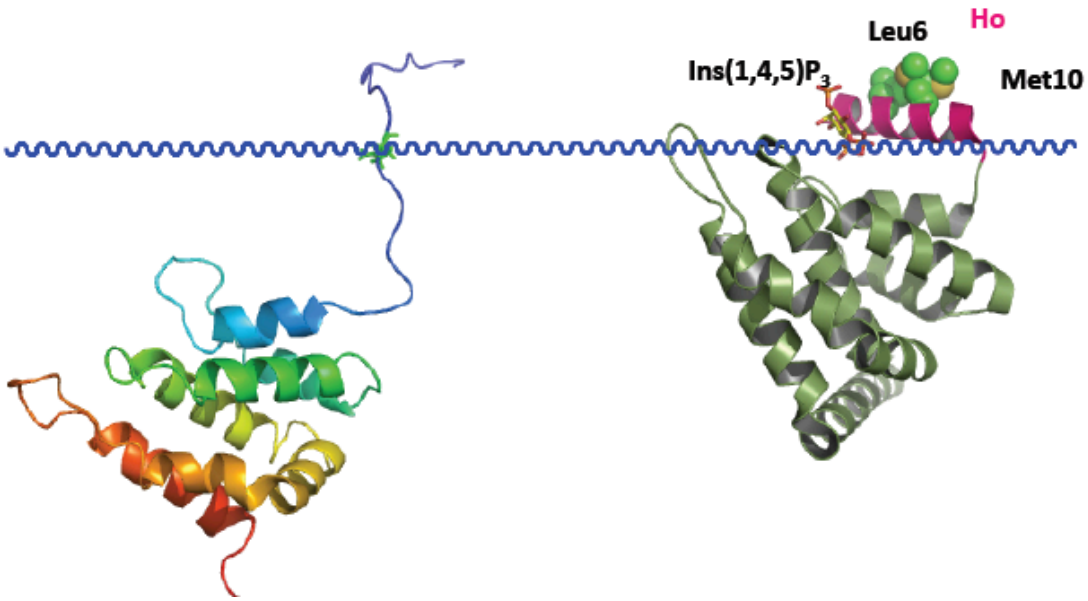

Figure 27. Binding of ENTH domain to the plasma membrane

PI(4,5)P2 binding induces conformational changes and membrane penetration of ENTH domain.

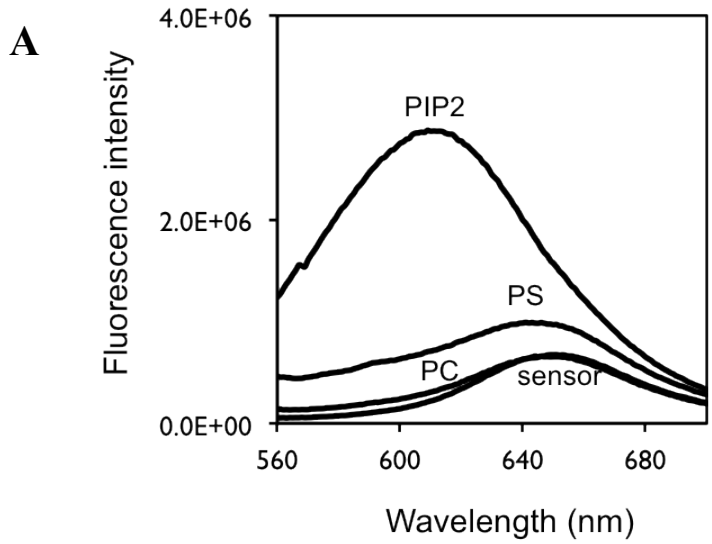

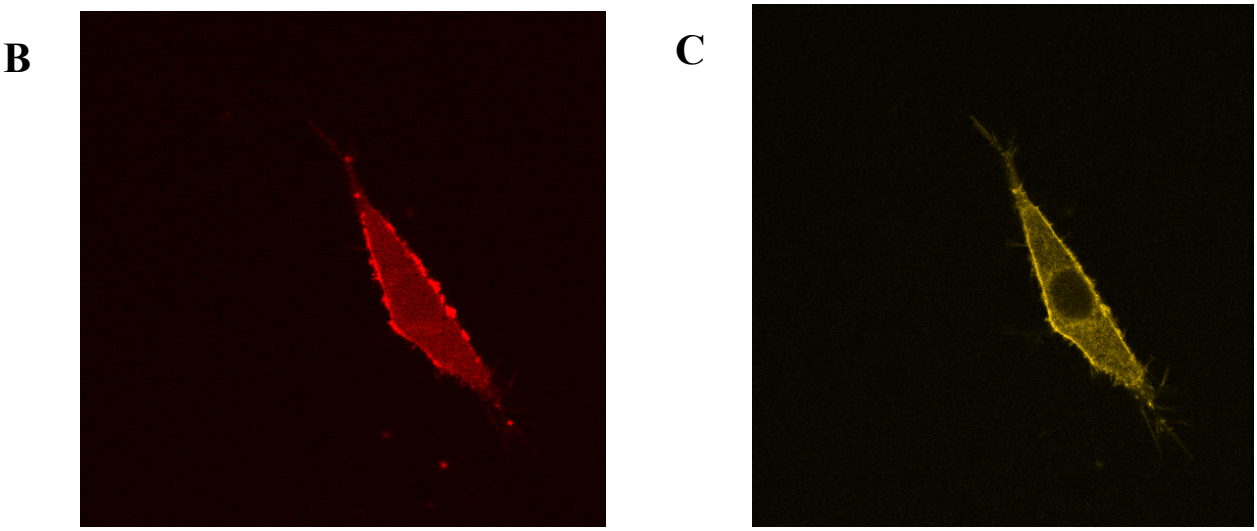

Figure 28. ENTH-NR3

(a) Emission spectrum of ENTH-NR3 sensor. (b-c) Images of ENTH-NR3 sensor registered in red (b) and yellow(c) channels. The PIP2 sensor was injected to NIH 3T3 cells.

3.6. Simultaneous quantification of two cellular lipids

In a living cell numerous signaling lipids are functionally and metabolically connected to each other. Moreover, a quantity of the same lipid can differ drastically between inner and outer leaflets of a cellular membrane. This distribution allows performing distinct cellular functions including the tightly regulated trans-bilayer asymmetry of lipids in the PM. Therefore an innovative strategy is required to accomplish orthogonal accurate determination of concentrations of multiple lipids at the same cellular membrane. To make a progress in solving this task, we elaborated a new approach for simultaneous quantification of two lipids in living cells. As described earlier, DAN and NR3 are dyes, which are sensitive to a polarity change, can be used for protein labeling and also have a good spectral separation.

To test this strategy, we chose three different pairs of lipid sensors: PS-NR3 – PS-DAN, PIP2-DAN – PIP3-NR3 and DAG-DAN – PIP2-NR3.

First, we constructed NR3- and DAN-labeled PS sensors for simultaneous quantification of the PS concentrations in inner and outer leaflets of the PM. PS is known as one of major lipids of PM and is mainly detected in the cytosolic leaflet of the PM under physiological conditions (Figure 29). It has been reported in literature numerously that PS translocates to the outer membrane layer during apoptosis (Figure 29). Contemporary, the information about the distribution and spatiotemporal dynamics of PS across the PM under normal conditions and during apoptosis is greatly limited because present optical imaging techniques forbid from simultaneous quantification of PS in the both leaflets of the cellular membrane.

To engineer PS sensors for each leaflet of the PM, we use the lactadherin C2 domain (LactC2), well known for its high binding affinity and specificity to PS and therefore widely employed as the PS probe for semi-quantitative measurements. We introduced a single cysteine residue in its

membrane-binding surface and labeled it with NR3 and DAN to acquire PS-NR3 and PS-DAN, respectively. Both PS-DAN and PS-NR3 showed characteristic spectral changes upon concentration-dependent manner binding to lipid vesicles containing PS. Then we performed *in vitro* ratiometric calibrations using GUVs with different PS content; after that we microinjected PS-DAN into NIH 3T3 cells and added PS-NR3 to the medium. To monitor the trans-membrane dynamics of PS we initiated the cell apoptosis using 1 μM doxorubicin treatment, and imaged PS-NR3 and PS-DAN bound to the PM at the same time by a four-channel two-photon microscope accompanied by two femtosecond-pulsed lasers. Because engineered PS sensors do not undergo the transbilayer movement, we could successfully separate the signals coming from each leaflet of the PM bilayer by examining fluorescence signals from four optical channels in situ [65]. The apoptosis study shows a clear local heterogeneity of PS in the outer layer of the PM. The described finding indicates that PS local enrichment exceeds a threshold value in that layer of the membrane and could form patches for the recognition of apoptotic cells by phagocytes such as it was shown for PIP2. Moreover, we observed a strong correlation between decrease of PS concentration in the inner PM and its increase in the outer PM. This relationship supports the hypothesis that the PS concentration is elevated due to a direct trans-bilayer translocation of PS. These results indicate the usefulness of the novel lipid sensor methodology as well as provide a new insight on the trans-bilayer translocation of PS and its lateral fluctuation. This ratiometric lipid quantification can be used for in situ detection and calculation of the content of other lipids including PIP2-PIP3, PS-PIP3 and DAG-PIP2. These studies could shed light on the location-specific and the trans-bilayer dynamics functions of many essential cellular lipids.

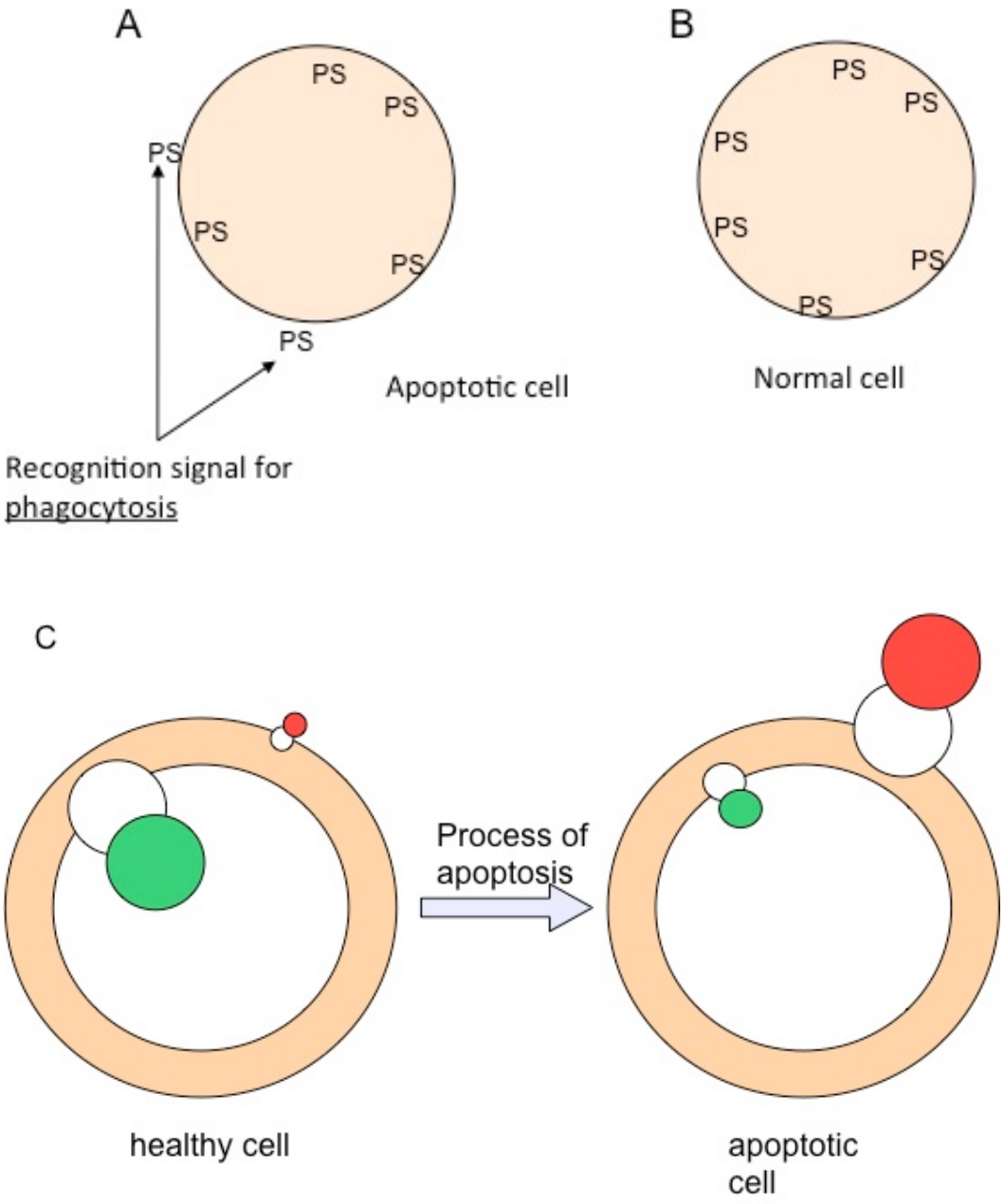

Figure 29. Schematic representation of simultaneous detection and quantification of PS in inner and outer PM

(a-b) During the apoptosis PS from the inner surface of the cellular membrane (b) relocates to the outer surface (a). (c) Scheme of apoptosis. PS is monitored by PS-DAN (microinjected; shown green) and PS-NR3 (added to the cellular media; shown red) in the inner and outer PM, respectively.

A novel lipid sensor methodology allowed us to perform simultaneous quantification of two metabolically linked signaling lipids, PIP_2 and phosphatidylinositol-3,4,5-trisphosphate (PIP_3). We were able to quantified PIP_2 and PIP_3 simultaneously in different mammalian cells using orthogonal sensors for PIP_2 and PIP_3. This experiment was outside of the current thesis, therefore the detailed description can be found in the original paper [65].

In this study, we illustrate the practicability of the novel methodology of simultaneous in situ quantification of two lipid pools in living mammalian cells. The described technique also demonstrates that orthogonal dual lipid quantification yields physiologically crucial details and novel perception unobtainable by current methodologies. Taking all together, this method gives a technical advantage toward understanding of complex lipid-mediated cell regulation.

3.7. DAG flip-flop

The chemical composition of the eukaryotic plasma membrane is asymmetric [11]. The cellular membranes are made of lipid bilayers where lipids are tightly packed next to each other. The outer membrane layer (outer leaflet) significantly differs from the inner leaflet of the membrane by lipid composition. These two layers can also be distinguished from each other by their lipid phase state and therefore cellular function. Lipids of the exterior leaflet of cellular PM form liquid-disordered (l_d) and phase-segregated liquid-ordered (l_o) structures whereas the interior leaflet has a composition that does not form and domains in vitro, whereas [12, 78, 79].

It is well known that some lipids such as ceramide and DAG are engaged in a quick transmembrane movement, moreover they often initiate flip-flop of other members of membrane molecules (Figure 30). The basal level of these lipids in cellular membranes is usually low; however it might be increased locally by 100 times by specific agonist activation [9-11, 46, 80, 81].

To investigate the phenomena of the transbilayer motion we determine an intracellular basal level of DAG as well as induced by ATP using DAG sensor (described in Section 3.4) (Figure 25). The result showed that the basal level of DAG at PM is 0.5% or below then after PI-PLC activation the concentration can reach 5-7%.

To identify the amount of DAG on the extracellular leaflet of PM we treated cells with DAG sensor by adding the sensor directly to the cell media. The preliminary data showed that there is a significant amount of DAG on outer membrane Figure 31. We might speculate that some DAG molecules flip-flop from outer to inner PM when its presence is required for any DAG-initiated pathways. To explore the correlation of DAG levels between two PM leaflets, we could use dual-sensor imaging as described above (Section 3.6) where one DAG sensor labeled with DAN is injected and another DAG sensor labeled with NR3 is added to the cell media. The challenging part is that DAG-NR3 does not show the specificity to DAG and actively binds to other lipids such as PC and PS (data not shown). In order to obtain working red-labeled DAG sensor, further investigation has to be done.

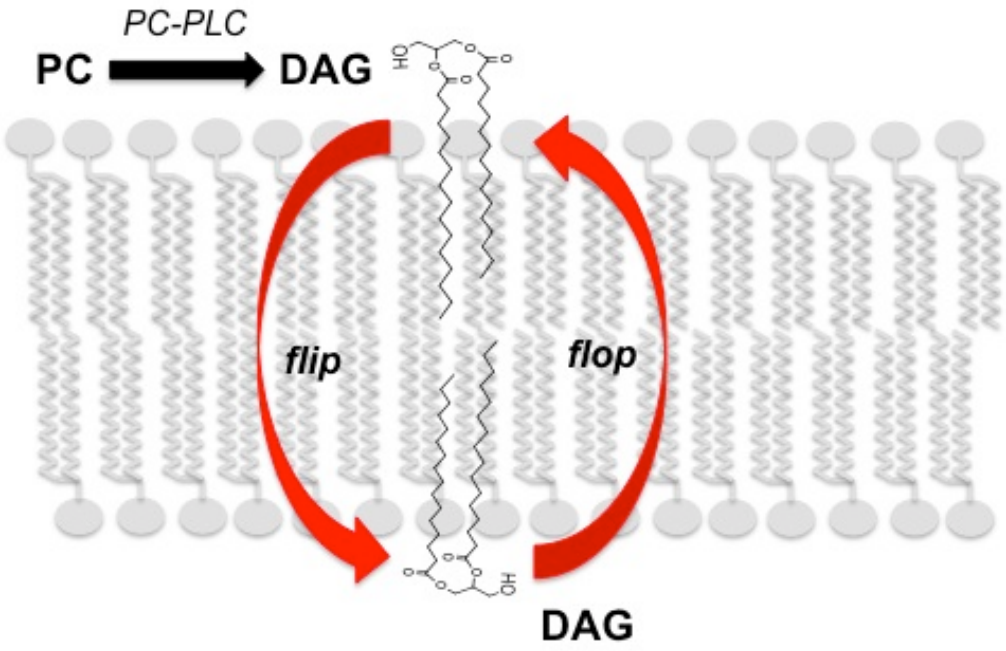

Figure 30. DAG transbilayer movement or flip-flop

The scheme represents the transbilayer movement (or flip-flop) of DAG between the two leaflets of the plasma membrane. After hydrolysis of PC by the PC-specific phospholipase C on the outer leaflet, movement of the produced DAG from the outer to the inner leaflet can be visualized by the membrane translocation of the fluorescent DAG-specific probe, EYFP-C1AB expressed in the cytosol. SM, sphingomyelin; GLPs, glycerophospholipids; PC, phosphatidyl choline.

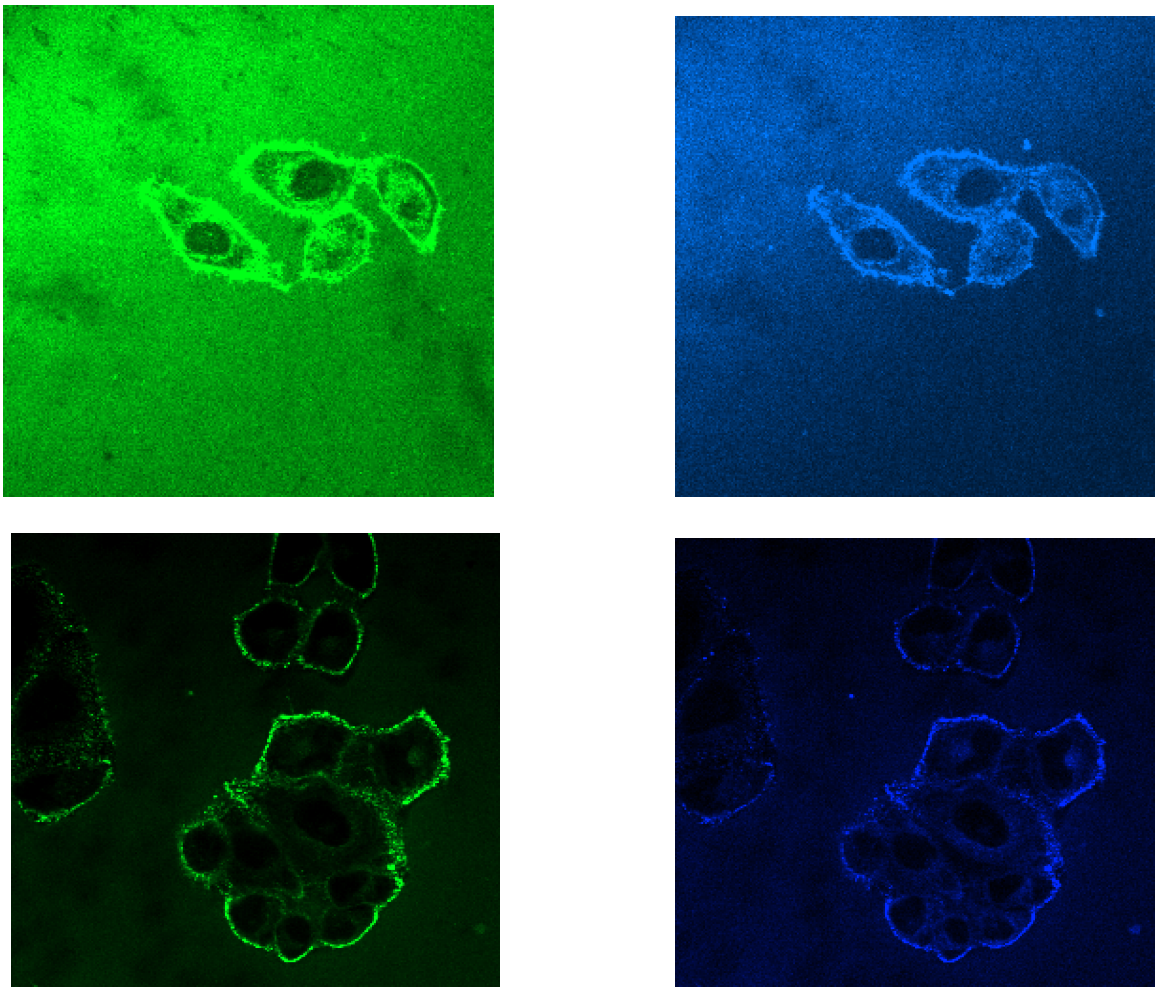

Figure 31. Detection of DAG in the inner PM in NIH 3T3 cells.

Two-channel images of NIH 3T3 cells after media-added DAG sensor. DAG in the outer PM was monitored by green and blue channels and the media-added sensor. Blue channel depicts the membrane bound sensor whereas green channel shows the membrane bound plus free sensors.

5. Cited literature

1. Wang, X.M., *Lipid signaling.* Current Opinion in Plant Biology, 2004. **7**(3): p. 329-336.
2. Escriba, P.V., et al., *Membranes: a meeting point for lipids, proteins and therapies.* Journal of Cellular and Molecular Medicine, 2008. **12**(3): p. 829-875.
3. Lemmon, M.A., *Membrane recognition by phospholipid-binding domains.* Nature Reviews Molecular Cell Biology, 2008. **9**(2): p. 99-111.
4. Testerink, C. and T. Munnik, *Molecular, cellular, and physiological responses to phosphatidic acid formation in plants.* Journal of Experimental Botany, 2011. **62**(7): p. 2349-2361.
5. Hughes, Z.E. and R.L. Mancera, *Molecular dynamics simulations of mixed DOPC-beta-sitosterol bilayers and their interactions with DMSO.* Soft Matter, 2013. **9**(10): p. 2920-2935.
6. Subramanian, D., et al., *Activation of membrane-permeant caged PtdIns(3)P induces endosomal fusion in cells.* Nature Chemical Biology, 2010. **6**(5): p. 324-326.
7. D'Souza, K. and R.M. Epand, *Enrichment of phosphatidylinositols with specific acyl chains.* Biochimica Et Biophysica Acta-Biomembranes, 2014. **1838**(6): p. 1501-1508.
8. Schultz, C., *Challenges in studying phospholipid signaling.* Nature Chemical Biology, 2010. **6**(7): p. 473-475.
9. Contreras, F.X., et al., *Transbilayer (flip-flop) lipid motion and lipid scrambling in membranes.* Febs Letters, 2010. **584**(9): p. 1779-1786.
10. Wei, C. and A. Pohorille, *Flip-Flop of Oleic Acid in a Phospholipid Membrane: Rate and Mechanism.* Journal of Physical Chemistry B, 2014. **118**(45): p. 12919-12926.
11. Ogushi, F., et al., *Rapid flip-flop motions of diacylglycerol and ceramide in phospholipid bilayers.* Chemical Physics Letters, 2012. **522**: p. 96-102.
12. Parisio, G., M.M. Sperotto, and A. Ferrarini, *Flip-Flop of Steroids in Phospholipid Bilayers: Effects of the Chemical Structure on Transbilayer Diffusion.* Journal of the American Chemical Society, 2012. **134**(29): p. 12198-12208.
13. Emoto, K., et al., *Local change in phospholipid composition at the cleavage furrow is essential for completion of cytokinesis.* Journal of Biological Chemistry, 2005. **280**(45): p. 37901-37907.
14. Wakelam, M.J.O., T.R. Pettitt, and A.D. Postle, *Lipidomic analysis of signaling pathways*, in *Lipidomics and Bioactive Lipids: Mass-Spectrometry-Based Lipid Analysis*, H.A. Brown, Editor. 2007. p. 233-246.
15. Atilla-Gokcumen, G.E., et al., *Dividing Cells Regulate Their Lipid Composition and Localization.* Cell, 2014. **156**(3): p. 428-439.
16. Hurley, J.H. and T. Meyer, *Subcellular targeting by membrane lipids.* Current Opinion in Cell Biology, 2001. **13**(2): p. 146-152.
17. DiPilato, L.M. and J. Zhang, *Fluorescent protein-based biosensors: resolving spatiotemporal dynamics of signaling.* Current Opinion in Chemical Biology, 2010. **14**(1): p. 37-42.
18. Di Paolo, G. and P. De Camilli, *Phosphoinositides in cell regulation and membrane dynamics.* Nature, 2006. **443**(7112): p. 651-657.
19. Yoon, Y., et al., *In situ quantitative imaging of cellular lipids using molecular sensors.* Nature Chemistry, 2011. **3**(11): p. 868-874.

20. Antal, C.E. and A.C. Newton, *Spatiotemporal Dynamics of Phosphorylation in Lipid Second Messenger Signaling.* Molecular & Cellular Proteomics, 2013. **12**(12): p. 3498-3508.
21. Idevall-Hagren, O. and P. De Camilli, *Detection and manipulation of phosphoinositides.* Biochimica et Biophysica Acta (BBA) - Molecular and Cell Biology of Lipids, 2015. **1851**(6): p. 736-745.
22. Morris, M.C., *Fluorescent biosensors — Probing protein kinase function in cancer and drug discovery.* Biochimica et Biophysica Acta (BBA) - Proteins and Proteomics, 2013. **1834**(7): p. 1387-1395.
23. Tamura, T. and I. Hamachi, *Recent Progress in Design of Protein-Based Fluorescent Biosensors and Their Cellular Applications.* Acs Chemical Biology, 2014. **9**(12): p. 2708-2717.
24. Ibraheem, A. and R.E. Campbell, *Designs and applications of fluorescent protein-based biosensors.* Current Opinion in Chemical Biology, 2010. **14**(1): p. 30-36.
25. Wang, H., E. Nakata, and I. Hamachi, *Recent Progress in Strategies for the Creation of Protein-Based Fluorescent Biosensors.* Chembiochem, 2009. **10**(16): p. 2560-2577.
26. Ohba, Y., et al., *Fluorescent Protein-Based Biosensors and Their Clinical Applications*, in *Fluorescence-Based Biosensors: From Concepts to Applications*, M.C. Morris, Editor. 2013. p. 313-348.
27. Welch, C.M., et al., *Imaging the coordination of multiple signalling activities in living cells.* Nature Reviews Molecular Cell Biology, 2011. **12**(11): p. 749-756.
28. Balla, T., *Phosphoinositides: Tiny lipids with giant impact on cell regulation.* Physiological Reviews, 2013. **93**(3): p. 1019-1137.
29. Wakelam, M.J.O., *The uses and limitations of the analysis of cellular phosphoinositides by lipidomic and imaging methodologies.* Biochimica et Biophysica Acta - Molecular and Cell Biology of Lipids, 2014. **1841**(8): p. 1102-1107.
30. Kim, Y., et al., *Mass spectrometry based cellular phosphoinositides profiling and phospholipid analysis: A brief review.* Experimental and Molecular Medicine, 2010. **42**(1): p. 1-11.
31. Rusten, T.E. and H. Stenmark, *Analyzing phosphoinositides and their interacting proteins.* Nature Methods, 2006. **3**(4): p. 251-258.
32. Nasuhoglu, C., et al., *Nonradioactive analysis of phosphatidylinositides and other anionic phospholipids by anion-exchange high-performance liquid chromatography with suppressed conductivity detection.* Analytical Biochemistry, 2002. **301**(2): p. 243-254.
33. Kraft, M.L. and H.A. Klitzing, *Imaging lipids with secondary ion mass spectrometry.* Biochimica et Biophysica Acta - Molecular and Cell Biology of Lipids, 2014. **1841**(8): p. 1108-1119.
34. Van Den Bogaart, G., et al., *Membrane protein sequestering by ionic protein-lipid interactions.* Nature, 2011. **479**(7374): p. 552-555.
35. Steyer, J.A. and W. Almers, *A real-time view of life within 100 NM of the plasma membrane.* Nature Reviews Molecular Cell Biology, 2001. **2**(4): p. 268-275.
36. Swanson, S.J., et al., *In Vivo Imaging of Ca2+, pH, and Reactive Oxygen Species Using Fluorescent Probes in Plants*, in *Annual Review of Plant Biology, Vol 62*, S.S. Merchant, W.R. Briggs, and D. Ort, Editors. 2011. p. 273-297.

37. Depry, C., S. Mehta, and J. Zhang, *Multiplexed visualization of dynamic signaling networks using genetically encoded fluorescent protein-based biosensors.* Pflugers Archiv-European Journal of Physiology, 2013. **465**(3): p. 373-381.
38. O'Connor, N. and R.B. Silver, *Chapter 16 - Ratio Imaging: Practical Considerations for Measuring Intracellular Ca2+ and pH in Living Cells*, in *Methods in Cell Biology*, S. Greenfield and E.W. David, Editors. 2013, Academic Press. p. 387-406.
39. Jiang, N., et al., *Ratiometric Fluorescence Imaging of Cellular Polarity: Decrease in Mitochondrial Polarity in Cancer Cells.* Angewandte Chemie-International Edition, 2015. **54**(8): p. 2510-2514.
40. Klymchenko, A.S. and Y. Mely, *Chapter Two - Fluorescent Environment-Sensitive Dyes as Reporters of Biomolecular Interactions*, in *Progress in Molecular Biology and Translational Science*, C.M. May, Editor. 2013, Academic Press. p. 35-58.
41. Pawlicki, M., et al., *Two-Photon Absorption and the Design of Two-Photon Dyes.* Angewandte Chemie International Edition, 2009. **48**(18): p. 3244-3266.
42. Ptaszek, M., *Chapter Three - Rational Design of Fluorophores for In Vivo Applications*, in *Progress in Molecular Biology and Translational Science*, C.M. May, Editor. 2013, Academic Press. p. 59-108.
43. Marks, K.M. and G.P. Nolan, *Chemical labeling strategies for cell biology.* Nat Meth, 2006. **3**(8): p. 591-596.
44. Killian, J.A. and G. von Heijne, *How proteins adapt to a membrane-water interface.* Trends in Biochemical Sciences, 2000. **25**(9): p. 429-434.
45. De Matteis, M.A. and A. Godi, *Protein-lipid interactions in membrane trafficking at the Golgi complex.* Biochimica Et Biophysica Acta-Biomembranes, 2004. **1666**(1-2): p. 264-274.
46. Ziemba, B.P. and J.J. Falke, *Lateral diffusion of peripheral membrane proteins on supported lipid bilayers is controlled by the additive frictional drags of (1) bound lipids and (2) protein domains penetrating into the bilayer hydrocarbon core.* Chemistry and Physics of Lipids, 2013. **172**: p. 67-77.
47. Dries, D.R., L.L. Gallegos, and A.C. Newton, *A single residue in the C1 domain sensitizes novel protein kinase C isoforms to cellular diacylglycerol production.* J Biol Chem, 2007. **282**(2): p. 826-30.
48. Borisov, S.M. and O.S. Wolfbeis, *Optical biosensors.* Chemical Reviews, 2008. **108**(2): p. 423-461.
49. Klymchenko, A.S., *Solvatochromic fluorescent dyes as universal tools for biological research.* Actualite Chimique, 2012(359): p. 20-26.
50. Loving, G.S., M. Sainlos, and B. Imperiali, *Monitoring protein interactions and dynamics with solvatochromic fluorophores.* Trends in Biotechnology, 2010. **28**(2): p. 73-83.
51. Demchenko, A.P., et al., *Monitoring biophysical properties of lipid membranes by environment-sensitive fluorescent probes.* Biophysical Journal, 2009. **96**(9): p. 3461-3470.
52. Grimm, J.B., L.M. Heckman, and L.D. Lavis, *The Chemistry of Small-Molecule Fluorogenic Probes*, in *Fluorescence-Based Biosensors: From Concepts to Applications*, M.C. Morris, Editor. 2013. p. 1-34.
53. Haidekker, M.A. and E.A. Theodorakis, *Molecular rotors - Fluorescent biosensors for viscosity and flow.* Organic and Biomolecular Chemistry, 2007. **5**(11): p. 1669-1678.

54. Lukinavičius, G. and K. Johnsson, *Switchable fluorophores for protein labeling in living cells.* Current Opinion in Chemical Biology, 2011. **15**(6): p. 768-774.
55. Reichardt, C., *Solvatochromic dyes as solvent polarity indicators.* Chemical Reviews, 1994. **94**(8): p. 2319-2358.
56. Hwan, M.K., et al., *Two-photon fluorescent turn-on probe for lipid rafts in live cell and tissue.* Journal of the American Chemical Society, 2008. **130**(13): p. 4246-4247.
57. Newton, A.C., *Regulation of the ABC kinases by phosphorylation: protein kinase C as a paradigm.* Biochemical Journal, 2003. **370**: p. 361-371.
58. Khandwal.As and C.B. Kasper, *MEMBRANE STRUCTURE - REACTIVITY OF TRYPTOPHAN, TYROSINE AND LYSINE IN PROTEINS OF MICROSOMAL MEMBRANE.* Biochimica Et Biophysica Acta, 1971. **233**(2): p. 348-&.
59. Kunkel, M.T. and A.C. Newton, *Calcium Transduces Plasma Membrane Receptor Signals to Produce Diacylglycerol at Golgi Membranes.* Journal of Biological Chemistry, 2010. **285**(30): p. 22746-22750.
60. Johnson, J.E., J. Giorgione, and A.C. Newton, *The C1 and C2 domains of protein kinase C are independent membrane targeting modules, with specificity for phosphatidylserine conferred by the C1 domain.* Biochemistry, 2000. **39**(37): p. 11360-11369.
61. Newton, A.C., *Protein kinase C: Structural and spatial regulation by phosphorylation, cofactors, and macromolecular interactions.* Chemical Reviews, 2001. **101**(8): p. 2353-2364.
62. Newton, A.C., *Protein kinase C: poised to signal.* American Journal of Physiology-Endocrinology and Metabolism, 2010. **298**(3): p. E395-E402.
63. Wu-Zhang, A.X. and A.C. Newton, *Protein kinase C pharmacology: refining the toolbox.* Biochemical Journal, 2013. **452**: p. 195-209.
64. Page, B.R., *A new methodology for quantitative and spatiotemporal sensing of key signaling lipids*, 2009, University of Illinois at Chicago: Ann Arbor. p. 136.
65. Liu, S.-L., et al., *Simultaneous In Situ Quantification of Two Cellular Lipid Pools Using Orthogonal Fluorescent Sensors.* Angewandte Chemie-International Edition, 2014. **53**(52): p. 14387-14391.
66. Entenberg, D., et al., *Setup and use of a two-laser multiphoton microscope for multichannel intravital fluorescence imaging.* Nature Protocols, 2011. **6**(10): p. 1500-1520.
67. Hibbs, R.E., T.T. Talley, and P. Taylor, *Acrylodan-conjugated cysteine side chains reveal conformational state and ligand site locations of the acetylcholine-binding protein.* Journal of Biological Chemistry, 2004. **279**(27): p. 28483-28491.
68. Jose, J. and K. Burgess, *Benzophenoxazine-based fluorescent dyes for labeling biomolecules.* Tetrahedron, 2006. **62**(48): p. 11021-11037.
69. Stahelin, R.V., et al., *Contrasting membrane interaction mechanisms of AP180 N-terminal homology (ANTH) and epsin N-terminal homology (ENTH) domains.* Journal of Biological Chemistry, 2003. **278**(31): p. 28993-28999.
70. Kim, Y., et al., *Efficient Site-Specific Labeling of Proteins via Cysteines.* Bioconjugate Chemistry, 2008. **19**(3): p. 786-791.
71. De Rosa, L., et al., *Site-specific protein double labeling by expressed protein ligation: applications to repeat proteins.* Organic & Biomolecular Chemistry, 2012. **10**(2): p. 273-280.

72. Blin, G., et al., *Quantitative analysis of the binding of ezrin to large unilamellar vesicles containing phosphatidylinositol 4,5 bisphosphate.* Biophysical Journal, 2008. **94**(3): p. 1021-1033.
73. Melowic, H.R., et al., *Mechanism of diacylglycerol-induced membrane targeting and activation of protein kinase C theta.* Journal of Biological Chemistry, 2007. **282**(29): p. 21467-21476.
74. Stewart, M.D., et al., *Probing the Determinants of Diacylglycerol Binding Affinity in the C1B Domain of Protein Kinase C alpha.* Journal of Molecular Biology, 2011. **408**(5): p. 949-970.
75. Giorgione, J.R., et al., *Increased membrane affinity of the C1 domain of protein kinase Cdelta compensates for the lack of involvement of its C2 domain in membrane recruitment.* J Biol Chem, 2006. **281**(3): p. 1660-9.
76. Rahman, G.M., et al., *Identification of the activator-binding residues in the second cysteine-rich regulatory domain of protein kinase C theta (PKC theta).* Biochemical Journal, 2013. **451**: p. 33-44.
77. Egea-Jimenez, A.L., S. Corbalan-Garcia, and J.C. Gomez-Fernandez, *The C1B domains of novel PKCepsilon and PKCeta have a higher membrane binding affinity than those of the also novel PKCdelta and PKCtheta.* Biochimica et biophysica acta, 2014. **1838**(7): p. 1898-909.
78. Das, C., M.G. Noro, and P.D. Olmsted, *Fast cholesterol flip-flop and lack of swelling in skin lipid multilayers.* Soft Matter, 2014. **10**(37): p. 7346-7352.
79. Rabinovich, A.L. and A.P. Lyubartsev, *Computer Simulation of Lipid Membranes: Methodology and Achievements.* Polymer Science Series C, 2013. **55**(1): p. 162-180.
80. Dibble, A.R.G., et al., *Lipid lateral heterogeneity in phosphatidylcholine/phosphatidylserine/diacylglycerol vesicles and its influence on protein kinase C activation.* Biophysical Journal, 1996. **71**(4): p. 1877-1890.
81. Perez-Lara, A., et al., *The membrane binding kinetics of full-length PKC alpha is determined by membrane lipid composition.* Biochimica Et Biophysica Acta-Molecular and Cell Biology of Lipids, 2012. **1821**(11): p. 1434-1442.

Chapter III

Concluding remarks

Concluding remarks

All organisms consist of cells, and cells are made of the complex of macromolecules, such as proteins, lipids, carbohydrates, and DNA. Each component plays its own role for survival and regulation of physiological functions in cells. Here we highlighted on lipids, especially diacylglycerol (DAG), and proteins that directly interact with DAG. Lipids are major component of plasma membrane and all other membranes of cellular organelles, such as mitochondria, Golgi, endoplasmic reticulum (ER), and etc. The valuable features of membrane are not only the walls to protect cells but also the regulation of almost all events inside of cells. As a second messenger DAG is a critically important lipid in cellular membranes. There is hardly a membrane-associated molecular event that is not regulated by DAG. The rapid formation, elimination, and conversion of this lipid in specific membrane compartments are ensured with unique localization and regulatory properties. DAG achieves direct signaling effects through the binding of their head groups to cytosolic proteins as well as hydrophobic interactions with acyl chains. In order to understand cellular processes in the cells, the researches should be focused on both dynamic features of lipids and their interacting proteins.

Lipids vary in not only in headgroups but also in the nature of the lipid acyl chains. It is been proved that the acyl chain of lipids plays an important role in a membrane curvature and signal transduction. Changes in the acyl chain composition of lipids can completely change its function and moreover lead to disease. In this work we difference of DAG interaction with the C1 domain depending on degree on unsaturation of the lipid acyl chain. Using fluorescence-quenching assay it is been shown that DAG with a highly unsaturated acyl chain binds tighter to C1 domain comparing with saturated DAG that has just very weak binding. Moreover, our single molecule tracking studies using supported lipid bilayers as a model system and NIH 3T3 cells

explain the kinetic aspect of that binding. Although more unsaturated DAG binds C1 domain tighter it dissociates from the membrane faster than in case of saturated DAG. This founding can explain why unsaturated lipids participate in cell signaling when saturated lipids mainly play a role of bulk lipids. This work provides the new inside about the dynamics of protein-lipid interaction.

Our novel strategy for lipid quantification overcame the limitations that conventional methods have. It is quantitative and cell 'undisruptive' method because the quantification of lipids was carried out using the shifted emission came from only lipid bound sensors by ratiometric analysis. We expect that our method could be extent to other lipid quantification using other lipid binding domains and environment-sensitive probes. We focused on engineering lipid binding domains to have high affinity and selectivity and developing other environment-sensitive dyes with different colors and found NR3. This dye allowed using simultaneous imaging and quantification of two lipids.

We might speculate that some DAG molecules flip-flop from outer to inner PM when its presence is required for any DAG-initiated pathways. To explore the correlation of DAG levels between two PM leaflets, we could use dual-sensor imaging as described above (Section 3.6) where one DAG sensor labeled with DAN is injected and another DAG sensor labeled with NR3 is added to the cell media. The challenging part is that DAG-NR3 does not show the specificity to DAG and actively binds to other lipids such as PC and PS (data not shown). In order to obtain working red-labeled DAG sensor, further investigation has to be done.

VITA

NAME SVETLANA KURILOVA

EDUCATION	2009-present	Ph.D.	University of Illinois at Chicago	CHEM
	2009-2014	M.S.	University of Illinois at Chicago	CHEM
	2003-2008	B.S.	Moscow State University	CHEM

CAREERS	2009-present	PhD Student	Department of Chemistry UIC, Chicago, IL
	2008-2009	Assistant Researcher	Department of Chemistry MSU, Moscow, Russia
TEACHING	2010-present	Teaching Assistant	Department of Chemistry UIC, Chicago, IL

ABSTRACTS **Poster presentation:**

Afsari, H. S., S. Kurilova and W. Cho (2013). "Orthogonal In Situ Quantification of Multiple Cellular Lipids." Faseb Journal 27.

Stec, E., H. S. Afsari, S. Kurilova and W. Cho (2013). "In situ Quantification of Cellular Cholesterol using a Molecular Sensor." Faseb Journal 27.

Kurilova, S., Y. Yoon, P. J. Lee, N. Bhardwaj, H. Lu and W. Cho (2010). "The effect of the sn-2 acyl chain of diacylglycerol on its interaction with C1 domains and its signaling role." Faseb Journal 24.

PUBLICATIONS

Liu, S.-L., R. Sheng, M. J. O'Connor, Y. Cui, Y. Yoon, S. Kurilova, D. Lee and W. Cho (2014). "Simultaneous In Situ Quantification of Two Cellular Lipid Pools Using Orthogonal Fluorescent Sensors." Angewandte Chemie-International Edition 53(52): 14387-14391.

Yao, L.-H., Y. Rao, C. Bang, S. Kurilova, K. Varga, C.-Y. Wang, B. D. Weller, W. Cho, J. Cheng and L.-W. Gong (2013). "Actin Polymerization Does Not Provide Direct Mechanical Forces for Vesicle Fission during Clathrin-Mediated Endocytosis." Journal of Neuroscience 33(40): 15793-15798.

Chen, Y., R. Sheng, M. Kaellberg, A. Silkov, M. P. Tun, N. Bhardwaj, S. Kurilova, R. A. Hall, B. Honig, H. Lu and W. Cho (2012). "Genome-wide Functional Annotation of Dual-Specificity Protein- and Lipid-Binding Modules that Regulate Protein Interactions." Molecular Cell 46(2): 226-237.

Yoon, Y., P. J. Lee, S. Kurilova and W. Cho (2011). "In situ quantitative imaging of cellular lipids using molecular sensors." Nature Chemistry 3(11): 868-874.

Alexander Majouga, D. P., Irina Ananieva, Svetlana Kurilova, Oleg Shpigun, Nikolay Kuz'menko, Nikolay Zyk (2010). "New separation materials based on gold nanoparticles." Journal of Manufacturing Technology Management 21(8): 950-955.

Appendix

Appendix

Table 3. Kd values and fraction of bound C1 domain for polyunsaturated and saturated DAG.

DAG	Relative K_d	Fraction bound
SAG	1	100%
DPG	3	40%

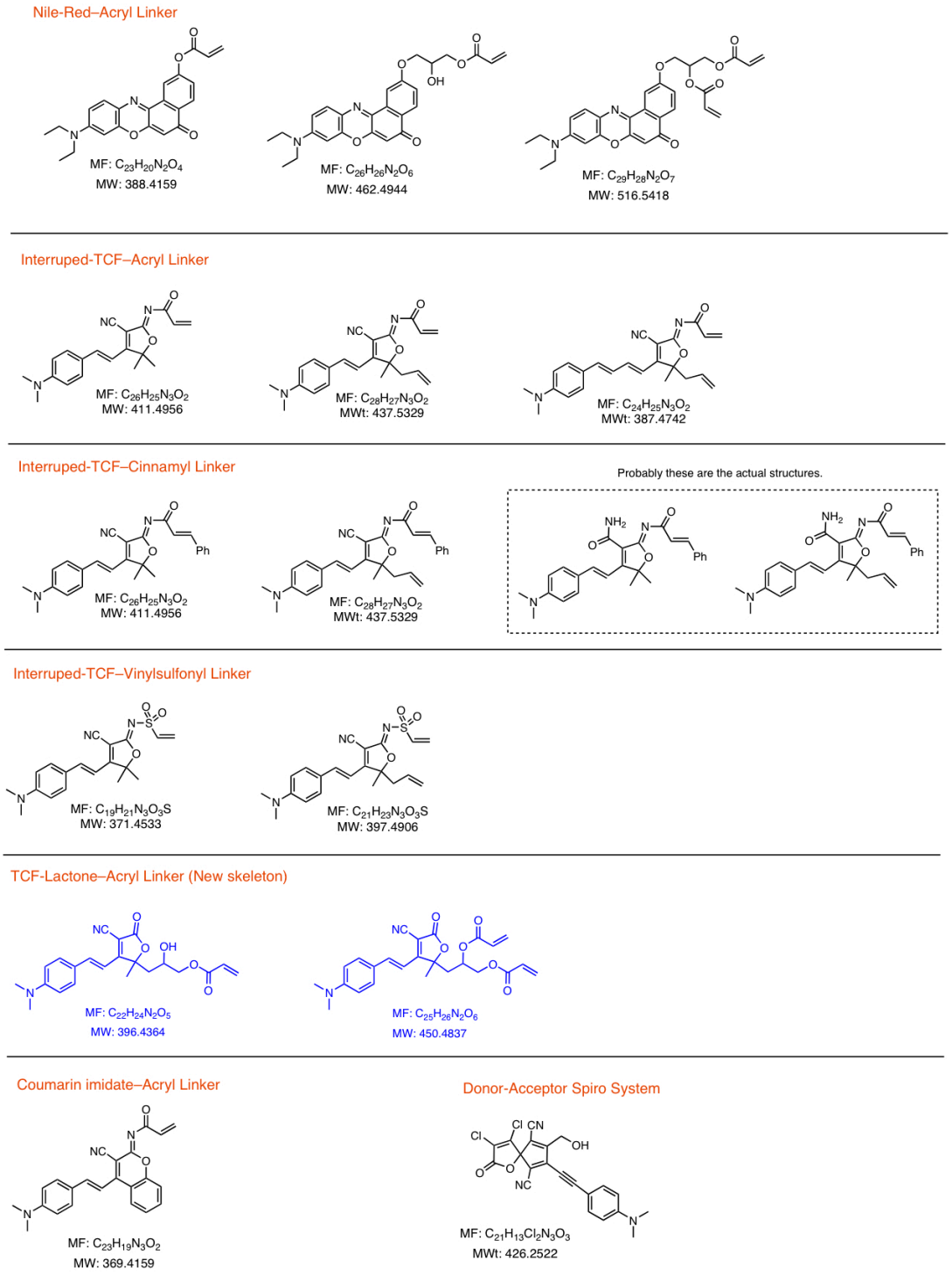

Figure 32. Environment sensitive fluorophores